

การสังเคราะห์คอมโพสิตของโพลีเอทิลีนชนิดโซ่ตรงซึ่งมีความหนาแน่นต่ำกับนาโนซิลิกา  
โดยวิธีอินไซตูปอลิเมอร์ไรเซชันด้วยตัวเร่งปฏิกิริยาเมทัลโลซีน



นายเอกราชชัย ไชยชนะ

สถาบันวิทยบริการ

วิทยานิพนธ์นี้เป็นส่วนหนึ่งของการศึกษาตามหลักสูตรปริญญาวิศวกรรมศาสตรมหาบัณฑิต

จุฬาลงกรณ์มหาวิทยาลัย

สาขาวิชาวิศวกรรมเคมี ภาควิชาวิศวกรรมเคมี

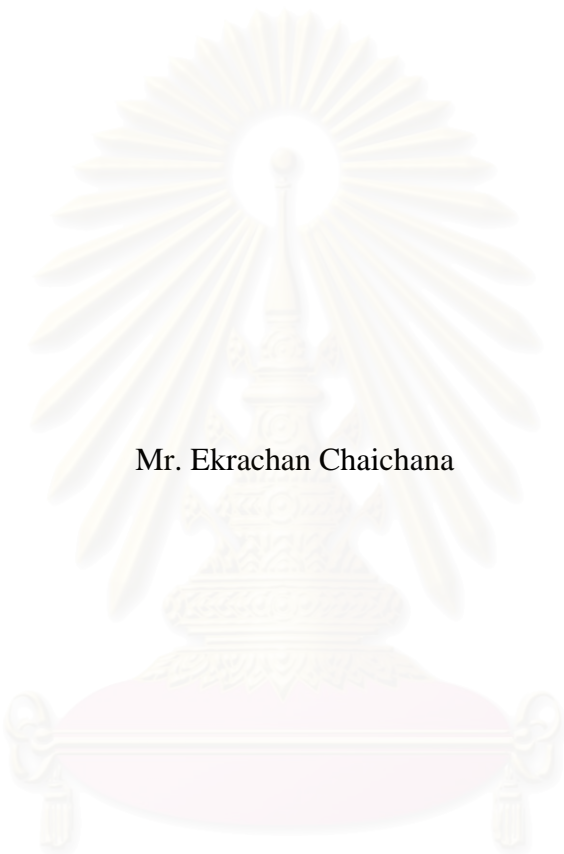
คณะวิศวกรรมศาสตร์ จุฬาลงกรณ์มหาวิทยาลัย

ปีการศึกษา 2548

ISBN:

ลิขสิทธิ์ของจุฬาลงกรณ์มหาวิทยาลัย

LINEAR LOW-DENSITY POLYETHYLENE / NANO-SILICA COMPOSITES  
SYNTHESIZED VIA *IN SITU* POLYMERIZATION WITH  
METALLOCENE CATALYSTS



Mr. Ekrachan Chaichana

สถาบันวิทยบริการ  
จุฬาลงกรณ์มหาวิทยาลัย

A Thesis Submitted in Partial Fulfillment of the Requirements  
for the Degree of Master of Engineering in Chemical Engineering

Department of Chemical Engineering

Faculty of Engineering

Chulalongkorn University

Academic Year 2005

ISBN:

Thesis Title                    LINEAR LOW-DENSITY POLYETHYLENE / NANO-SILICA  
   COMPOSITES SYNTHESIZED VIA *IN SITU*  
   POLYMERIZATION WITH METALLOCENE CATALYSTS


By                                    Mr. Ekrachan Chaichana

Field of Study                    Chemical Engineering

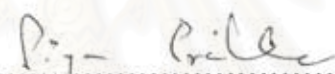
Thesis Advisor                 Bunjerd Jongsomjit, Ph.D.

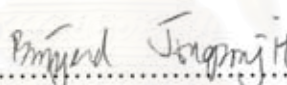
---

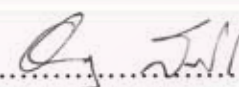
Accepted by the Faculty of Engineering, Chulalongkorn University in Partial  
Fulfillment of the Requirements for the Master's Degree

  
..... Dean of the Faculty of Engineering  
(Professor Direk Lavansiri, Ph.D.)

THESIS COMMITTEE

  
..... Chairman  
(Professor Piyasan Praserthdam, Dr.Ing.)

  
..... Thesis Advisor  
(Assistant Professor Bunjerd Jongsomjit, Ph.D.)

  
..... Member  
(Anongnat Somwangthanaroj, Ph.D.)

  
..... Member  
(Assistant Professor Joongjai Panpranot, Ph.D.)

สถาบันวิจัยสาร  
จุฬาลงกรณ์มหาวิทยาลัย

เอกราชชัย ไชยชนะ : การสังเคราะห์คอมโพสิตของโพลีเอทิลีนชนิดโซ่ตรงซึ่งมีความหนาแน่นต่ำกับนาโนซิลิกาโดยวิธีอินไซตูปอลิเมอร์ไรเซชันด้วยตัวเร่งปฏิกิริยาเมทัลโลซีน

( LINEAR LOW-DENSITY POLYETHYLENE / NANO-SILICA COMPOSITES SYNTHESIZED VIA *IN SITU* POLYMERIZATION WITH METALLOCENE CATALYST)

อ. ที่ปรึกษา: ผศ.ดร. บรรเจิด จงสมจิตร, 96 หน้า. ISBN : 974-17-3899-4

ในปัจจุบันเป็นที่ทราบกันดีว่าปฏิกิริยาการเตรียมโคพอลิเมอร์ของเอทิลีนกับ1-โอเลฟินโดยใช้ตัวเร่งปฏิกิริยาเมทัลโลซีน สามารถสังเคราะห์โพลีเอทิลีนชนิดโซ่ตรงซึ่งมีความหนาแน่นต่ำได้ คุณสมบัติทางกลของโพลีเอทิลีนตัวดังกล่าวที่สังเคราะห์ขึ้นสามารถปรับปรุงได้ โดยการเติมสารปรุงแต่งประเภทอินทรีย์หรืออนินทรีย์บางตัวลงไป สำหรับการเติมสารปรุงแต่งที่มีขนาดอยู่ในระดับนาโนเมตรลงไปโคพอลิเมอร์ จะเรียกพอลิเมอร์เหล่านั้นว่าเป็นพอลิเมอร์นาโนคอมโพสิต วิธีในการเตรียมพอลิเมอร์นาโนคอมโพสิตมีอยู่หลายวิธี เช่น การผสมโดยใช้ตัวทำละลาย, การผสมโดยการหลอมความร้อน และ วิธีอินไซตูปอลิเมอร์ไรเซชัน โดยวิธีอินไซตูปอลิเมอร์ไรเซชันได้รับการยอมรับว่าเป็นวิธีการเตรียมพอลิเมอร์นาโนคอมโพสิตที่ช่วยทำให้อนุภาคของสารปรุงแต่งที่ใส่ลงไปมีการกระจายตัวได้เป็นอย่างดี ทั้งนี้เนื่องมาจากการเกิดพันธะกันโดยตรงระหว่างตัวเร่งปฏิกิริยากับพื้นผิวของอนุภาคระดับนาโนเมตรของสารปรุงแต่ง ดังนั้นระหว่างขั้นตอนการสังเคราะห์พอลิเมอร์ดังกล่าว จะต้องมีการตรึงตัวเร่งปฏิกิริยาที่ใช้ไว้บนพื้นผิวของอนุภาคระดับนาโนเมตรของสารปรุงแต่ง ในการศึกษาจะสังเคราะห์พอลิเมอร์นาโนคอมโพสิตโดยวิธีอินไซตูปอลิเมอร์ไรเซชันโดยใช้เซอร์โคโนซีนเป็นตัวเร่งปฏิกิริยา และ เมทิลอะลูมิเนียมออกเซนเป็นตัวเร่งปฏิกิริยาร่วม ซิลิกา 2 ชนิดจะถูกนำมาใช้เป็นสารปรุงแต่ง ชนิดแรกคือซิลิกาที่เตรียมขึ้นโดยวิธีการโซล-เจล และ อีกชนิดคือซิลิกาที่ทำการซื้อมาจากบริษัทผู้ค้าซึ่งมีด้วยกัน 2 ขนาด คือ 10 นาโนเมตร และ 15 นาโนเมตร ซิลิกาที่ใช้รวมทั้งพอลิเมอร์นาโนคอมโพสิตที่สังเคราะห์ได้จะถูกนำไปทดสอบคุณสมบัติต่อไป

## สถาบันวิทยบริการ จุฬาลงกรณ์มหาวิทยาลัย

ภาควิชา.....วิศวกรรมเคมี.....ลายมือชื่อนิสิต.....  
สาขาวิชา.....วิศวกรรมเคมี.....ลายมือชื่ออาจารย์ที่ปรึกษา.....  
ปีการศึกษา .....2548.....

# #4670617421 : MAJOR CHEMICAL ENGINEERING  
 KEY WORD : ZIRCONOCENE CATALYST/SILICA/LLDPE  
 /SUPPORTED CATALYST/POLYMER NANOCOMPOSITES

EKRACHAN CHAICHANA: LINEAR LOW-DENSITY POLYETHYLENE /  
 NANO-SILICA COMPOSITES SYNTHESIZED VIA *IN SITU*  
 POLYMERIZATION WITH METALLOCENE CATALYST  
 THESIS ADVISOR: BUNJERD JONGSOMJIT, Ph.D., 96 pp.  
 ISBN : 974-17-3899-4

It is known that linear low-density polyethylene (LLDPE) can be synthesized by copolymerization of ethylene and 1-olefins using metallocene catalysts. However, the mechanical properties of LLDPE can be improved by adding organic or inorganic fillers. It should be mentioned that by adding nanoscale fillers into LLDPE, LLDPE-nanocomposites can be achieved. Among methods to produce polymer nanocomposites such as solution blending, melt mixing process and *in situ* polymerization, the *in situ* polymerization is perhaps the most promising method to produce LLDPE-nanocomposite with an exceptional dispersion of nanoparticles throughout the polymer matrix. This is due to the direct linkage of active centers to the surface of nanoparticles. Therefore, it is necessary to immobilize the active centers onto nanoparticle surface or fillers. In this present study, LLDPE/SiO<sub>2</sub>-nanocomposites were synthesized by the *in situ* polymerization with methylaluminoxane (MAO)/zirconocene catalyst. Two types of SiO<sub>2</sub> were as the fillers. One type was the SiO<sub>2</sub> prepared by sol-gel method. The other was the commercial nanopowder silica with two different sizes (10 nm and 15 nm). All particles and the obtained LLDPE/SiO<sub>2</sub>-nanocomposites were further characterized.

สถาบันวิทยบริการ  
 จุฬาลงกรณ์มหาวิทยาลัย

Department ...Chemical Engineering.....

Field of study...Chemical Engineering...

Academic year.....2005.....

Student's signature.....

Advisor's signature.....

## ACKNOWLEDGEMENTS

The author would like to express his sincere gratitude and appreciation to his advisor, Dr. Bunjerd Jongsomjit, for his invaluable suggestions, stimulating, useful discussions throughout this research and devotion to revise this thesis otherwise it can not be completed in a short time. In addition, the author would also be grateful to Professor Dr. Piyasan Prasertdam, as the chairman, and Dr. Joongjai Panpranot, Dr. Anongnat Somwangthanaroj, as the members of the thesis committee. The financial supports from the National Research Council of Thailand (NRCT), Thailand Research Fund (TRF) and Thailand Japan Technology Transfer Project (TJTTP-JBIC) are also gratefully acknowledged.

Most of all, the author would like to express his highest gratitude to his parents who always pay attention to his all the times for suggestions and have provided his support and encouragement. The most success of graduation is devoted to his parents.

Finally, the author wishes to thank the members of the Center of Excellence on Catalysis and Catalytic Reaction Engineering, Department of Chemical Engineering, Faculty of Engineering, Chulalongkorn University for their assistance especially Miss Pramrutai Kruachot.

สถาบันวิทยบริการ  
จุฬาลงกรณ์มหาวิทยาลัย

# CONTENTS

	Page
<b>ABSTRACT ( IN THAI )</b> .....	iv
<b>ABSTRACT ( IN ENGLISH )</b> .....	v
<b>ACKNOWLEDGMENTS</b> .....	vi
<b>CONTENTS</b> .....	vii
<b>LIST OF TABLES</b> .....	x
<b>LIST OF FIGURES</b> .....	xi
<b>CHAPTER I INTRODUCTION</b> .....	1
1.1 Objective of the Thesis .....	4
1.2 Scope of the Thesis .....	4
<b>CHAPTER II LITERATURE REVIEWS</b> .....	5
2.1 Background on Polyolefin Catalysts .....	5
2.1.1 Catalyst Structure.....	5
2.1.2 Polymerization mechanism.....	8
2.1.3 Cocatalysts.....	11
2.1.4 Catalyst Activity.....	14
2.1.5 Copolymerization.....	15
2.2 Heterogenous Systems.....	19
2.2.1 Catalyst Chemistry.....	19
2.2.2 Supporting Methods.....	20
2.3 Polymer nanocomposites.....	21
2.4 Linear low density polyethylene (LLDPE) nanocomposites.....	25
2.5 Silica nanocomposites.....	27
<b>CHAPTER III EXPERIMENTAL</b> .....	30
3.1 Chemicals.....	30
3.2 Equipments.....	31
3.2.1 Cooling System.....	31
3.2.2 Inert Gas Supply.....	31
3.2.3 Magnetic Stirrer and Heater.....	32
3.2.4 Reactor.....	32
3.2.5 Schlenk Line.....	32

	Page
3.2.6 Schlenk Tube .....	33
3.2.7 Vacuum Pump.....	34
3.2.8 Polymerization line.....	34
3.3 Characterizing Instruments.....	34
3.3.1 Differential Scanning Calorimetry (DSC).....	34
3.3.2 Nuclear Magnetic Resonance (NMR).....	35
3.3.3 Scanning Electron Microscope (SEM) and (EDX).....	35
3.3.4 X-ray diffraction (XRD).....	35
3.3.5 Transmission Electron Microscopy (TEM).....	35
3.4 Preparation of fillers.....	36
3.4.1 Preparation of nano-materials.....	36
3.4.2 Impregnation.....	36
3.5 Ethylene and hexene Copolymerization Procedure.....	36
3.6 Characterization.....	39
3.6.1 Nano-materials.....	39
3.6.2 Catalyst precursor MAO filled (filler).....	39
3.6.3 LLDPE-nanocomposites.....	39
<b>CHAPTER IV RESULTS AND DISCUSSIONS.....</b>	<b>41</b>
4.1 Sol-gel silica as a filler of LLDPE-SiO <sub>2</sub> nanocomposite synthesized via <i>insitu</i> polymerization with zirconocene/MAO catalyst.....	41
4.1.1 Characterization of fillers with X-ray diffraction (XRD).....	41
4.1.2 Effect of the amount of filler on catalytic activity.....	42
4.1.3 Characterization of supports and catalyst precursors with fourier transformed infrared spectroscopy (FT- IR).....	44
4.1.4 The distribution of nano- SiO <sub>2</sub> in LLDPE-nanocomposites.....	45
4.2 Nanopowder silica as a filler of LLDPE-SiO <sub>2</sub> nanocomposite synthesized via in situ polymerization with zirconocene/MAO catalysts.....	46
4.2.1 The Effect of particle size of nano-SiO <sub>2</sub> .....	46
4.2.1.1 Characterization of fillers and catalyst precursors with X- ray diffraction (XRD).....	46
4.2.1.2 Characterization of fillers and catalyst precursors with Transmission electron microscope (TEM).....	46



	Page
4.2.1.3 Effect of particle size on activity and characteristics of LLDPE-SiO <sub>2</sub> nanocomposites.....	46
4.2.1.4 The effect of nanopowder-silica on the morphologies of LLDPE-nanocomposites.....	50
4.2.1.5 Characterization of LLDPE-nanocomposites with Transmission electron microscope (TEM).....	52
4.2.1.6 Characterization of LLDPE-nanocomposites with Nuclear Magnetic Resonance (NMR).....	54
4.2.2 Effect of the amount of nano-SiO <sub>2</sub> .....	55
4.2.2.1 Effect of the amount of nano-SiO <sub>2</sub> on activity and characteristics of LLDPE-SiO <sub>2</sub> nanocomposites.....	55
4.2.2.2 The effect of the amount of nanopowder-silica on the morphologies of LLDPE-nanocomposites.....	56
4.2.2.3 Characterization of LLDPE-nanocomposites ( fixed ratio of [Al] <sub>MAO</sub> /[Zr] )with Transmission electron microscope (TEM).....	57
4.2.2.4 Characterization of LLDPE-nanocomposites( fixed ratio of [Al] <sub>MAO</sub> /[Zr] ) with Nuclear Magnetic Resonance (NMR).....	58
<b>CHAPTER V CONCLUSIONS &amp; RECOMMENDATIONS.....</b>	<b>59</b>
5.1 Conclusions.....	59
5.2 Recommendations.....	59
<b>REFERENCES.....</b>	<b>60</b>
<b>APPENDICES.....</b>	<b>64</b>
<b>APPENDIX A.....</b>	<b>65</b>
<b>APPENDIX B.....</b>	<b>74</b>
<b>APPENDIX C.....</b>	<b>83</b>
<b>APPENDIX D.....</b>	<b>86</b>
<b>VITAE.....</b>	<b>87</b>

## LIST OF TABLES

Table	Page
2.1 Representative Examples of Metallocenes.....	6
4.1 Activity and yield of LLDPE/nano-composites via <i>in situ</i> polymerization with metallocene catalyst.....	43
4.2 Activity and characteristics of LLDPE-SiO <sub>2</sub> nanocomposites.....	48
4.3 Triad distribution obtained from <sup>13</sup> C NMR of LLDPE-SiO <sub>2</sub> nanocomposites.....	54
4.4 Activity and characteristics of LLDPE-SiO <sub>2</sub> nanocomposites at [Al] <sub>MAO</sub> /[Zr] = 2270.....	56



สถาบันวิทยบริการ  
จุฬาลงกรณ์มหาวิทยาลัย

## LIST OF FIGURES

Figure	Page
1.1 (a) Surface area per unit volume vs. particle size.....	3
1.2 (b) Interparticle distance.....	3
2.1 Molecular structure of metallocene .....	5
2.2 Some of zirconocene catalysts structure .....	6
2.3 Scheme of the different metallocene complex structures.....	7
2.4 Cossee mechanism for Ziegler-Natta olefin polymerization.....	8
2.5 The propagation step according to the trigger mechanism.....	9
2.6 Propagation mechanism in polymerization.....	9
2.7 Chain transfer via $\beta$ -H elimination.....	10
2.8 Chain transfer via $\beta$ -CH <sub>3</sub> elimination.....	10
2.9 Chain transfer to aluminum.....	11
2.10 Chain transfer to monomer.....	11
2.11 Chain transfer to hydrogen.....	11
2.12 Early structure models for MAO.....	12
2.13 Representation of MAO showing the substitution of one bridging methyl group by X ligand extracted from $\text{racEt}(\text{Ind})_2\text{ZrCl}_2$ (X = Cl, NMe <sub>2</sub> , CH <sub>2</sub> Ph).....	13
2.14 (a) Pure polypropylene and (b) polypropylene with 9.2% volume filler.....	22
2.15 Debonding around 50 and 12 nm particles.....	24
3.1 Inert gas supply system.....	32
3.2 Schlenk line.....	33
3.3 Schlenk tube.....	33
3.4 diagram of system in slurry phase polymerization.....	34
4.1 XRD patterns of nano-SiO <sub>2</sub> and nano-SiO <sub>2</sub> -Al <sub>2</sub> O <sub>3</sub> .....	42
4.2 Activity profile with various amounts of support used.....	43
4.3 Morphologies of LLDPE/nano composites.....	44
4.4 EDX mapping of LLDPE/nano-SiO <sub>2</sub> composite with SiO <sub>2</sub> .....	45
4.5 XRD patterns of nanopowder-SiO <sub>2</sub> before and after impregnation procedure.....	46

<b>Figure</b>	<b>Page</b>
4.6 TEM micrographs of the nano-SiO <sub>2</sub> before and after impregnation with MAO.....	47
4.7 Catalytic activity of LLDPE-SiO <sub>2</sub> nanocomposites with two particle size of nanosilica as a filler.....	49
4.8 The conceptual model of nano-particle interacting with MAO.....	50
4.9 Morphologies of LLDPE/nano composites with two particle size of nanosilica as a filler.....	51
4.10 EDX mapping of LLDPE/nano-SiO <sub>2</sub> composite with SiO <sub>2</sub> (0.3 g) indicating distribution of Si and O.....	52
4.11 TEM micrographs of LLDPE/nanocomposites with two particle size of nanosilica as a filler.....	53
4.12 Morphologies of LLDPE/nano composites with 15nm silica as a filler.....	57
4.13 TEM micrographs of LLDPE/nano-SiO <sub>2</sub> with 15 nm silica as a filler.....	57
A-1. DSC curve of LLDPE-nanocomposites with 0.1 g of 10 nm-silica.....	67
A-2. DSC curve of LLDPE-nanocomposites with 0.2 g of 10 nm-silica.....	68
A-3. DSC curve of LLDPE-nanocomposites with 0.3 g of 10 nm-silica.....	69
A-4. DSC curve of LLDPE-nanocomposites with 0.1 g of 15 nm-silica .....	70
A-5. DSC curve of LLDPE-nanocomposites with 0.2 g of 15 nm-silica.....	71
A-6. DSC curve of LLDPE-nanocomposites with 0.3 g of 15 nm-silica.....	72
A-7. DSC curve of LLDPE-nanocomposites with 0.1 g of 15 nm-silica ( fixed ratio of Al/Zr).....	73
A-8. DSC curve of LLDPE-nanocomposites with 0.3 g of 15 nm-silica ( fixed ratio of Al/Zr).....	74
B-1. <sup>13</sup> C-NMR spectrum of LLDPE-nanocomposites with 0.1 g of 10 nm-silica.	76
B-2. <sup>13</sup> C-NMR spectrum of LLDPE-nanocomposites with 0.2 g of 10 nm-silica.	77
B-3. <sup>13</sup> C-NMR spectrum of LLDPE-nanocomposites with 0.3 g of 10 nm-silica.	78
B-4. <sup>13</sup> C-NMR spectrum of LLDPE-nanocomposites with 0.1 g of 15 nm-silica.	79
B-5. <sup>13</sup> C-NMR spectrum of LLDPE-nanocomposites with 0.2 g of 15 nm-silica.	80
B-6. <sup>13</sup> C-NMR spectrum of LLDPE-nanocomposites with 0.3 g of 15 nm-silica.	81
B-7. <sup>13</sup> C-NMR spectrum of LLDPE-nanocomposites with 0.1 g of 15 nm-silica (fixed ratio of Al/Zr).....	82
B-8. <sup>13</sup> C-NMR spectrum of LLDPE-nanocomposites with 0.3 g of 15 nm-silica (fixed ratio of Al/Zr).....	83

# CHAPTER I

## INTRODUCTION

Introduced in the early 1990s, metallocene catalysts were engineered to radically change the molecular structure of polyolefins and create new application markets. This new catalysts system was estimated to have the same impact on the polymers industry as the discovery of Ziegler-Natta (ZN) catalysts in the 1950s [1]. ZN catalysts are still the workhorse of the global polyethylene (PE) and polypropylene (PP) industries. The course of this revolution would draw on the unique characteristics offered by metallocenes:

- The ability to polymerize almost any vinyl unsaturated monomer
- Inherent ability to produce extremely uniform homopolymers and copolymers of very narrow molecular weight distribution (MWD) and composition distribution
- Capability to control stereoselectivity of the catalysts and produce new molecular structures such as highly syndiotactic polymers
- Unprecedented precision in assembling polymers of predictable structure and properties as if each metallocene holds the genetic code for a specific family of polymers

The metallocene catalyst technologies became a “must do” R&D objective for many global polyolefins companies. The development field soon broadened to include systems that were not true metallocenes. However these catalysts have the same characteristics derived from single active site or species (SSC). The early expectations of SSC usage for low-density PEs has been met well and exceeded for some resin types such as for linear low-density polyethylene (LLDPE) large volume applications.

It is known that the copolymerization of ethylene with higher 1-olefins is a commercial importance for productions of LLDPE. LLDPE (density 0.920 to 0.940) is one

of the most widely used polyolefins in many applications, especially, for plastic films. However, in some cases, the use of polyolefins or LLDPE is limited by their drawbacks such as low mechanical strength, low thermal resistance, poor optical properties and so on. Thus, in order to improve the specific properties of these polymers, some additives need to be blended with them.

It has been known that blending polymer with inorganic materials is recognized as a powerful method to produce new materials called polymer composites or filled polymers. However, due to the significant development in nanotechnologies in the recent years, nano-inorganic materials such as  $\text{SiO}_2$ ,  $\text{Al}_2\text{O}_3$  and  $\text{TiO}_2$  have brought much attention to this research field.

There are several reasons for many researchers to consider the nano-material replace the traditional micro-material. One of the important reasons is the effect of size on particle properties[2], the small size of the filler leads to an exceptionally large interfacial area in the composites. Figure 1a shows the surface area per unit volume as a function of particle size for spherical particles that are ideally dispersed. The increase in surface area below 100 nm is dramatic.

As defined in traditional composites, the interfacial region is the region of altered chemistry, altered polymer chain mobility, altered degree of cure, and altered crystallinity. Interface size has been reported to be as small as 2 nm and as large as about 50 nm. Figure 1b shows interparticle spacing as a function of particle size for an ideally dispersed nanoparticle composite: at low volume fractions the entire matrix is essentially part of the interfacial region. Even if the interfacial region is only a few nanometers, very quickly the entire polymer matrix has a different behavior than the bulk. If the interfacial region is more extended, then the polymer matrix behavior can be altered at much smaller loadings. Therefore, by controlling the degree of interaction between the polymer and the nanofiller, the properties of the entire matrix can be controlled.

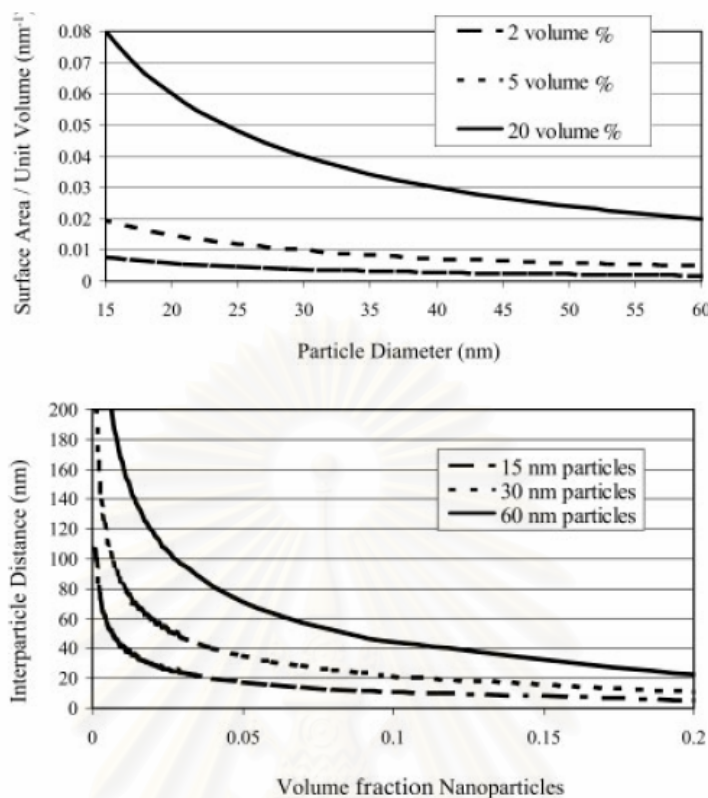


**Figure 1.1**

- (a) Surface area per unit volume vs. particle size for spherical particles that are ideally dispersed.
- (b) Interparticle distance for spherical that are ideally dispersed.[2]

The polymer composites filled with nano-inorganic materials are well recognized as polymer nano-composites. Basically, there are probably three methods used to produce the filled polymer; (i) melt blending, (ii) solution blending, and (iii) *in situ* polymerization. Due to the direct synthesis via polymerization along with the presence of nano materials, the *in situ* polymerization is perhaps considered to be the most powerful techniques to produce polymer nano-composites with good dispersion of the nanoparticles into polymer matrix. Although, LLDPE composites have been investigated by many authors [3-8], no such a study has been done on synthesizing polymer nano-composites via the *in situ* polymerization.

In the present study, LLDPE/nano-SiO<sub>2</sub> composites synthesized via the *in situ* polymerization with MAO/zirconocene catalyst was investigated for the first time. For

the first part of this study, the nano-SiO<sub>2</sub> filled materials will be synthesized using sol-gel method. For the second part ,the two different sizes of filler used were obtained from Sigma-Aldrich .In the both parts, the amounts of nano-materials filler were also varied. Yields, activities, and polymer properties were further investigated and discussed.

### 1.1. Objective of the Thesis

- To synthesize LLDPE nano – SiO<sub>2</sub> composites with zirconocene and MAO by *in situ* polymerization method.
- To study properties of LLDPE nano – SiO<sub>2</sub> composites prepared by *in situ* polymerization method.

### 1.2. Scope of the Thesis

- Synthesize nano – SiO<sub>2</sub> by sol-gel method with trimethylorthosilicate (TEOS) as a precursor.
- Prepare LLDPE nano – SiO<sub>2</sub> composites by *in situ* polymerization with [*rac*-ethylene bis-(indenyl)] zirconium(IV) dichloride with MAO.
- Characterize fillers and catalyst precursors using XRD ,SEM, TEM and EDX.
- Characterize the obtained LLDPE nano-SiO<sub>2</sub> composites using SEM, TEM, DSC, GPC and <sup>13</sup>C -NMR.

สถาบันวิทยบริการ  
จุฬาลงกรณ์มหาวิทยาลัย



## CHAPTER II

### LITERATURE REVIEW

#### 2.1. Background on Polyolefin Catalysts

Polyolefins can be produced with free radical initiators, Phillips type catalysts, Ziegler-Natta catalysts and metallocene catalysts. Ziegler-Natta catalysts have been most widely used because of their broad range of application. However, Ziegler-Natta catalyst provides polymers having broad molecular weight distribution (MWD) and composition distribution due to multiple active sites formed [9].

Metallocene catalysts have been used to polymerize ethylene and  $\alpha$ -olefins commercially. The structural change of metallocene catalysts can control composition distribution, incorporation of various comonomers, MWD and stereoregularity [10].

##### 2.1.1. Catalyst Structure

Metallocene is a class of compounds in which cyclopentadienyl or substituted cyclopentadienyl ligands are  $\pi$ -bonded to the metal atom. The stereochemistry of biscyclopentadienyl (or substituted cyclopentadienyl)-metal bis (unibidentate ligand) complexes can be most simply described as distorted tetrahedral, with each  $\eta^5$ -L group ( L = ligand ) occupying a single co-ordination position, as in Figure 2.1 [11].

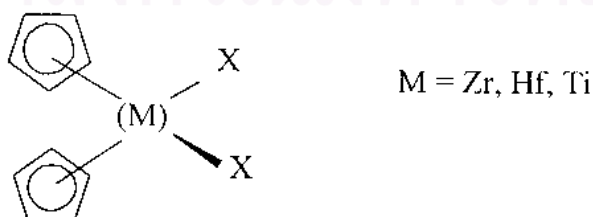


**Figure 2.1** Molecular structure of metallocene

Representative examples of each category of metallocenes and some of zirconocene catalysts are shown in Table 2.1 and Figure 2.2, respectively.

**Table 2.1 Representative Examples of Metallocenes [11]**

Category of metallocenes	Metallocene Catalysts
[A] Nonstereorigid metallocenes	1) $\text{Cp}_2\text{MCl}_2$ (M = Ti, Zr, Hf) 2) $\text{Cp}_2\text{ZrR}_2$ (M = Me, Ph, $\text{CH}_2\text{Ph}$ , $\text{CH}_2\text{SiMe}_3$ ) 3) $(\text{Ind})_2\text{ZrMe}_2$
[B] Nonstereorigid ring-substituted metallocenes	1) $(\text{Me}_5\text{C}_5)_2\text{MCl}_2$ (M = Ti, Zr, Hf) 2) $(\text{Me}_3\text{SiCp})_2\text{ZrCl}_2$
[C] Stereorigid metallocenes	1) $\text{Et}(\text{Ind})_2\text{ZrCl}_2$ 2) $\text{Et}(\text{Ind})_2\text{ZrMe}_2$ 3) $\text{Et}(\text{IndH}_4)_2\text{ZrCl}_2$
[D] Cationic metallocenes	1) $\text{Cp}_2\text{MR}(\text{L})^+[\text{BPh}_4]^-$ (M = Ti, Zr) 2) $[\text{Et}(\text{Ind})_2\text{ZrMe}]^+[\text{B}(\text{C}_6\text{F}_5)_4]^-$ 3) $[\text{Cp}_2\text{ZrMe}]^+[(\text{C}_2\text{B}_9\text{H}_{11})_2\text{M}]^-$ (M = Co)
[E] Supported metallocenes	1) $\text{Al}_2\text{O}_3\text{-Et}(\text{IndH}_4)_2\text{ZrCl}_2$ 2) $\text{MgCl}_2\text{-Cp}_2\text{ZrCl}_2$ 3) $\text{SiO}_2\text{-Et}(\text{Ind})_2\text{ZrCl}_2$

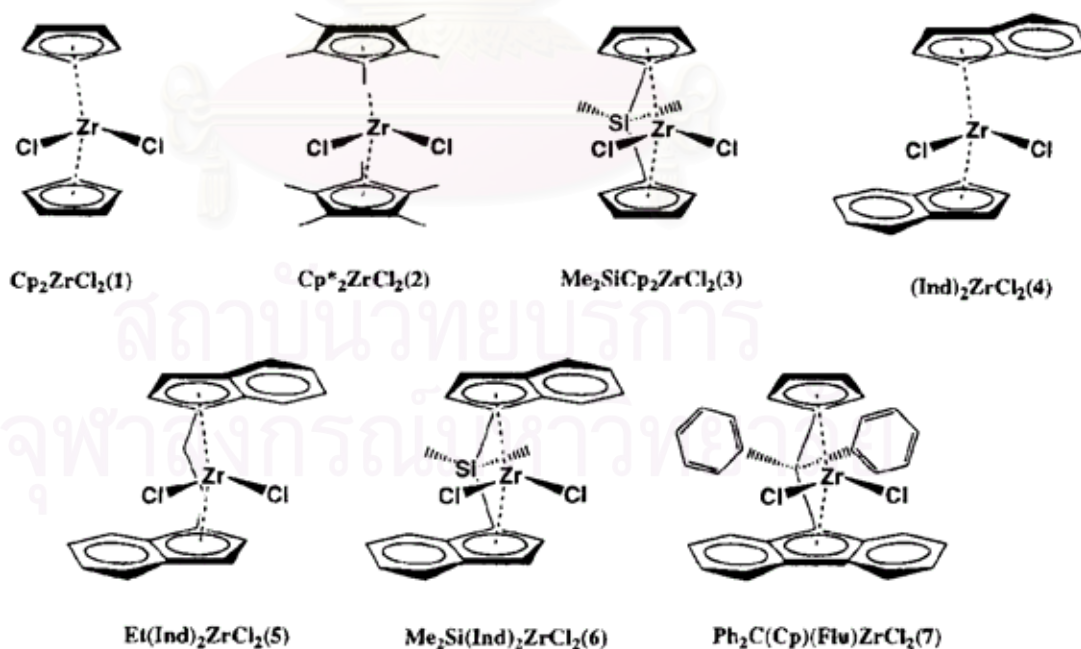


**Figure 2.2** Some of zirconocene catalysts structure [12]

Composition and types of metallocene have several varieties. When the two cyclopentadienyl (Cp) rings on either side of the transition metal are unbridged, the metallocene is nonstereorigid and it is characterized by  $C_{2v}$  symmetry. The  $Cp_2M$  ( $M = \text{metal}$ ) fragment is bent back with the centroid-metal-centroid angle  $\theta$  about  $140^\circ$  due to an interaction with the other two  $\sigma$  bonding ligands [13]. When the Cp rings are bridged (two Cp rings arranged in a chiral array and connected together with chemical bonds by a bridging group), the stereorigid metallocene, so-called ansa-metallocene, could be characterized by either a  $C_1$ ,  $C_2$ , or  $C_s$  symmetry depending upon the substituents on two Cp rings and the structure of the bridging unit as schematically illustrated in Figure 2.3[11].

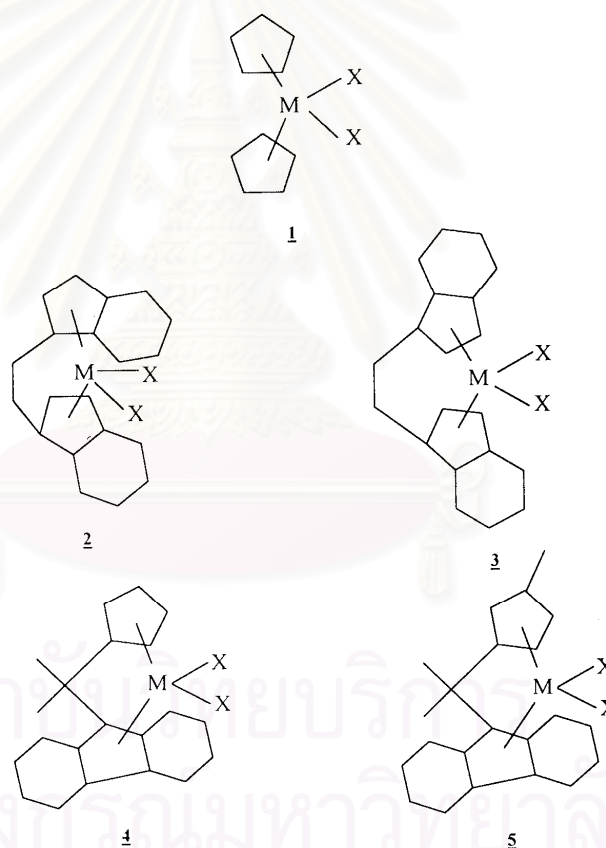


**Figure 2.3** Scheme of the different metallocene complex structures [11]. Type 1 is  $C_{2v}$ -symmetric; Type 2 is  $C_2$ -symmetric; Type 3 is  $C_s$ -symmetric; Type 4 is  $C_s$ -symmetric; Type 5 is  $C_1$ -symmetric.

### 2.1.2. Polymerization Mechanism

The mechanism of catalyst activation is not clearly understood. However, alkylation and reduction of the metal site by a cocatalyst (generally alkyl aluminum or alkyl aluminoxane) is believed to generate the cationic active catalyst species.

First, in the polymerization, the initial mechanism started with formation of cationic species catalyst that is shown below.

#### Initiation



Propagation proceeds by coordination and insertion of new monomer unit in the metal carbon bond. Cossee mechanism is still one of the most generally accepted polymerization mechanism (Figure 2.4) [14]. In the first step, monomer forms a complex with the vacant coordination site at the active catalyst center. Then through a four-centered transition state, bond between monomer and metal center and between monomer and polymer chain are formed, increasing the length of the polymer chain by one monomer unit and generating another vacant site.

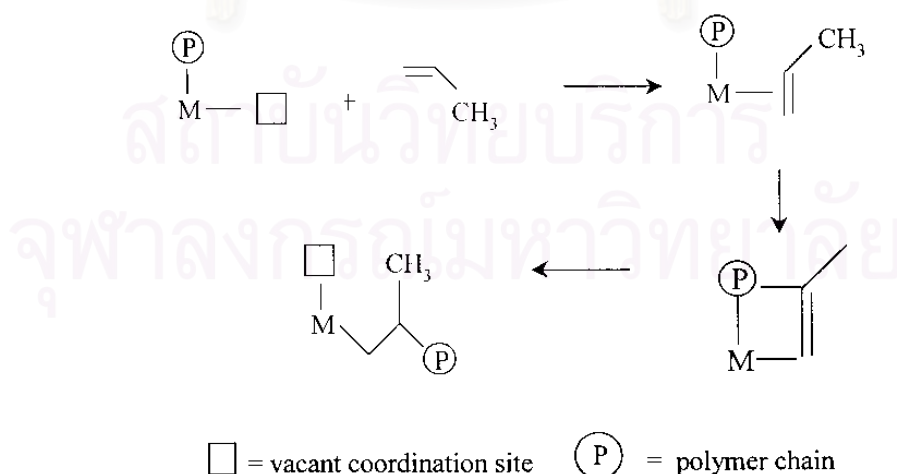


**Figure 2.4** Cossee mechanism for Ziegler-Natta olefin polymerization [14].

The trigger mechanism has been proposed for the polymerization of  $\alpha$ -olefin with Ziegler-Natta catalysts [15]. In this mechanism, two monomers interact with one active catalytic center in the transition state. A second monomer is required to form a new complex with the existing catalyst-monomer complex, thus trigger a chain propagation step. No vacant site is involved in this model. The trigger mechanism has been used to explain the rate enhancement effect observed when ethylene is copolymerized with  $\alpha$ -olefins.

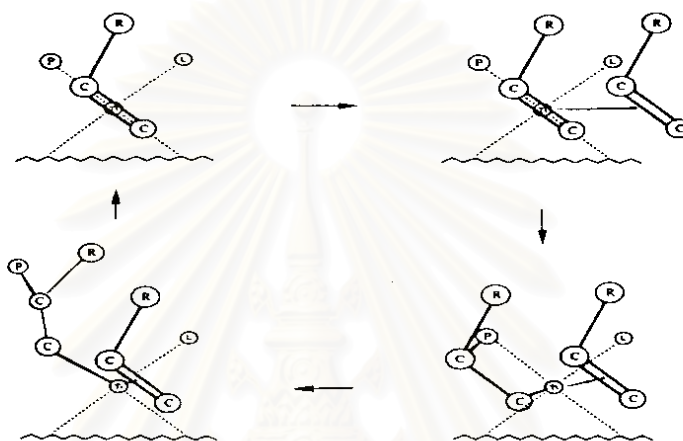


**Figure 2.5** The propagation step according to the trigger mechanism [15].

After that, the propagation mechanism in polymerization shown in Figure 2.6.

#### Propagation

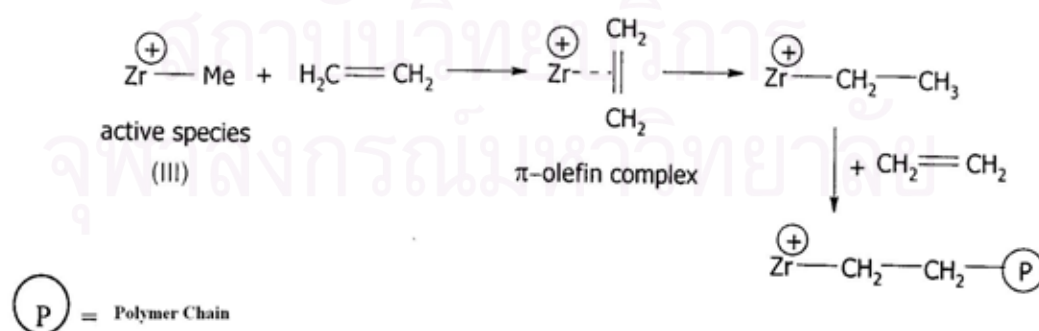


**Figure 2.6** Propagation mechanism in polymerization

Finally, the termination of polymer chains can be formed by 1) chain transfer via  $\beta$ -H elimination, 2) chain transfer via  $\beta$ -Me elimination, 3) chain transfer to aluminum, 4) chain transfer to monomer, and 5) chain transfer to hydrogen ( Figure 2.7-2.11 ) [11]. The first two transfer reactions form the polymer chains containing terminal double bonds.

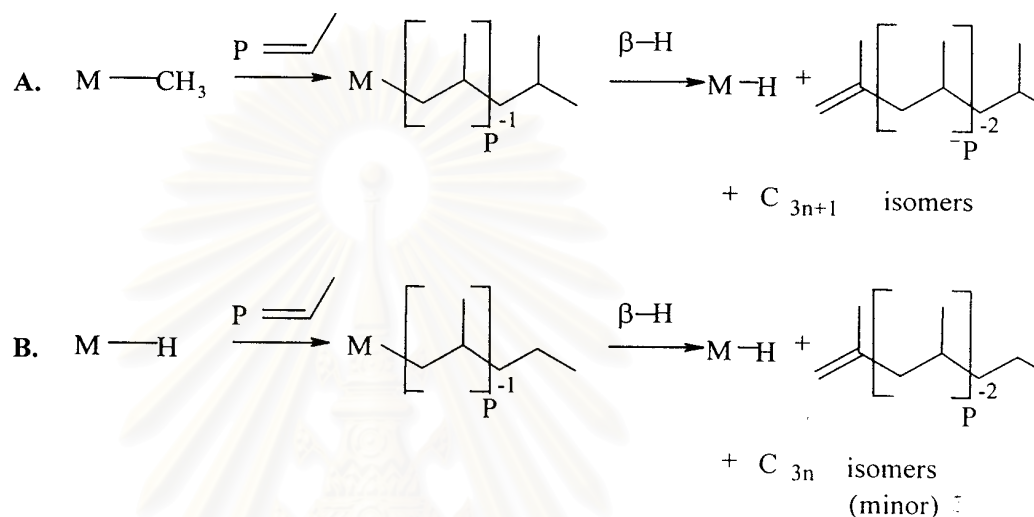


**Figure 2.7** Chain transfer via  $\beta$ -H elimination [11]

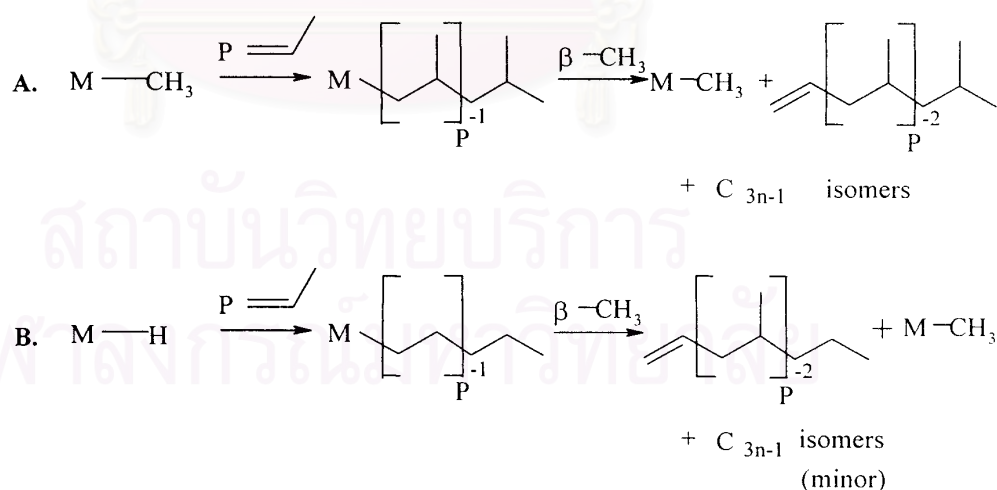


**Figure 2.8** Chain transfer via  $\beta$ -CH<sub>3</sub> elimination [11]

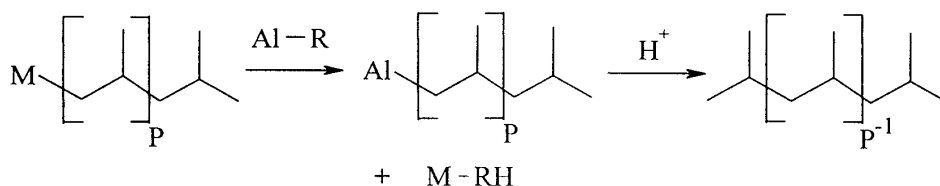


**Figure 2.9** Chain transfer to aluminum [11]

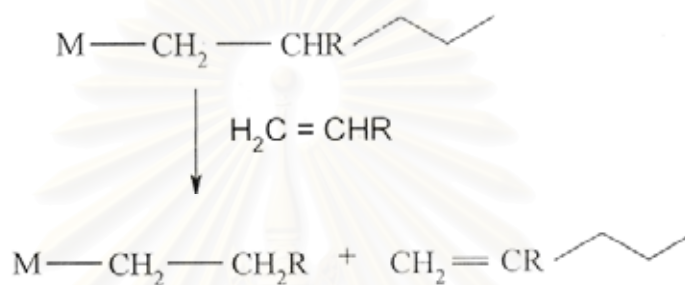


**Figure 2.10** Chain transfer to monomer [11]

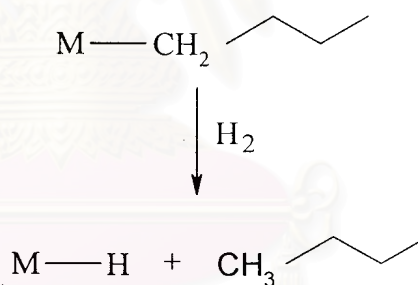


**Figure 2.11** Chain transfer to hydrogen [11]

### 2.1.3. Cocatalysts

Metallocene catalysts have to be activated by a cocatalyst. The most common types of cocatalysts are alkylaluminums including methylaluminoxane (MAO), trimethylaluminum (TMA), triethylaluminum (TEA), triisobutylaluminum (TIBA) and cation forming agents such as  $(\text{C}_6\text{H}_5)_3\text{C}^+(\text{C}_6\text{F}_5)_4\text{B}^-$  and  $\text{B}(\text{C}_6\text{F}_5)_3$  [16].

Among these, MAO is a very effective cocatalyst for metallocene. However, due to the difficulties and costs involved in the synthesis of MAO, there has been considerable effort done to reduce or elimination the use of MAO. Due to difficulties in separation, most commercially available MAO contains a significant fraction of TMA (about 10-30%) [17]. This TMA in MAO could be substantially eliminated by toluene-evaporation at 25°C.

Indeed, the difficulties encountered to better understand the important factors for an efficient activation are mainly due to the poor knowledge of the MAO composition and structure. Several types of macromolecular arrangements, involving linear chains, monocycles and/or various three-dimensional structures have been successively postulated. These are shown in Figure 2.12. In recent work, a more detailed image of MAO was proposed as a cage molecule, with a general formula  $\text{Me}_{6m}\text{Al}_{4m}\text{O}_{3m}$  (m equal to 3 or 4) [18].

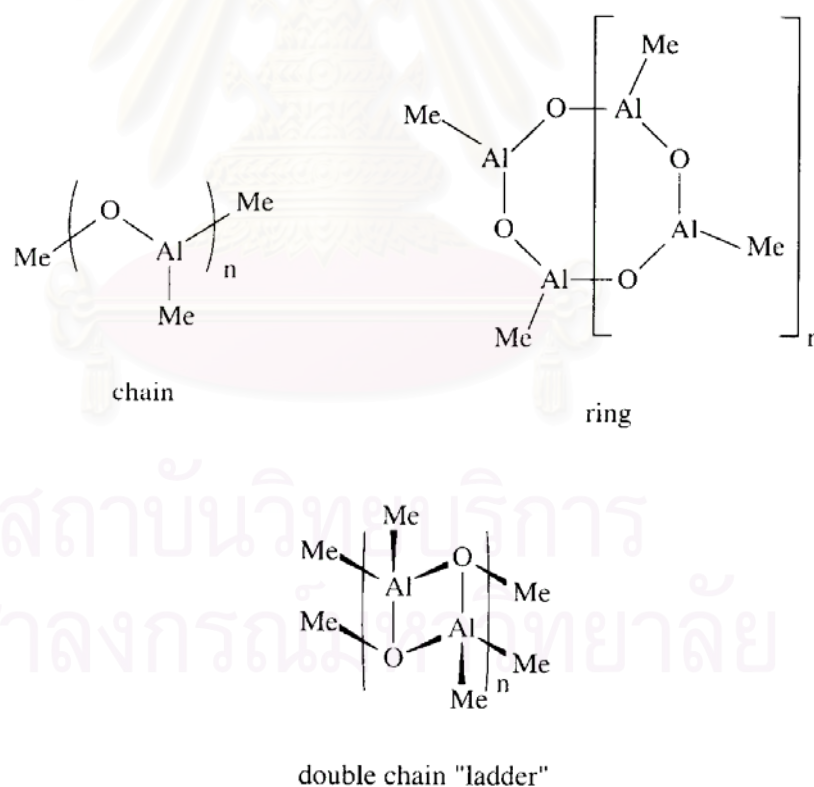


**Figure 2.12** Early structure models for MAO [18]



In the case of  $\text{rac-Et(Ind)}_2\text{ZrMe}_2$  as precursor, the extracted methyl ligands do not yield any modification in the structure and reactivity of the MAO counter-anion, thus allowing zirconium coordination site available for olefin that presented in Figure 2.13 [19].

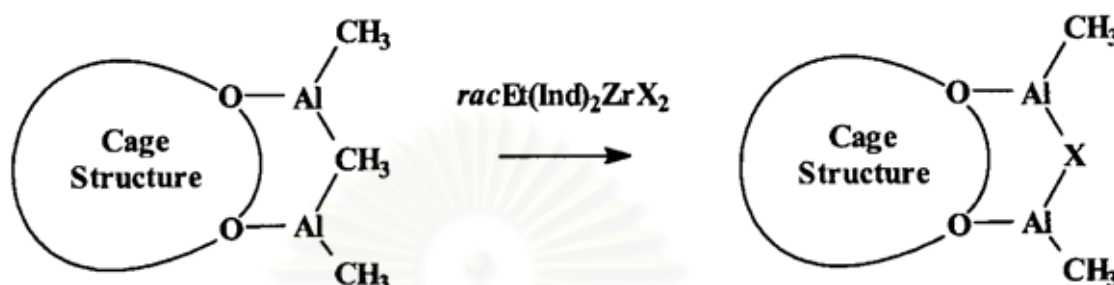


**Figure 2.13** Representation of MAO showing the substitution of one bridging methyl group by X ligand extracted from  $\text{racEt(Ind)}_2\text{ZrCl}_2$  ( $\text{X} = \text{Cl}, \text{NMe}_2, \text{CH}_2\text{Ph}$ ) [19].

Cam and Giannini [20] investigated the role of TMA present in MAO by a direct analysis of  $\text{Cp}_2\text{ZrCl}_2/\text{MAO}$  solution in toluene- $d_8$  using  $^1\text{H-NMR}$ . Their observation indicated that TMA might be the major alkylating agent and that MAO acted mainly as a polarization agent. However, in general it is believed that MAO is the key cocatalyst in polymerizations involving metallocene catalysts. The role of MAO included 1) alkylation of metallocene, thus forming catalyst active species, 2) scavenging impurities, 3) stabilizing the cationic center by ion-pair interaction and 4) preventing bimetallic deactivation of the active species.

The homogeneous metallocene catalyst cannot be activated by common trialkylaluminum only. However, Soga *et al.*[21] were able to produce polyethylene with modified homogeneous  $\text{Cp}_2\text{ZrCl}_2$  activated by common trialkylaluminum in the presence of  $\text{Si(CH}_3)_3\text{OH}$ . Their results show that for an “optimum” yield aging of the catalyst and  $\text{Si(CH}_3)_3\text{OH}$  mixture for four hours is required. However, MWD of the produced polymers is bimodal although the polymers obtained in the presence of MAO have narrow MWD.

Ethylene/ $\alpha$ -olefins copolymers with bimodal CCD were produced with homogeneous  $\text{Cp}_2\text{ZrCl}_2$  with different cocatalysts such as MAO and mixture of

TEA/borate or TIBA/borate [22]. It seemed that the active species generated with different cocatalysts have different activities and produce polymers with different molecular weights.

#### 2.1.4. Catalyst Activity

The ethylene polymerization rate of the copolymerization reaction with the catalyst system  $\text{SiO}_2/\text{MAO}/\text{rac-Me}_2\text{Si} [2\text{-Me-4-Ph-Ind}]_2\text{ZrCl}_2$  was studied by Fink *et al.* [23]. The temperature was varied from 40 to 57°C. Small amount of hexene in the reaction solution increased the polymerization rate. The extent of the "comonomer effect" depended on the polymerization temperature. At 57°C the maximum activity of the ethylene/hexene copolymerization was 8 times higher than the homopolymerization under the same conditions. At 40°C the highest reaction rate for the copolymerization is only 5 times higher than that for the ethylene homopolymerization. For the polymer properties of the ethylene/ $\alpha$ -olefin copolymerization, the molecular weights of the polymers decreased with increasing comonomer incorporation. Ethylene/hexene copolymers produced by a metallocene catalyst also have the same melting point and glass transition temperature.

Series of ethylene copolymerization with 1-hexene or 1-hexadecene over four different siloxy-substituted ansa-metallocene/methylaluminoxane (MAO) catalyst systems were studied by Seppala *et al.* [24]. Metallocene catalysts  $\text{rac-Et}[2\text{-(t-BuMe}_2\text{SiO)Ind}]_2\text{ZrCl}_2$  (1),  $\text{rac-Et}[1\text{-(t-BuMe}_2\text{SiO)Ind}]_2\text{ZrCl}_2$  (2),  $\text{rac-Et}[2\text{-(i-Pr}_3\text{SiO)Ind}]_2\text{ZrCl}_2$  (3) and  $\text{rac-Et}[1\text{-(i-Pr}_3\text{SiO)Ind}]_2\text{ZrCl}_2$  (4) were used. The effects of minor changes in the catalyst structure, more precisely changes in the ligand substitution pattern were studied. They found that series of polymerization with siloxy-substituted bis(indenyl) ansa-metallocene are highly active catalyst precursors for ethylene- $\alpha$ -olefins copolymerizations. The comonomer response of all four catalyst precursors was good. Under the same conditions the order of copolymerization ability of the catalyst was  $\text{rac-Et}[2\text{-(i-Pr}_3\text{SiO)Ind}]_2\text{ZrCl}_2 > \text{rac-Et}[2\text{-(t-BuMe}_2\text{SiO)Ind}]_2\text{ZrCl}_2$  and  $\text{rac-Et}[1\text{-(i-Pr}_3\text{SiO)Ind}]_2\text{ZrCl}_2 > \text{rac-Et}[1\text{-(t-BuMe}_2\text{SiO)Ind}]_2\text{ZrCl}_2$ . These catalysts are able to produce high molecular weight copolymers.

### 2.1.5. Copolymerization

By adding a small amount of comonomer to the polymerization reactor, the final polymer characteristics can be dramatically changed. For example, the Unipol process for linear low density polyethylene (LLDPE) uses hexene and the British Petroleum process (BP) uses 4-methylpentene to produce high-performance copolymers [25]. The comonomer can be affected the overall crystallinity, melting point, softening range, transparency and also structural, thermochemical, and rheological properties of the formed polymer. Copolymers can also be used to enhance mechanical properties by improving the miscibility in polymer blending [26].

Ethylene is copolymerized with  $\alpha$ -olefin to produce polymers with lower densities. It is commonly observed that the addition of a comonomer generally increases the polymerization rate significantly. This comonomer effect is sometimes linked to the reduction of diffusion limitations by producing a lower crystallinity polymer or to the activation of catalytic sites by the comonomer. The polymer molecular weight often decreases with comonomer addition, possibly because of a transfer to comonomer reactions. Heterogeneous polymerization tends to be less sensitive to changes in the aluminum/transition metal ratio. Chain transfer to aluminum is also favored at high aluminum concentrations. This increase in chain transfer would presumably produce a lower molecular weight polymer. In addition, some researchers observed the decrease, and some observed no change in the molecular weight with increasing aluminum concentration [27].

The effect of polymerization conditions and molecular structure of the catalyst on ethylene/ $\alpha$ -olefin copolymerization have been investigated extensively. Pietikainen and Seppala [28] investigated the effect of polymerization temperature on catalyst activity and viscosity average molecular weights for low molecular weight ethylene/propylene copolymers produced with homogeneous  $\text{Cp}_2\text{ZrCl}_2$ . Soga and Kaminaka [29] compared copolymerizations (ethylene/propylene, ethylene/1-hexene, and propylene/1-hexene) with  $\text{Et}(\text{H}_4\text{Ind})_2\text{ZrCl}_2$  supported on  $\text{SiO}_2$ ,  $\text{Al}_2\text{O}_3$  or  $\text{MgCl}_2$ . Broadness of MWD was found to be related to the combination of support types and types of monomers. The effect of silica and magnesium supports on

copolymerization characteristics was also investigated by Nowlin *et al.* [30]. Their results indicated that comonomer incorporation was significantly affected by the way that support was treated based on the reactivity ratio estimation calculated with simplified Finemann Ross method. However, it should be noted that Finemann Ross method could be misleading due to linear estimation of nonlinear system.

Copolymer based on ethylene with different incorporation of 1-hexene, 1-octene, and 1-decene were investigated by Quijada [31]. The type and the concentration of the comonomer in the feed do not have a strong influence on the catalytic activity of the system, but the presence of the comonomer increases the activity compared with that in the absence of it. From  $^{13}\text{C}$ -NMR it was found that the size of the lateral chain influences the percentage of comonomer incorporated, 1-hexene being the highest one incorporated. The molecular weight of the copolymers obtained was found to be dependent on the comonomer concentration in the feed, showing that there is a transfer reaction with the comonomer. The polydispersity ( $M_w/M_n$ ) of the copolymers is rather narrow and dependent on the concentration of the comonomer incorporation.

Soga *et al.* [32] noted that some metallocene catalysts produce two-different types of copolymers in terms of crystallinity. They copolymerized ethylene and 1-alkenes using 6 different catalysts such as  $\text{Cp}_2\text{ZrCl}_2$ ,  $\text{Cp}_2\text{TiCl}_2$ ,  $\text{Cp}_2\text{HfCl}_2$ ,  $\text{Cp}_2\text{Zr}(\text{CH}_3)_2$ ,  $\text{Et}(\text{Ind H}_4)_2\text{ZrCl}_2$  and  $i\text{-Pr}(\text{Cp})(\text{Flu})\text{ZrCl}_2$ . Polymers with bimodal crystallinity distribution (as measured by TREF-GPC analysis) were produced with some catalytic systems. Only  $\text{Cp}_2\text{TiCl}_2\text{-MAO}$  and  $\text{Et}(\text{H}_4\text{Ind})_2\text{ZrCl}_2\text{-MAO}$  produced polymers that have unimodal crystallinity distribution. The results seem to indicate that more than one active site type are present in some of these catalysts. However, it is also possible that unsteady-state polymerization conditions might have caused the broad distributions since the polymerization times were very short (5 minutes for most cases).

Marques *et al.* [33] investigated copolymerization of ethylene and 1-octene by using the homogeneous catalyst system based on  $\text{Et}(\text{Flu})_2\text{ZrCl}_2/\text{MAO}$ . A study was performed to compare this system with that of  $\text{Cp}_2\text{ZrCl}_2/\text{MAO}$ . The influence of different support materials for the  $\text{Cp}_2\text{ZrCl}_2$  was also evaluated, using

silica,  $\text{MgCl}_2$ , and the zeolite sodic mordenite NaM. The copolymer produced by the  $\text{Et(Ind)}_2\text{ZrCl}_2/\text{MAO}$  system showed higher molecular weight and narrower molecular weight distribution, compared with that produced by  $\text{Cp}_2\text{ZrCl}_2/\text{MAO}$  system. Because of the extremely congested environment of the fluorenyl rings surrounding the transition metal, which hinders the beta hydrogen interaction, and therefore, the chain transference. Moreover, the most active catalyst was the one supported on  $\text{SiO}_2$ , whereas the zeolite sodic mordenite support resulted in a catalyst that produced copolymer with higher molecular weight and narrower molecular weight distribution. Both homogeneous catalytic systems showed the comonomer effect, considering that a significant increase was observed in the activity with the addition of a larger comonomer in the reaction medium.

The effect of different catalyst support treatments in the 1-hexene/ethylene copolymerization with supported metallocene catalyst was investigated by Soares *et al.* [34]. The catalysts in the study were supported catalysts containing  $\text{SiO}_2$ , commercial MAO supported on silica (SMAO) and MAO pretreated silica (MAO/silica) with  $\text{Cp}_2\text{HfCl}_2$ ,  $\text{Et(Ind)}_2\text{HfCl}_2$ ,  $\text{Cp}_2\text{ZrCl}_2$  and  $\text{Et(Ind)}_2\text{ZrCl}_2$ . All the investigated supported catalysts showed good activities for the ethylene polymerization (400-3000 kg polymer/mol metal.h). Non-bridged catalysts tend to produce polymers with higher molecular weight when supported on to SMAO and narrow polydispersity. The polymer produced with  $\text{Cp}_2\text{HfCl}_2$  supported on silica has only a single low crystallinity peak. On the other hand,  $\text{Cp}_2\text{HfCl}_2$  supported on SMAO and MAO/silica produced ethylene/1-hexene copolymers having bimodal CCDs. For the case of  $\text{Cp}_2\text{ZrCl}_2$  and  $\text{Et(Ind)}_2\text{ZrCl}_2$ , only unimodal CCDs were obtained. It seems that silica-MAO-metallocene and silica-metallocene site differ slightly in their ability to incorporate comonomer into the growing polymer chain, but not enough to form bimodals CCDs.

Soares *et al.* [35] studied copolymerization of ethylene and 1-hexene. It was carried out with different catalyst systems (homogeneous  $\text{Et(Ind)}_2\text{ZrCl}_2$ , supported  $\text{Et(Ind)}_2\text{ZrCl}_2$  and in-situ supported  $\text{Et(Ind)}_2\text{ZrCl}_2$ ). Supported  $\text{Et(Ind)}_2\text{ZrCl}_2$ : an  $\text{Et(Ind)}_2\text{ZrCl}_2$  solution was supported on SMAO. It was used for polymerization of ethylene and 1-hexene. In-situ supported  $\text{Et(Ind)}_2\text{ZrCl}_2$ : an  $\text{Et(Ind)}_2\text{ZrCl}_2$  solution was directly added to SMAO in the polymerization reactor, in

the absence of soluble MAO. Homogeneous  $\text{Et(Ind)}_2\text{ZrCl}_2$  showed higher catalytic activity than the corresponding supported and in-situ supported metallocene catalysts. The relative reactivity of 1-hexene increased in the following order: supported metallocene  $\approx$  in-situ supported metallocene  $<$  homogeneous metallocene catalysts. The MWD and short chain branching distribution (SCBD) of the copolymer made with the in-situ supported metallocene were broader than those made with homogeneous and supported metallocene catalysts. They concluded that there are at least two different active species on the in-situ supported metallocene catalyst for the copolymerization of ethylene and 1-hexene.

Soares *et al.* [36] investigated copolymerization of ethylene and 1-hexene with different catalysts: homogeneous  $\text{Et(Ind)}_2\text{ZrCl}_2$ ,  $\text{Cp}_2\text{HfCl}_2$  and  $[(\text{C}_5\text{Me}_4)\text{SiMe}_2\text{N(tert-Bu)}]\text{TiCl}_2$ , the corresponding in-situ supported metallocene and combined in-situ supported metallocene catalyst (mixture of  $\text{Et(Ind)}_2\text{ZrCl}_2$  and  $\text{Cp}_2\text{HfCl}_2$  and mixture of  $[(\text{C}_5\text{Me}_4)\text{SiMe}_2\text{N(tert-Bu)}]\text{TiCl}_2$ ). They studied properties of copolymers by using  $^{13}\text{C}$ -NMR, gel permeation chromatography (GPC) and crystallization analysis fractionation (CRYSTAF) and compared with the corresponding homogeneous metallocene. The in-situ supported metallocene produced polymers having different 1-hexene fractions, SCBD and MDW. It was also demonstrated that polymers with broader MWD and SCBD can be produced by combining two different in-situ supported metallocenes.

In addition, Soares *et al.* [37] studied copolymerization of ethylene and 1-hexene with an in-situ supported metallocene catalysts. Copolymer was produced with alkylaluminum activator and effect on MWD and SCBD was examined. They found that TMA exhibited the highest activity while TEA and TIBA had significantly lower activities. Molecular weight distributions of copolymers produced by using the different activator types were unimodal and narrow, however, short chain branching distributions were very different. Each activator exhibited unique comonomer incorporation characteristics that can produce bimodal SCBD with the use of a single activator. They used individual and mixed activator system for controlling the SCBDs of the resulting copolymers while maintaining narrow MWDs.

## 2.2 Heterogeneous System

The new metallocene/MAO systems offer more possibilities in olefin polymerization compared to conventional Ziegler-Natta catalysts, such as narrow stereoregularity, molecular weight and chemical composition distributions (CCDs) through ligand design. However, only heterogeneous catalysts can be practically used for the existing gas phase and slurry polymerization processes. Without using a heterogeneous system, high bulk density and narrow size distribution of polymer particles cannot be achieved. The advantages of supporting catalysts include improved morphology, less reactor fouling, lower Al/metal mole ratios required to obtain the maximum activities in some cases the elimination of the use of MAO, and improved stability of the catalyst due to much slower deactivation by bimolecular catalyst interactions. Therefore, developing heterogeneous metallocene catalysts, that still have all the advantages of homogeneous systems, became one of the main research objectives of applied metallocene catalysis.

Steinmetz *et al.* [38] examined the particle growth of polypropylene made with a supported metallocene catalyst using scanning electron microscopy (SEM). They noticed formation of a polymer layer only on the outer surface of catalyst particles during the initial induction period. As the polymerization continued, the whole particle was filled with polymer. Particle fragmentation pattern depended on the type of supported metallocene.

### 2.2.1. Catalyst Chemistry

The nature of the active sites affects the polymer morphology, catalyst stability and activity, and the characteristics of the polymer produced. However, structure and chemistry of the active sites in supported catalysts are not clearly understood. Catalytic activities for supported metallocene are usually much lower than that of their counterpart homogeneous system. Formation of different active species, deactivation of catalyst during supporting procedure, and mass transfer resistance may contribute to decreased catalyst activity.

Tait *et al.* [39] reported general effects of support type, treatment, supporting procedure, and type of diluents on reaction kinetics and physical properties of polymer produced. Although the activities of supported catalysts are much lower compared to homogeneous systems. The activity of catalysts increased slightly when *o*-dichlorobenzene was introduced in toluene

The catalytic activities of supported catalyst depended on the percentage of the incorporated metallocene was reported by Quijada *et al.* [40]. However, in the case of metallocenes supported on MAO pretreated silica, depending on how the surface bound MAO complex with the catalyst, the activity can be as high as that of homogeneous system. According to the experiment by Chein *et al.* [41], if a single MAO is attached to silica, it would complex with zirconocene and lowers its activity. On the other hand, if multiple MAOs are attached to the surface silanol, the supported zirconocene will not be further complexed with MAO and have activity.

### 2.2.2. Supporting Methods

In the case of carriers like silica or other inorganic compounds with OH group on the surface, the resulting catalyst displayed very poor activities even combined with MAO. The reaction of metallocene complexes with the Si-OH groups might cause the decomposition of active species. Such decomposition could be suppressed by fixing MAO on the silica surface and then reacting with metallocenes [42]. Therefore, silica must be pretreated before the interaction with metallocene, to reduce the OH concentration and to prepare an adequate surface for metallocene adsorption and reaction in a non-deactivating way [43]. Metallocene immobilization methods can be divided in to three main groups. The first method is the direct support of catalyst onto an inert support. The second method involves the pretreatment of the inert support with MAO or other alkylaluminum followed by metallocene supporting. The third method, the catalyst is chemically anchored to the support, which often involves in-situ catalyst synthesis. These methods produce catalysts with distinct activities, comonomer reactivity ratios, and stereospecificities.



### 2.3 Polymer nanocomposites

From the many previous study results, we observe that different composite systems can lead to very different results. One important observation is that composites with nano-sized inclusions generally have different properties than composites with larger scale inclusions [44]. The specific reasons why the polymer matrix composites with nano-sized reinforcement have different properties than composites with micron-sized reinforcement are not fully understood, but several theories have been introduced to explain some of the changes in material morphology and behavior that are seen at the nano-scale. It is important to point out, however, that most of these theories were developed to explain particular results and, therefore, are not necessarily applicable to a large number of polymer nanocomposites.

Chan et al. [45] proposed that properties such as elastic modulus, tensile strength, and yield strength decrease in nanocomposites with polypropylene matrix due to the change in nucleation caused by the nanoparticles (Fig.2.14). The nanoparticles produce a much larger number of nucleating sites but, in turn, greatly reduce the size of these spherulites. In their experimental work, no spherulites were found in the nanocomposites by SEM indicating that either none were present or they were reduced to such a small size that SEM could not detect them. It was further proposed that there was another mechanism which was causing these same properties to increase. The increase occurred when there was a strong interaction between the polymer and filler. This interaction had larger impact in nanocomposites due to the large interfacial area between the filler particles and the matrix.

Other investigators have suggested that this interaction leads to a layer of polymer that is directly adsorbed and bound to the particles [46,47,48,49]. Experimental work that has been performed on a polystyrene-cobalt nanocomposite with cobalt nanoparticles with an average size of 21 nm has shown that the polymer layer was about 24 nm, and varied non-linearly with molecular weight [50].

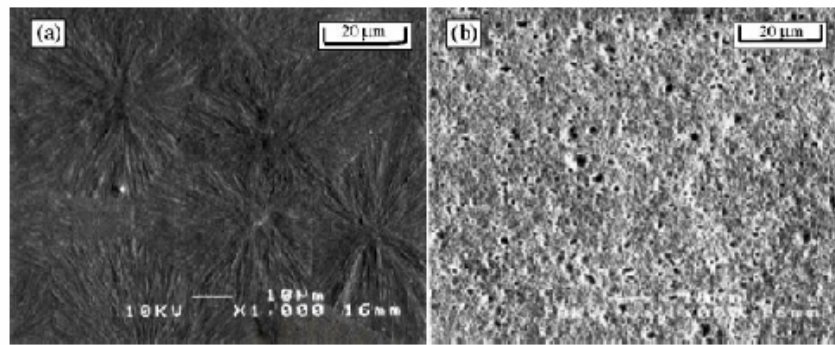


**Figure 2.14** (a) Pure polypropylene (b) polypropylene with 9.2% volume filler [45].

An increase in yield and tensile strength and modulus in nanocomposite systems as compared to microcomposites can be partially explained on the basis of the interaction between the filler and the matrix. It has been found that a greater adhesion between the matrix and inclusion causes less debonding when a stress is applied and, consequently the elastic modulus and strength are improved [51].

Vollenberg and Heikens [46] explained that if there is a strong interaction between the polymer and the particle, the polymer layer in the immediate proximity of the particle will have a higher density. For most systems, density is proportional to elastic modulus, so the region directly surrounding the inclusions will be a region of high modulus. The polymer right outside this high modulus region will have a lower density due to the polymer chains that are moved towards the particle. For large particles, the size of the low density region will be relatively large, and the contribution of the high modulus filler will be diminished. For nanoparticles, the number of particles for a given volume fraction is much larger, thus the particles will be much closer to one another. If the particles are densely packed, then the boundary layer of polymer at the interface will comprise a large percentage of the matrix and can create a system where there is no space for a low modulus region to form. This results in the elastic modulus of composites with smaller particle size (nano) being greater than the modulus of composites with larger inclusions [46,47].

The small interparticle distance in nanocomposites was used as another parameter to explain the changes in the elastic modulus and strength of these materials when compared with the composites with micron-sized particles. The same

parameter also plays a role in the glass transition temperature changes observed in nanocomposites versus composites with micron-sized reinforcement. Ash et al. [49] found that for their system the glass transition temperature was constant until around 0.5% weight fraction of particles, then had a sharp drop, and then it remained constant for weight fractions above 1%. When there is little or no interfacial interaction between the filler and matrix and the interparticle distance is small enough, the polymer between two particles acts as a thin film. For a thin film, the glass transition temperature decreases as film thickness decreases. The distance between particles in a composite with the filler weight fraction below 0.5% is relatively large, and hence, in this case the polymer between each particle is not considered to belong to the thin film regime. As the filler concentration increases, the interparticle distance and the resulting thickness of the film, decrease. This theory, however, does not explain why the glass transition temperature levels off rather than continues to drop as a function of increasing weight fraction of the filler. A drop-off in Young's modulus was found for the same filler weight fraction as the drop in glass transition temperature. It was proposed that as the glass transition temperature decreased, the relative testing temperature increased. Also, the elastic modulus of the matrix, PMMA, decreases as temperature increases, so the drop in glass transition temperature is correlated with the drop in modulus [48,49].

Reynaud et al. [52] found that during tensile testing, the volume of polymer nanocomposites increased, with the greatest increase occurring in systems with the smallest particles. To explain this, the debonding process of the polymer next to the inclusions was examined, as shown in Fig. 2.15. It was proposed that the smallest particles tend to aggregate and debonding occurs around each individual particle. As a result, the large clusters of small particles act as larger soft particles. On the other hand, the larger filler particles do not aggregate and each particle undergoes a single debonding process.

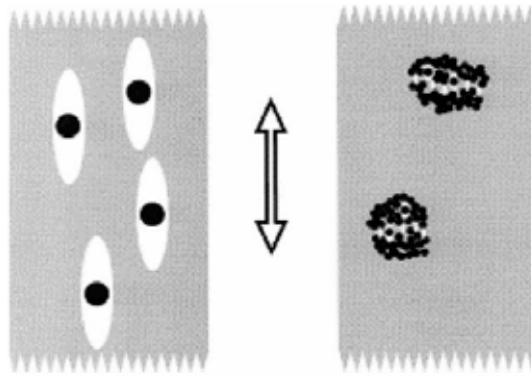


**Figure 2.15** Debonding around 50 and 12 nm particle [52].

Due to the different results obtained and the different nature of the various polymer nanocomposite systems, there is no observed universal trend that can be modeled and explained.

There are, however, observations that show the behavior of nanocomposites different from composites with larger scale inclusions. The particle size and the polymer and particle morphology tend to play a very important role. In addition, the nature of dispersion and aggregation of particles can affect the properties of composites significantly. Filler–matrix interaction is another factor that influences the properties. The strength of the interaction plays a role in the thickness and density of the interphase, which consists of a layer of high density polymer around the particle. The effects of the interface on the behavior of a composite depend upon the interparticle distance. For constant filler content, with reduction in particle size, number of filler particles increases, bringing the particles closer to one another. Thus, the interface layers from adjacent particles overlap, altering the bulk properties significantly. These issues play a major role in the effect of nano-sized inclusions in a polymer matrix. For nanoparticles, any configuration changes in the matrix will have a significant effect when the characteristic radius of polymer chains is of the same order as the inclusions [51,53]. There are other areas addressed in literature.

For example, L’opez et al. [54] examined the processing and thermal and mechanical properties of magnetic nanocomposites. In another work the mechanical properties of clay nanocomposites were analyzed as a function of filler loading and orientation [55]. Zhang et al. [56] provided a look at matrix–filler interfacial

properties. Effect of matrix on the polymer matrix composites were examined by Friedlander et al. [57].

#### **2.4 Linear low density polyethylene (LLDPE) nanocomposites**

Although the high amount of nanocomposite researches have done, there still have the low amount of them relating to LLDPE. The adequately experimental made by some researchers include here.

Hotta and Paul [58] studied L-clay nanocomposites. It was prepared by melt compounding various combinations of a maleic anhydride grafted linear low density polyethylene (LLDPE-g-MA), a linear low density polyethylene (LLDPE), and two organoclays. The two types of organoclay were selected to show the effect of the number of alkyl groups attached to the nitrogen of the organic modifier on exfoliation and improvement of mechanical properties. Nanocomposites derived from the organoclay having two alkyl tails, M2(HT)2, exhibited better dispersion and improvement of mechanical properties than nanocomposites based on the organoclay having one alkyl tail M3(HT)1. This result is the opposite of what is observed for nylon-6 nanocomposites. In addition, the rheological properties and gas permeability of the nanocomposites derived from the organoclay having two alkyl tails, M2(HT)2 were investigated. Both melt viscosity and melt tension (melt strength) increased with increased content of clay (MMT) and LLDPE-g-MA. Gas permeability was decreased by the addition of MMT.

Ki Hyun Wang et al. [59] studied maleic anhydride grafted polyethylene (maleated polyethylene)/clay nanocomposites prepared by simple melt compounding. The exfoliation and intercalation behaviors depended on the hydrophilicity of polyethylene grafted with maleic anhydride and the chain length of organic modifier in the clay. When the number of methylene groups in alkylamine (organic modifier) was larger than 16, the exfoliated nanocomposite was obtained, and the maleic anhydride grafting level was higher than about 0.1 wt% for the exfoliated nanocomposite with the clay modified with dimethyl dihydrogenated tallow ammonium ion or octadecylammonium ion. The pure LLDPE showed only the intercalation, which does not depend on the initial spacing between clay layers.

Lew et al. [60] studied LLDPE-organoclay nanocomposites containing a synthetic tetrasilic fluoromica prepared from metallocene-catalyzed and conventional Ziegler-Natta-catalyzed linear low-density polyethylenes (LLDPE) by means of melt-compounding. The effects of maleic-anhydride grafted compatibilizer (PE-g-MA) level, clay concentration, and blending procedure were investigated and compared. Morphology and structural analysis using transmission electron microscopy (TEM) and X-ray diffraction (XRD) suggested the clay exfoliation was more intense in the metallocene LLDPE matrix, conceivably because of the controlled short-chain branching and viscosity effects. When exfoliated, these silicate sheets were shown to restrict the lamellar crystallization, as seen by the decrease in crystallinity using differential scanning calorimetry analysis (DSC). The dynamic mechanical thermal analysis (DMTA) study suggested that the three  $\alpha$ ,  $\beta$  and  $\gamma$  -relaxations of the LLDPE were affected by polymer chain branching and clay exfoliation level.

Sometime LLDPE was used as a form of blending polymer to investigate the properties of nanocomposites. Tsu-Hwang Chuang et al. [61] blended ethylene-vinyl acetate copolymer (EVA)/montmorillonite (MMT) composite with a linear low density polyethylene (LLDPE). X-ray diffraction and transmission electron microscopy (TEM) image of the EVA/MMT composite are in support of an intercalated with partially delaminated nanocomposite. The tensile strength of the nanocomposite is about 20% higher than that without layered silicates, MMT. Furthermore, the incorporation of MMT into polymer blend delays the main thermo-oxidative degradation. Cone calorimeter test points out that the addition of layered silicates into the pristine EVA/LLDPE blend or the blend with a low smoke non-halogen (LSNH) fire retardants, aluminum trihydroxide, and antimony trioxide, can reduce the maximum heat release rate by 30–40%. The smoke suppressing effect of layered silicates is only observed in the nanocomposite containing flame retardants. According to the limiting oxygen index (LOI) data and cone calorimeter test, the addition of the nanodispersed layered silicate and LSNH flame retardants to the EVA/LLDPE exhibits a synergistic effect on the flame retardancy and smoke suppression.

## 2.5 Silica nanocomposites

In heterogeneous polymerization research field, many inorganic support such as  $\text{SiO}_2$ ,  $\text{Al}_2\text{O}_3$  and  $\text{MgCl}_2$  have been investigated. It was reported that  $\text{SiO}_2$  is perhaps the most attractive support so far. Beside be the excellent support, silica also be claimed to be the excellent filler in the polymer composites. Hence when talking about the study of nanocomposites, silica is usually the first filler that the most of researchers thinking of. To fill the silica into polymer matrix, melting method and solution mixing method is more favor than in situ polymerization in the present time. However the in situ polymerization was found to be the promising method.

Fayna Mammeri et al [62] investigated thin film from in situ polymerization of tetraethoxysilane in poly(methyl methacrylate). The sol-gel process allows to design hybrid organic-inorganic materials constituted by organic molecules or macromolecules and inorganic metal oxo-polymers interpenetrated at the nanometer scale. These hybrids were deposited as functional coatings with tunable thickness on float glass substrates. Good adhesion and mechanical behaviour of the coatings are required to keep their functionality in time hence; the performance of the PMMA- $\text{SiO}_2$  based thin films was investigated using nanoindentation. This study validates nanoindentation measurements as an appropriate technique to characterize hybrid organic-inorganic thin films, despite visco-elastic behaviours. Specific analysis procedures and the use of appropriate models allowed us to determine the indentation modulus and hardness of the hybrid layers reproductively. The structure and the mechanical behaviour are reported for thin films as a function of the fraction of silica.

Liu et al [63] prepared poly(ethylene oxide)- $\text{SiO}_2$  composite polymer electrolytes by in situ method. Amorphous poly(ethylene oxide) (PEO)- $\text{SiO}_2$  composites are prepared by in situ reactions that involve the simultaneous formation of the polymer network and inorganic nanoparticles. The polymer matrix is formed by ultraviolet irradiation of a PEO macromer, and silica is produced in situ by the sol-gel method. The PEO- $\text{SiO}_2$  composite mixed with  $\text{LiBF}_4$  is used as a lithium-ion

conducting solid electrolyte and electrochemical transport properties such as ionic conductivity and  $\text{Li}^+$  transference number are measured. A significant increase in the  $\text{Li}^+$  transference number, up to 0.56, is found together with a slight decrease in the ionic conductivity. The results are interpreted in terms of interactions between the surface OH groups of the inorganic particles, the cations, the anions, and the ether oxygen atoms on the PEO backbone.

Feng-Xian Qiu et al.[64]. studied the synthesis and characteristic of 6FDA-6FHP-NLO polyimide/ $\text{SiO}_2$  nanohybrid materials. Hybrid nanocomposite films of silica ( $\text{SiO}_2$ ) in polyimide (PI) from 4,4'-(hexafluoroisopropylidene) diphthalic anhydride (6FDA), 2,2-Bis (3-amino-4-hydroxyphenyl) hexafluoropropane (6FHP) and nonlinear optical (NLO) molecule have been successfully fabricated by an in situ sol-gel process. The silica content in the hybrid films was varied from 0 to 22.5 wt%. These nanocomposite films exhibit fair good optical transparency. Fourier transform infrared (FTIR) spectroscopy results confirm the formation of  $\text{SiO}_2$  particles in PI matrix. Scanning electron microscope (SEM) images show that the  $\text{SiO}_2$  phase is well dispersed in the polymer matrix. Their glass transition behavior and thermal stability were investigated by differential scanning calorimeter (DSC) and thermal gravimetric analysis (TG).

Papageorgiou et al. [65] studied Crystallization kinetics and nucleation activity of filler in polypropylene/surface-treated  $\text{SiO}_2$  nanocomposites. Isothermal and non-isothermal crystallization kinetics of polypropylene (PP)/surface-treated  $\text{SiO}_2$  nanocomposites were extensively studied. Analysis of the isothermal crystallization showed that the phenomenon is characterized by faster rates as the amount of silica is increased. In the case of non-isothermal crystallization, it was found that the Ozawa analysis was rather inapplicable for the nanocomposites. In contrast, the modified Avrami method, as well as the method proposed by Mo was applied giving satisfactory results. The effective energy barrier for non-isothermal crystallization was estimated as a function of the relative degree of crystallinity using the isoconversional analysis of calorimetric data. This was found to vary with the degree of conversion, as well as with the presence of filler. Finally, the nucleation activity of the silica



nanoparticles on the polymer matrix was explored and it was proved that when the content of filler exceeds 7.5 wt.% the nucleation is not drastically improved.



สถาบันวิทยบริการ  
จุฬาลงกรณ์มหาวิทยาลัย

## CHAPTER III

### EXPERIMENTAL

In the present study of LLDPE-SiO<sub>2</sub> nanocomposite synthesized via in situ polymerization with zirconocene/MAO catalyst was investigated. The experiments were divided into four parts:

- (i) Preparation of nano-SiO<sub>2</sub> by sol-gel method
- (ii) Preparation of catalyst precursor nano-SiO<sub>2</sub>/MAO
- (iii) Ethylene and hexene copolymerization Procedure
- (iv) Characterization of nano-SiO<sub>2</sub> , catalyst precursor nano-SiO<sub>2</sub>/MAO and ethylene and hexene copolymer products

The details of the experiments are explained as follows.

#### 3.1 Chemicals

The chemicals used in these experiments were analytical grade, but only major materials are specified as follows:

1. rac-Ethylenebis(indenyl)zirconium dichloride (Et(Ind)<sub>2</sub>ZrCl<sub>2</sub>) was supplied from Aldrich Chemical Company, Inc. and used without further purification.

2. Ethylene gas (99.96%) was devoted from National Petrochemical Co., Ltd., Thailand and used as received.

3. 1-Hexene (99+%) was purchased from Aldrich Chemical Company, Inc. and purified by distilling over sodium under argon atmosphere before use.

4. Methylaluminoxane (MAO) 2.667 M in toluene was donated from Tosoh Akso, Japan and used without further purification.

5. Trimethylaluminum [Al(CH<sub>3</sub>)<sub>3</sub>] 2.0 M in toluene was supplied from Nippon Aluminum Alkyls Ltd., Japan and used without further purification.

6. Triethyl ortho silicated (TEOS).

7. Silica nanopowder, 10 nm, 99.5% from Sigma-Aldrich (surface area 590-690 m<sup>2</sup>/g) was calcined at 400 °C for 6 hours under vacuum.

8. Silica nanopowder, 15 nm, 99.5% from Sigma-Aldrich (surface area 140-180 m<sup>2</sup>/g) was calcined at 400 °C for 6 hours under vacuum.

9. Hydrochloric acid (Fuming 36.7%) was supplied from Sigma.

10. Methanol (Commercial grade) was purchased from SR lab.

11. Toluene was devolved from EXXON Chemical Ltd., Thailand. This solvent was dried over dehydrated CaCl<sub>2</sub> and distilled over sodium/benzophenone under argon atmosphere before use.

12. Ultra high purity argon gas (99.999%) was purchased from Thai Industrial Gas Co., Ltd., and further purified by passing through columns packed with molecular sieve 3 A, BASF Catalyst R3-11G, sodium hydroxide (NaOH) and phosphorus pentoxide (P<sub>2</sub>O<sub>5</sub>) to remove traces of oxygen and moisture.

### **3.2 Equipments**

All types of equipments used in the catalyst precursor preparation and polymerization are listed below:

#### **3.2.1 Cooling system**

The cooling system was in the solvent distillation in order to condense the freshly evaporated solvent.

#### **3.2.2 Inert gas supply**

The inert gas (argon) was passed through columns of BASF catalyst R3-11G as oxygen scavenger, molecular sieve  $3 \times 10^{-10}$  m to remove moisture. The BASF catalyst was regenerated by treatment with hydrogen at 300 °C overnight before flowing the argon gas through all the above columns. The inert gas supply system is shown in Figure 3.1.

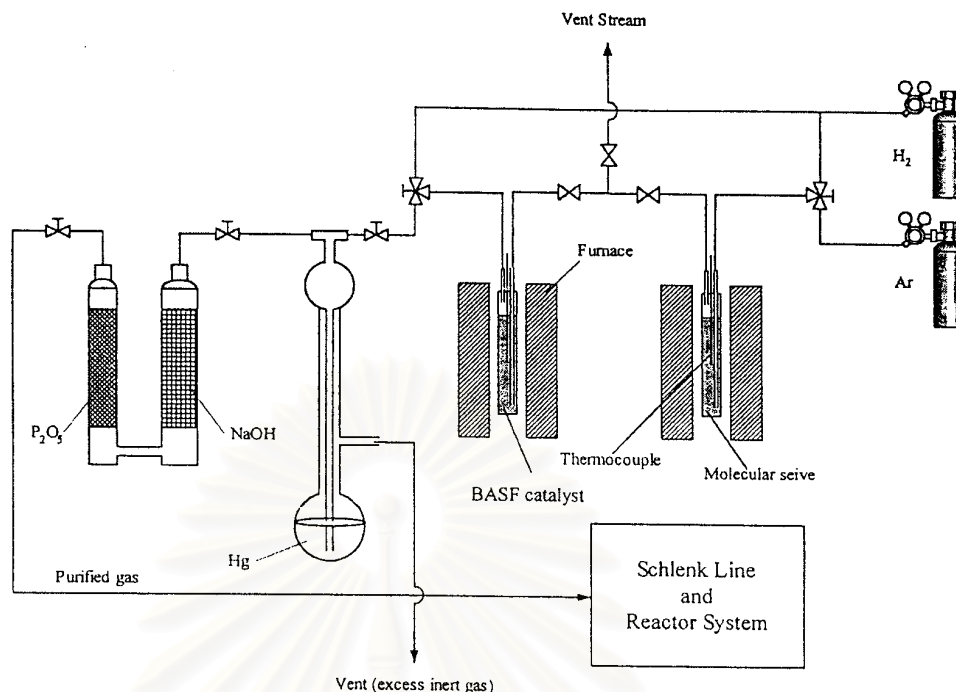


**Figure 3.1** Inert gas supply system

### 3.2.3 Magnetic stirrer and heater

The magnetic stirrer and heater model RTC basis from IKA Labortechnik were used.

### 3.2.4 Reactor

A 100 ml stainless steel autoclave was used as the copolymerization reactor.

### 3.2.5 Schlenk line

Schlenk line consists of vacuum and argon lines. The vacuum line was equipped with the solvent trap and vacuum pump, respectively. The argon line was connected with the trap and the mercury bubbler that was a manometer tube and contain enough mercury to provide a seal from the atmosphere when argon line was evacuated. The Schlenk line was shown in Figure 3.2.

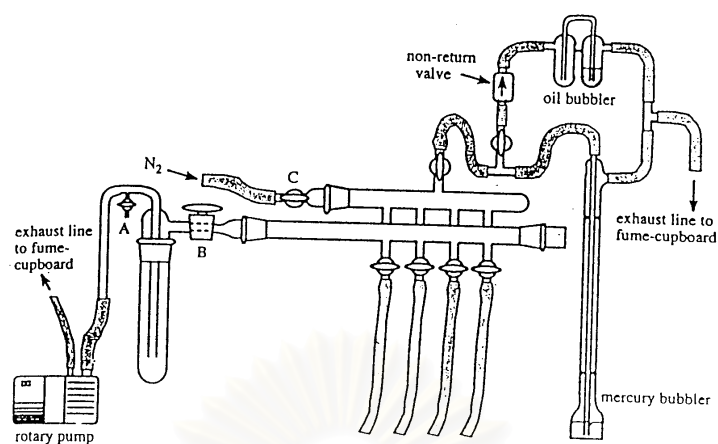


**Figure 3.2** Schlenk line

### 3.2.6 Schlenk tube

A tube with a ground glass joint and side arm, which was three-way glass valve as shown in Figure 3.3. Sizes of Schlenk tubes were 50, 100 and 200 ml used to prepare catalyst and store materials which were sensitive to oxygen and moisture.

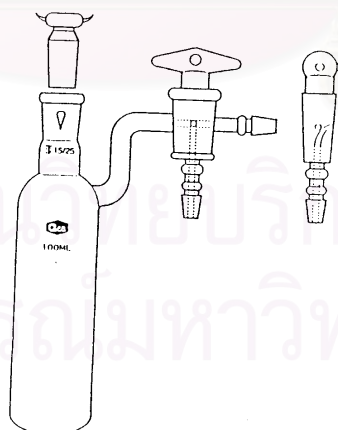


**Figure 3.3** Schlenk tube

### 3.2.7 Vacuum pump

The vacuum pump model 195 from Labconco Corporation was used. A pressure of  $10^{-1}$  to  $10^{-3}$  mmHg was adequate for the vacuum supply to the vacuum line in the Schlenk line.

### 3.2.8 Polymerization line

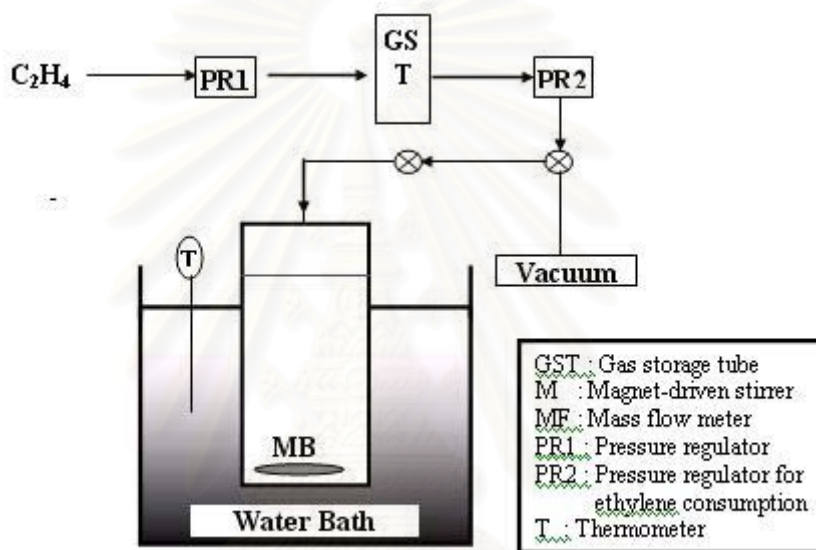


**Figure 3.4** diagram of system in slurry phase polymerization

## 3.3 Characterizing instruments

The instruments used for characterizing catalysts and ethylene/ $\alpha$ -olefin copolymer products are specified below.

### 3.3.1 Differential scanning calorimetry (DSC)

The melting temperature of ethylene/ $\alpha$ -olefin copolymer products was determined with a Perkin-Elmer diamond DSC from MEKTEC, at the Center of Excellence on Catalysis and Catalytic Reaction Engineering, Department of Chemical Engineering, Chulalongkorn University. The analyses were performed at the heating

rate of 20 °C/ min in the temperature range of 50-150 °C. The heating cycle was run twice. In the first scan, samples were heated and the cooled to room temperature. In the second, samples were reheated at the same rate, but only the results of the second scan were reported because the first scan was influenced by the mechanical and thermal history of samples.

### **3.3.2 Nuclear magnetic resonance (NMR)**

The  $^{13}\text{C}$ -NMR spectra were recorded at 100°C using JEOL JNM-A500 operating at 125 MHz. Copolymer solutions were prepared using 1,2 - dichlorobenzene as solvent and benzene- $\text{d}_6$  for internal lock.

### **3.3.3 Scanning electron microscope (SEM) and energy dispersive X-ray spectroscopy (EDX)**

SEM observation with a JSM-5800 LV Scanning Microscope, Microspec WDX at Scientific Technological Research Equipment Center, Chulalongkorn University was employed to investigate the morphology of catalyst precursor and polymer. The polymer samples for SEM analysis were coated with gold particles by ion sputtering device to provide electrical contact to the specimen. EDX was performed using Link Isis series 300 program.

### **3.3.4 X-ray diffraction (XRD)**

XRD was performed to determine the bulk crystalline phases of sample. It was conducted using a SIEMENS D-5000 X-ray diffractometer with  $\text{CuK}_\alpha$  ( $\lambda = 1.54439 \times 10^{-10}$  m). The spectra were scanned at a rate 2.4 degree/min in the range  $2\theta = 20$ -80 degrees.

### **3.3.5 Transmission Electron Microscopy (TEM)**

Transmission Electron Microscopy (TEM) was used to determine the distribution of nano- $\text{SiO}_2$  within polymer matrix. The sample was dispersed in ethanol before using TEM (JEOL JEM-2010) for microstructural characterizations.

### 3.4 Preparation of fillers.

All reactions were conducted under argon atmosphere using Schlenk techniques and glove box

#### 3.4.1 Preparation of nano- SiO<sub>2</sub>

The nano-SiO<sub>2</sub> filled materials were synthesized using sol-gel method [66] to obtain the nano-SiO<sub>2</sub> with particle size of ca. 50 nm.

#### 3.4.2 Impregnation

In order to impregnate MAO onto the nano-materials used the method as follows was described. First, 1 g of the nano-materials (sol-gel silica or commercial nanopowder silica) was reacted with the desired amount of MAO at room temperature and stirred for 30 min. The solvent was then removed from the mixture. About 20 ml of toluene was added into the obtained precipitate, stirred the mixture for 5 min, and then removed the solvent. This procedure was done for 5 times to ensure the removal of impurities. Then, the solid part was dried under vacuum at room temperature to obtain white powder of nano-materials/ MAO.

### 3.5 Ethylen and hexene Copolymerization Procedure

Polymerization was conducted upon the methods as follows. The ethylene /1-hexene copolymerization reaction was carried out in a 100 ml semi-batch stainless steel autoclave reactor equipped with a magnetic stirrer. At first, 0.1, 0.2, and 0.3 g of the nano-materials/MAO ( $[Al]_{MAO}/[Zr] = 1135$ ) and 0.018 mole of 1-hexene along with toluene (to make the total volume of 30 ml) were put into the reactor. The desired amount of Et(Ind)<sub>2</sub>ZrCl<sub>2</sub> ( $5 \times 10^{-5}$  M) and TMA ( $[Al]_{TMA}/[Zr] = 2500$ ) was mixed and stirred for 5-min aging at room temperature, separately, then was injected into the reactor. The reactor was frozen in liquid nitrogen to stop reaction for 15 min and then the reactor was evacuated to remove argon. The reactor was heated up to polymerization temperature (70°C). To start reaction, 0.018 mole of ethylene was fed into the reactor containing the comonomer and catalyst mixtures. After all ethylene was consumed, the reaction was terminated by addition of acidic methanol (0.1% HCl

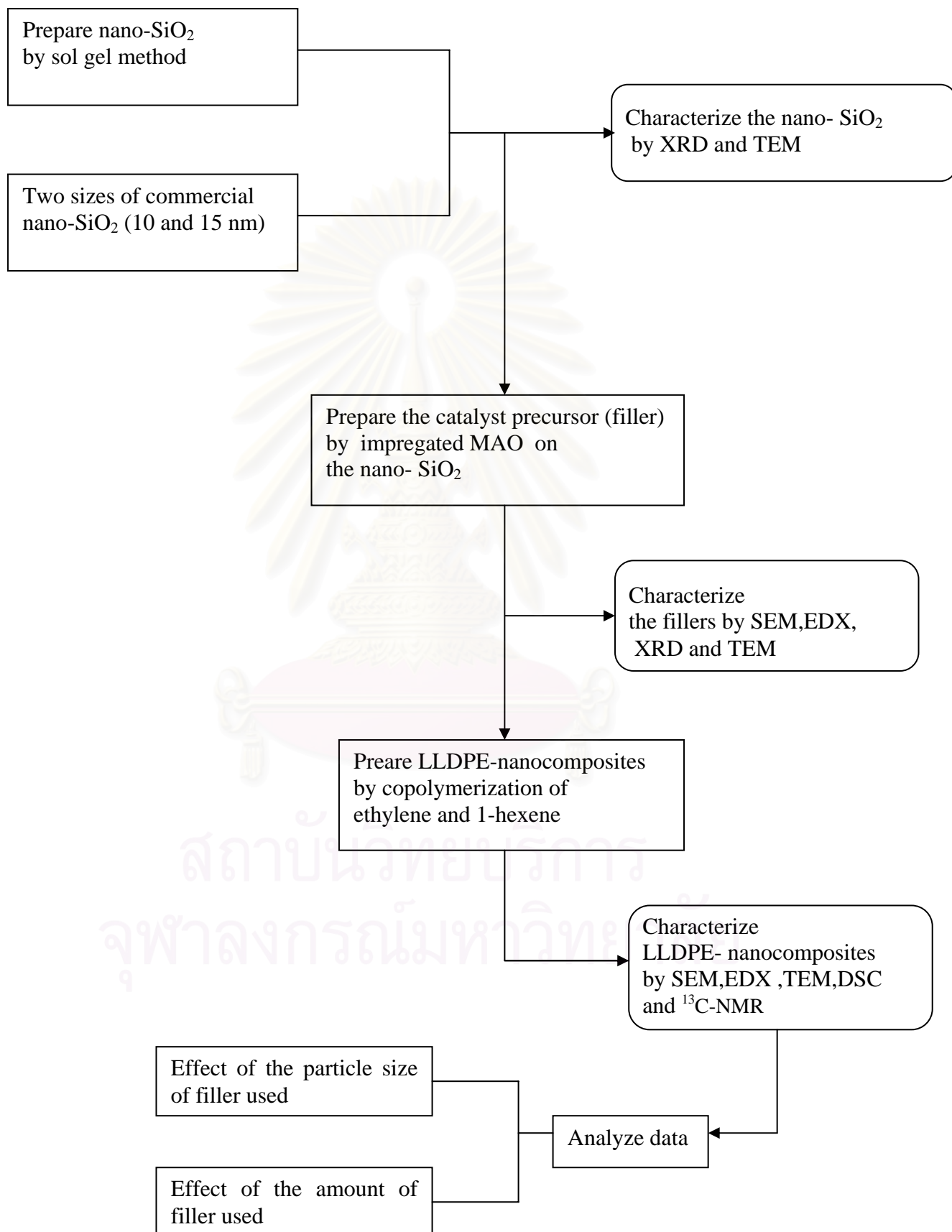


in methanol) and stirred for 30 min. After filtration, the obtained copolymer (white powder) was washed with methanol and dried at room temperature.

The various effects on the ethylene/1-hexene copolymerization with silica-supported metallocene catalyst and optimized condition were investigated. The effects of copolymerization on production of ethylene/1-hexene copolymer were systematically varied as follow in the next page.



สถาบันวิทยบริการ  
จุฬาลงกรณ์มหาวิทยาลัย

**Research Methodology**

### 3.6 Characterization

#### 3.6.1 Nano-SiO<sub>2</sub>

- Crystallinity

X-ray diffraction (XRD) was performed to determine the bulk crystalline phases of each nano-SiO<sub>2</sub> sample.

- The distribution of particle

Transmission electron microscope (TEM) was performed to determine the distribution and agglomeration of nano-material particle before they were impregnated with MAO .

#### 3.6.2 Catalyst precursor nano- SiO<sub>2</sub>/MAO

- Morphology

Scanning electron microscopic (SEM) technique was the effective method to investigate catalyst precursor morphologies. The term of morphology was referred to shape, texture or form of catalyst precursor.

- The distribution of particle

Transmission electron microscope (TEM) was performed to determine the distribution and agglomeration of filler particle before they were in the polymer matrix after copolymerization procedure.

#### 3.6.3 LLDPE-nanocomposites

- Morphology

The morphology of LLDPE-nanocomposites obtained was observed with scanning electron microscopy (SEM).

- Melting temperature ( $T_m$ )

Differential scanning calorimetry (DSC) was an instrument designed to measure the thermal properties especially melting temperature ( $T_m$ ). The melting

temperature of LLDPE-nanocomposites were determined from the critical point of DSC curve.

- Microstructure

$^{13}\text{C}$ -NMR spectroscopy was widely used to determine comonomer incorporation and polymer structure. Comparison of the positions of peak in the  $^{13}\text{C}$ -NMR spectrum of polymer sample with characteristic led to identification of the sequence of the comonomer incorporation.

- The distribution of particle

Energy-dispersive X-ray Spectrometer (EDX) and Transmission Electron Microscopy (TEM) were used to determined the distribution and agglomeration of nano-SiO<sub>2</sub> within polymer matrix.



สถาบันวิทยบริการ  
จุฬาลงกรณ์มหาวิทยาลัย

## CHAPTER IV

### RESULTS AND DISCUSSIONS

In this present study, results and discussion were divided into two parts. In the first portion, the study of the activities and characteristics of LLDPE/nanocomposite with using sol-gel silica as a filler was obtained. The second portion was based on the study of first portion, but a filler was replaced by the commercial nanopowder silica with two different sizes (10 and 15 nm). Thus, the particle size effect was then reported. In addition, the effect of the amounts of nano-SiO<sub>2</sub> when the ratio of [Al]<sub>MAO</sub>/[Zr] was fixed at 2270 was also reported in this study.

#### **4.1 Sol-gel silica as a filler of LLDPE-SiO<sub>2</sub> nanocomposite synthesized via *in situ* polymerization with zirconocene/MAO catalyst.**

##### **4.1.1 Characterization of fillers with X-ray diffraction (XRD)**

Pure silica and silica doped alumina prepared by sol-gel method and then were characterized by X-ray diffraction (XRD), the XRD patterns are shown in Figure 4.1. It was found that XRD patterns for both materials exhibited similar patterns assigning to amorphous silica. No XRD peaks of Al<sub>2</sub>O<sub>3</sub> were detected indicating highly dispersed forms of its.

สถาบันวิทยบริการ  
จุฬาลงกรณ์มหาวิทยาลัย

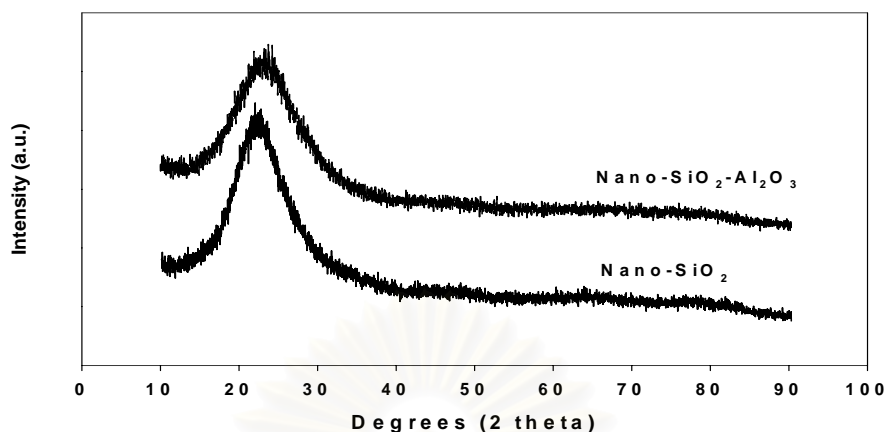


**Figure 4.1** XRD patterns of nano-SiO<sub>2</sub> and nano-SiO<sub>2</sub>-Al<sub>2</sub>O<sub>3</sub>

#### 4.1.2 Effect of the amount of filler on catalytic activity.

After impregnation of MAO onto the nano-SiO<sub>2</sub>, copolymerization of ethylene/1-hexene was performed with various conditions based on changing types and/or amounts of the nano-SiO<sub>2</sub> (SiO<sub>2</sub>-Al<sub>2</sub>O<sub>3</sub>) used. Activities and yields of LLDPE/nano-composites are shown in Table 4.1. It was observed that activities and yields dramatically increased with increasing the amounts of silica (SiO<sub>2</sub>) particles used due to increased MAO as a cocatalyst. However, at the same amount (0.1 g) of particles, the SiO<sub>2</sub>-Al<sub>2</sub>O<sub>3</sub> exhibited the lowest yield and activity of any other samples. A comparison of activities is also shown in Figure 4.2. It should be noted that activities of LLDPE/nano-SiO<sub>2</sub> composites obtained in this present study were much lower (about 3 times) compared to the LLDPE/micron-SiO<sub>2</sub> composite as reported by Jongsomjit *et al* [67]. This was probably due to more steric hindrance arising from the nano-particles.

**Table 4.1** Activity and yield of LLDPE/nano-composites via *in situ* polymerization with metallocene catalyst.

Filler	Weight (g)	Polymer yield (g)	Time (s)	Activity <sup>a</sup>	%SiO <sub>2</sub> <sup>b</sup>
SiO <sub>2</sub>	0.1	0.1147	360	882	46.58
	0.2	0.4070	318	3544	32.95
	0.3	0.5382	315	4731	35.79
SiO <sub>2</sub> -Al <sub>2</sub> O <sub>3</sub>	0.1	0.1006	450	619	49.85

<sup>a</sup> Activities (kg of polym/mol of Zr.h) were measured at polymerization temperature of 70°C, [ethylene] = 0.018 mole, [1-hexene] = 0.018 mole, [Al]<sub>MAO</sub>/[Zr] = 1135 to 3405, [Al]<sub>TMA</sub>/[Zr] = 2500, in toluene with total volume = 30 ml and [Zr] = 5 x 10<sup>-5</sup> M.

<sup>b</sup> The amount of SiO<sub>2</sub> present in the LLDPE composites based on yield

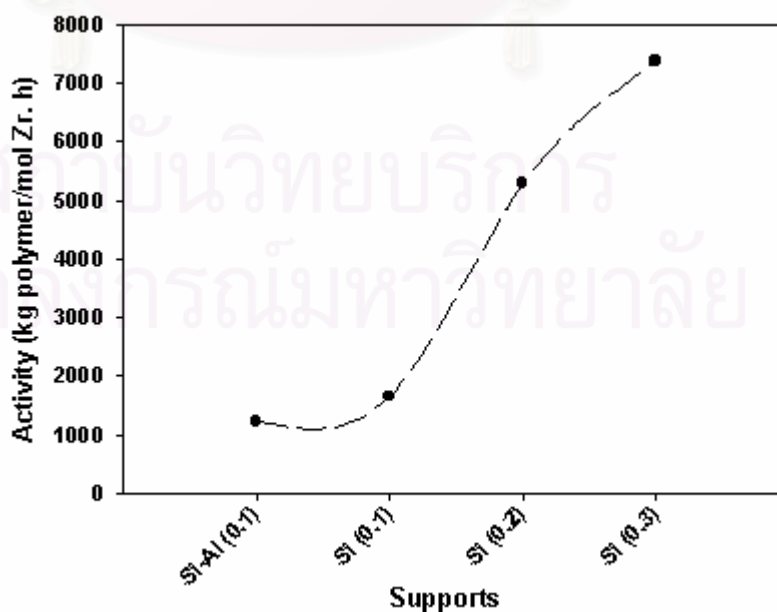
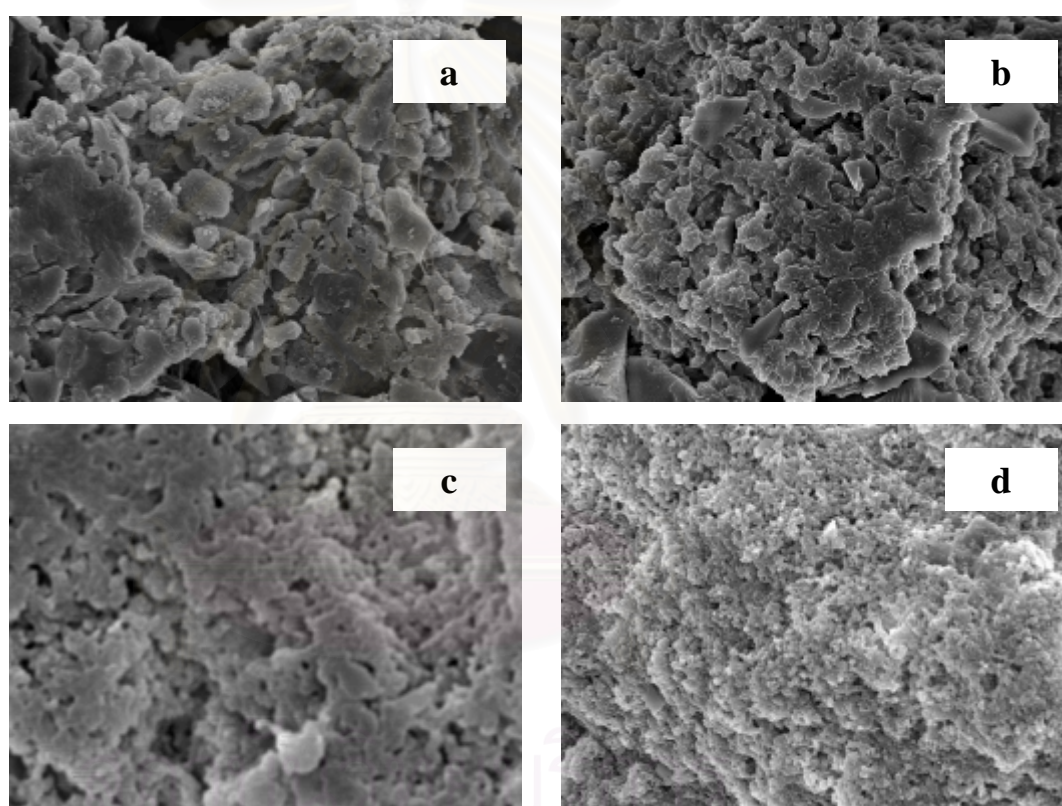


**Figure 4.2** Activity profile with various amounts of support used.

#### 4.1.3 The effect of nano-silica on the morphologies of LLDPE-nanocomposites.

Morphologies of LLDPE/nano composites are shown in Figure 4.3. It can be observed that with using  $\text{SiO}_2\text{-Al}_2\text{O}_3$  (0.1 g),  $\text{SiO}_2$  (0.1 g), and  $\text{SiO}_2$  (0.2 g), morphologies [Figure 4.3 (a) to (c)] were found to be similar indicating only the polymer texture as seen in ref. [8]. However, with increasing the amount of nano- $\text{SiO}_2$  to 0.3 g, the morphology as shown in Figure 4.3 (d) was significant changed indicating better combination between the silica and polymer textures. This was suggested that the LLDPE/nano- $\text{SiO}_2$  composite can be obtained at a certain amount of the nano- $\text{SiO}_2$  particles used.



x 1500

**Figure 4.3** Morphologies of LLDPE/nano composites with ; (a)  $\text{SiO}_2\text{-Al}_2\text{O}_3$  (0.1 g), (b)  $\text{SiO}_2$  (0.1 g), (c)  $\text{SiO}_2$  (0.2 g), and (d)  $\text{SiO}_2$  (0.3 g)



#### 4.1.4 The distribution of nano- SiO<sub>2</sub> in LLDPE-nanocomposites.

In order to identify the distribution of SiO<sub>2</sub> particles in the polymer matrix, EDX mapping was performed on the distribution of Si and O elements as shown in Figure 4.4. It can be observed that Si and O elements exhibited good distribution all over the polymer matrix.

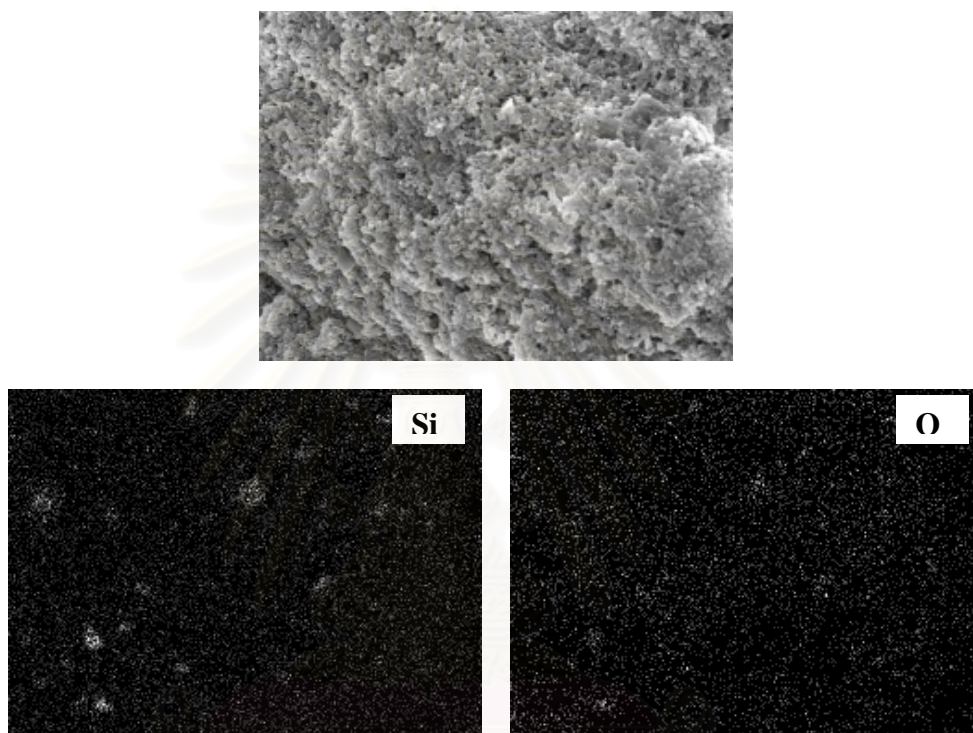


**Figure 4.4** .EDX mapping of LLDPE/nano-SiO<sub>2</sub> composite with SiO<sub>2</sub> (0.3 g) indicating distribution of Si and O.

In this part, we can prove that the nano-SiO<sub>2</sub> had the ability to use as the filler in the process of polymerization. Although its activity was lower than that of conventional SiO<sub>2</sub> (microscale), we still can not conclude in this part that the reason for the low activity was arising from the steric effect of the small particle only. Because the particle size distribution of prepared sol-gel SiO<sub>2</sub> can not be controlled and some impurity may be exist in the SiO<sub>2</sub>. To confirm that the particle size distribution of SiO<sub>2</sub> used was suitably narrow and the purity of SiO<sub>2</sub> was acceptable. In the next part, we chose the commercial nano-SiO<sub>2</sub> from Sigma-Aldrich which have the specification cover our

requirement replace to the sol-gel  $\text{SiO}_2$ . And we also used the two different particle size (10 and 15 nm) of these commercial  $\text{SiO}_2$  to study the effect of particle size.

## 4.2 Nanopowder silica as a filler of LLDPE- $\text{SiO}_2$ nanocomposite synthesized via in situ polymerization with zirconocene/MAO catalysts

### 4.2.1 Effect of particle size of nano- $\text{SiO}_2$

#### 4.2.1.1 Characterization of fillers and catalyst precursors with X-ray diffraction (XRD).

The XRD patterns for the nano- $\text{SiO}_2$  before and after impregnation with MAO are shown in Figure 4.5. Only broad XRD peaks can be observed indicating amorphous  $\text{SiO}_2$ . There was no significant change regarding after impregnation with MAO.

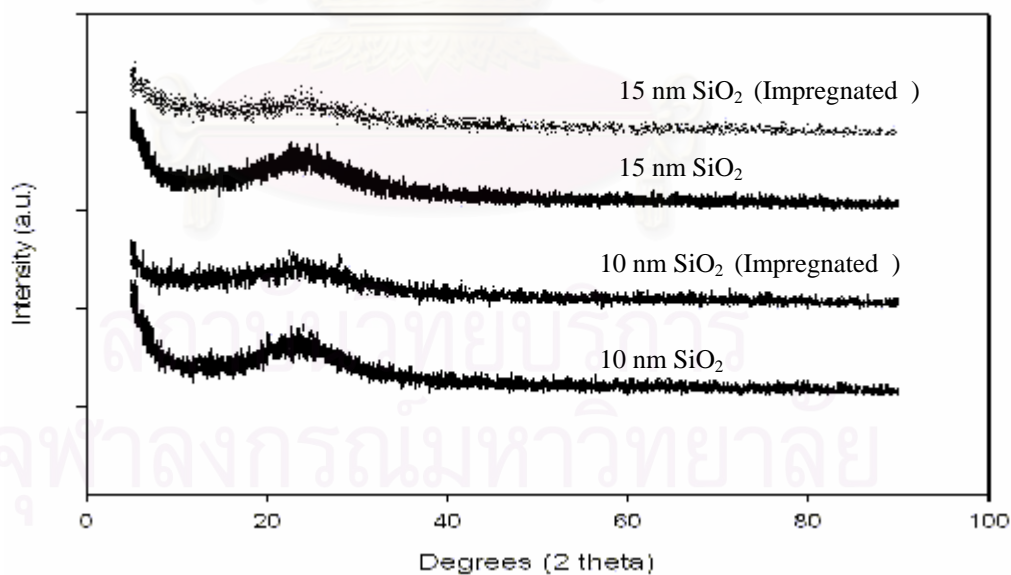


**Figure 4.5** XRD patterns of nanopowder- $\text{SiO}_2$  before and after impregnation procedure.

#### 4.2.1.2 Characterization of fillers and catalyst precursors with Transmission electron microscope (TEM)

TEM micrographs of the nano-SiO<sub>2</sub> before and after impregnation with MAO are shown in Figure 4.6 , 4.6a and 4.6b showed the 10 nm-SiO<sub>2</sub> before and after impregnation with MAO, respectively. The images of 15 nm-SiO<sub>2</sub> before and after impregnation with MAO are shown in Figure 4.6c and 4.6d, respectively. In all images, they indicated that the dense of amorphous SiO<sub>2</sub> did actually agglomerate. There was no significant change regarding before and after impregnation with MAO for both 10 and 15 nm-SiO<sub>2</sub>.

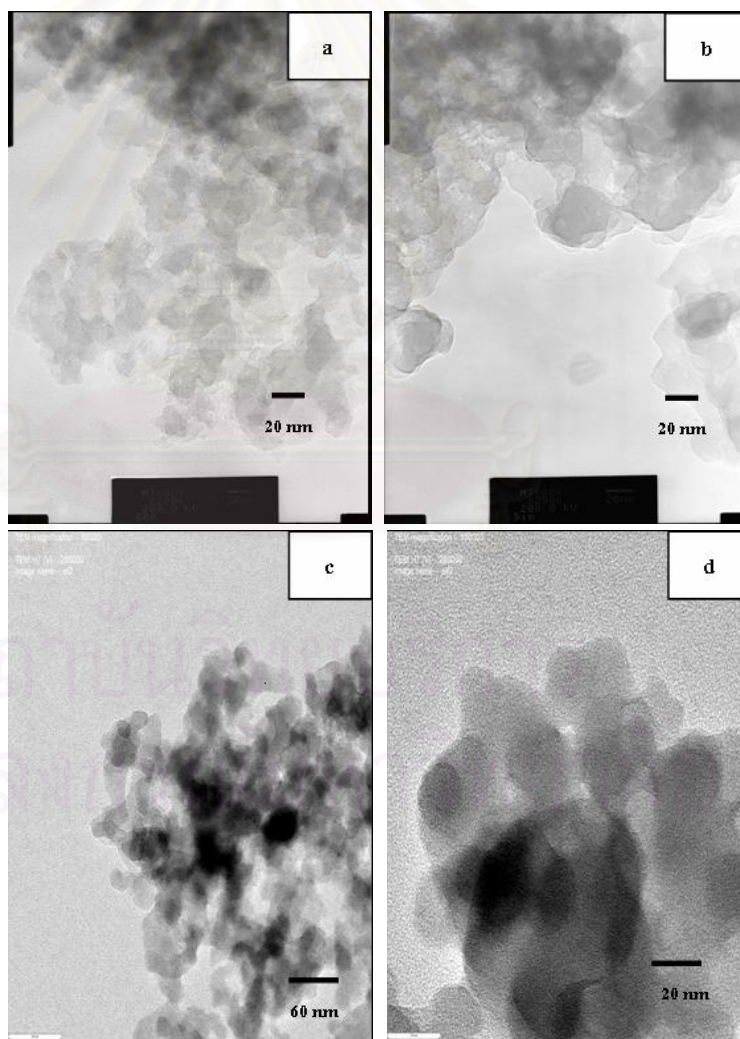


**Figure 4.6** TEM micrographs of the nano-SiO<sub>2</sub> before and after impregnation with MAO.  
(a) 10 nm-SiO<sub>2</sub> before impregnation (b) 10 nm-SiO<sub>2</sub> after impregnation  
(c) 15 nm-SiO<sub>2</sub> before impregnation (d) 15 nm-SiO<sub>2</sub> after impregnation

### 4.2.1.3 Effect of particle size on activity and characteristics of LLDPE-SiO<sub>2</sub> nanocomposites.

After the *in situ* polymerization was done, the polymerization time and yield were recorded. They are listed in Table 4. 2 along with some other characteristics of polymers. To better illustrate the effect of particle size of nano-SiO<sub>2</sub> on the activities at the same amounts of it, a plot of activity versus the weight of nano-SiO<sub>2</sub> used corresponding to different ratios of [Al]<sub>MAO</sub>/[Zr] is shown in Figure 4. 7.

**Table 4.2** Activity and characteristics of LLDPE-SiO<sub>2</sub> nanocomposites

Filler	Weight (g)	Polym. yield (g)	Time (s)	Activity <sup>a</sup>	%SiO <sub>2</sub> <sup>b</sup>	T <sub>m</sub> (°C)	1-Hexene insertion <sup>d</sup> (%)
Nano-SiO <sub>2</sub> (10 nm)	0.1	0.1355	1714	380	42.5	102.3	25.7
	0.2	0.9164	326	9483	17.9	70.4	47.7
	0.3	0.8633	330	9762	25.8	86.3	38.7
Nano-SiO <sub>2</sub> (15 nm)	0.1	0.5505	400	3811	15.4	99.6	29.7
	0.2	0.9555	149	17758	17.3	89.7	54.5
	0.3	1.002	134	20707	23.1	87.7	70.0

<sup>a</sup> Activities (kg of polym/mol of Zr.h) were measured at polymerization temperature of 70°C, [ethylene] = 0.018 mole, [1-hexene] = 0.018 mole, [Al]<sub>MAO</sub>/[Zr] = 1135 to 3405, [Al]<sub>TMA</sub>/[Zr] = 2500, in toluene with total volume = 30 ml and [Zr] = 5 x 10<sup>-5</sup> M.

<sup>b</sup> The amount of SiO<sub>2</sub> present in the LLDPE composites based on yield

<sup>c</sup> Melting temperature (T<sub>m</sub>) was obtained from the DSC measurement

<sup>d</sup> 1-hexene insertion or incorporation was calculated based on <sup>13</sup>C NMR

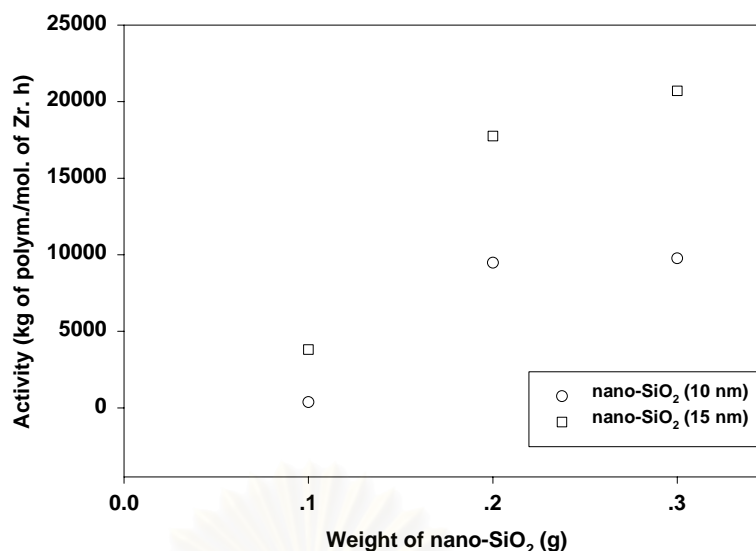


**Figure 4.7** Catalytic activity of LLDPE-SiO<sub>2</sub> nanocomposites with two particle sizes of nano-SiO<sub>2</sub> as a filler.

It can be observed that increased amounts of nano-SiO<sub>2</sub> resulted in increased activities during polymerization for both 10 and 15 nm-SiO<sub>2</sub>. This can be attributed to an increase in the  $[Al]_{MAO}/[Zr]$  ratios from 1135 to 2270 and, then to 3405 corresponding to 0.1, 0.2, and 0.3 g of the nano-SiO<sub>2</sub>, respectively as also mentioned in our previous work[68]. It was reported that the greater amounts of MAO resulted in more active species being present during polymerization[69]. It was proposed that MAO possibly had many functions, such as an alkylating agent, a stabilizer for a cationic metallocene alkyl and/or counterion, an ionizing and/or reducing agent for the transition element, and a scavenger for the metallocene catalytic system. However, one of the most important roles of MAO is apparently to prevent the formation of ZrCH<sub>2</sub>CH<sub>2</sub>Zr species, which is formed via a bimolecular process[70].

Considering, activities for both 10 and 15 nm-SiO<sub>2</sub>, it was found that the 15 nm-SiO<sub>2</sub> exhibited higher activities with the same ratios of  $[Al]_{MAO}/[Zr]$  as seen in Figure 4.7. The higher activities can be attributed to fewer interactions between SiO<sub>2</sub> and MAO arising from the larger particles. It should be noted that SiO<sub>2</sub> is one of materials having strong interaction with species being present on its surface[71]. A wide range of variables including particle size, types of material, and pretreatment condition can affect the particle interaction[72]. The smaller particles may interact more with MAO resulting in decreased activities because it is more difficult for metallocene to react with the strongly interacted MAO on SiO<sub>2</sub> surface. Besides, the strong interaction between

SiO<sub>2</sub> and MAO, it should be mentioned that the smaller particles also render more steric hindrance. Apparently, the more steric hindrance results in more difficulty for monomer insertion. Hence, low activities for the 10 nm-SiO<sub>2</sub> was observed. In order to give a better point of view on the particle size effect, the conceptual model drawn based on the resulted activities is illustrated in Figure 4.8.

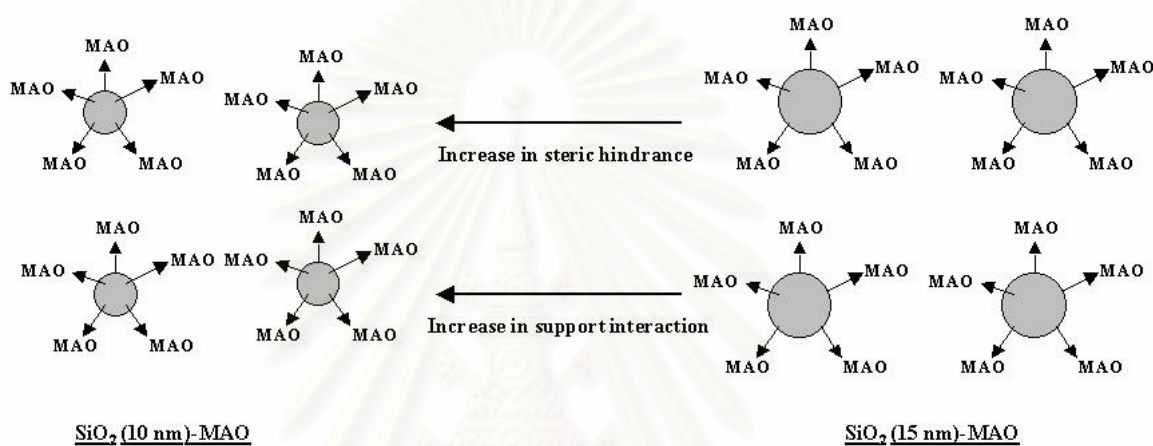


**Figure 4.8.** The conceptual model of nano-particle interacting with MAO.

#### 4.2.1.4 The effect of nanopowder-silica on the morphologies of LLDPE-nanocomposites.

Morphologies of LLDPE/nano-SiO<sub>2</sub> composites are shown in Figure 4.9.

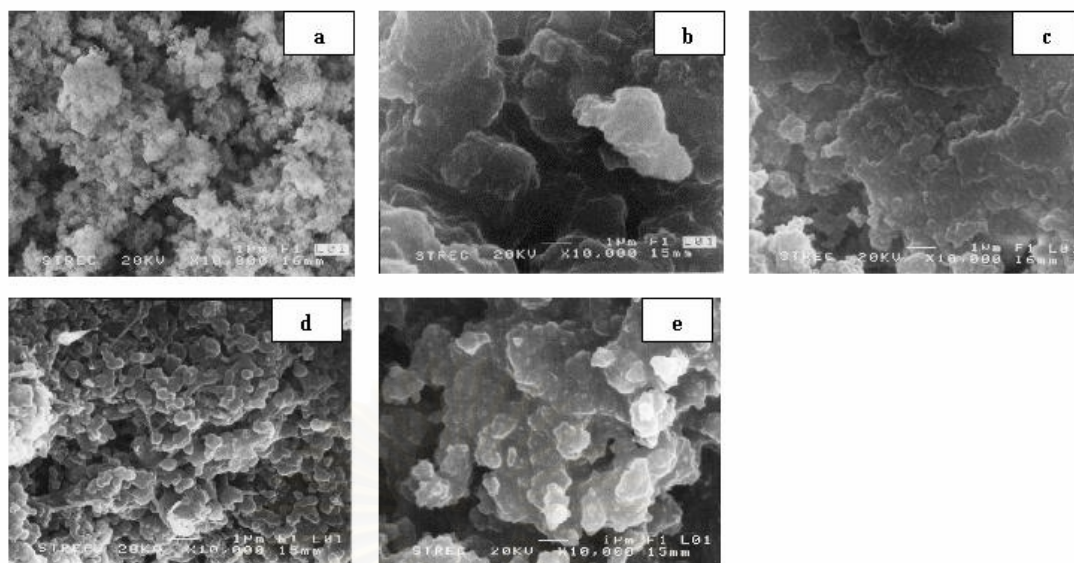


**Figure 4.9** Morphologies of LLDPE/nano composites with two particle sizes of nano-SiO<sub>2</sub> as a filler.

: 10 nm-SiO<sub>2</sub> (a) 0.1 g (b) 0.2 g (c) 0.3 g  
 : 15 nm-SiO<sub>2</sub> (c) 0.1 g (d) 0.2 g

Figure 4.9a, 4.9b, and 4.9c represented LLDPE with 10 nm-SiO<sub>2</sub> at 0.1, 0.2, and 0.3 g of SiO<sub>2</sub>, respectively. Figure 4.9d and 4.9e showed LLDPE containing 15 nm-SiO<sub>2</sub> at 0.1 and 0.2 g of SiO<sub>2</sub>, respectively. However, there was no SEM micrograph for the LLDPE with 15 nm-SiO<sub>2</sub> at 0.3 g of SiO<sub>2</sub> due to its gel-like form, which was unable to be seen by SEM. Based on the SEM results, there was no significant change in polymer morphologies for LLDPE nanocomposites containing 10 and 15 nm-SiO<sub>2</sub> with the same amounts of SiO<sub>2</sub>. However, significant differences can be observed with changing amounts of nano-SiO<sub>2</sub> in the LLDPE composites. As seen, increased amounts of the nano-SiO<sub>2</sub> resulted in more agglomeration of particles. Therefore, the bigger patches of LLDPE can be observed with larger amounts of the nano-SiO<sub>2</sub> added. It should be mentioned that EDX was also used to identify the elemental distribution in LLDPE/nano-SiO<sub>2</sub> composites. EDX mapping in Figure 4.10 revealed that even with agglomeration, the nano-SiO<sub>2</sub> had good distribution inside the polymer matrix as well.

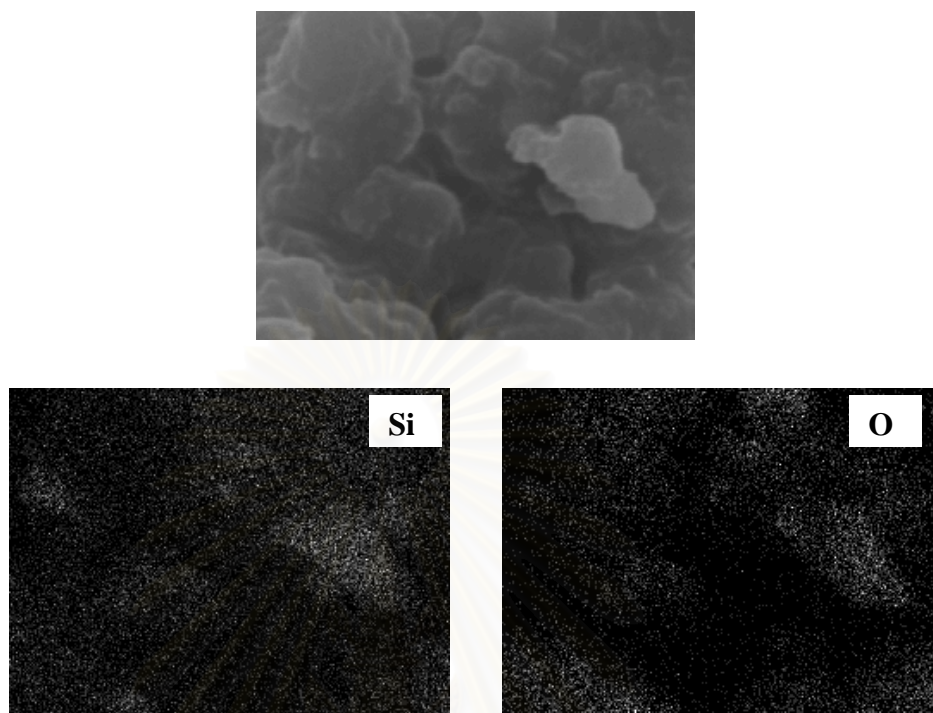


**Figure 4.10** EDX mapping of LLDPE/nano-SiO<sub>2</sub> composite with SiO<sub>2</sub> (0.3 g) indicating distribution of Si and O.

#### **4.2.1.5 Characterization of LLDPE-nanocomposites with transmission electron microscope (TEM).**

As known, images from high resolution transmission electron microscopy (TEM) is an essential component of nanoscience, therefore TEM was performed to identify the dispersion of nano-SiO<sub>2</sub> in LLDPE. The TEM micrographs of LLDPE/nano-SiO<sub>2</sub> are shown in Figure 4.11.



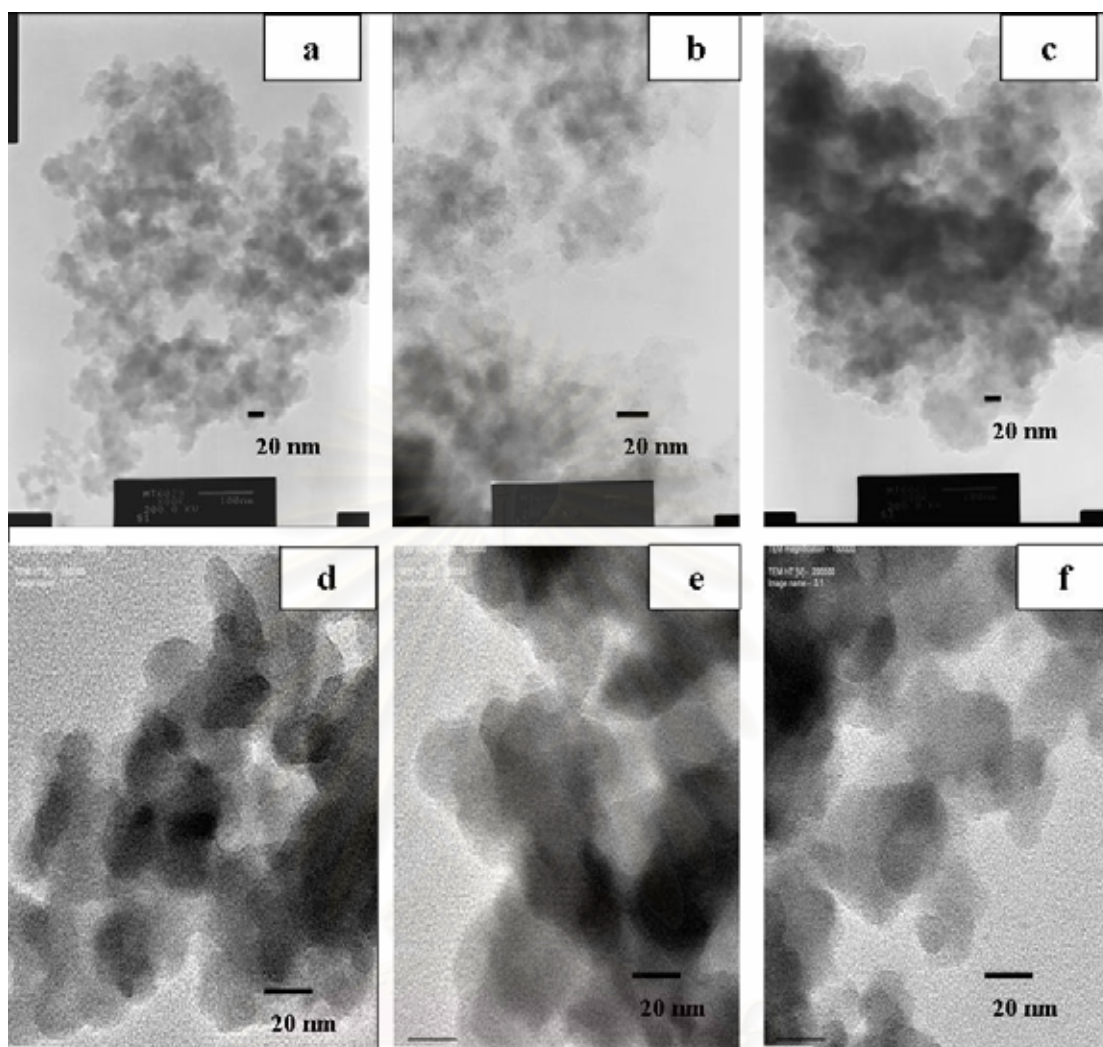


**Figure 4.11** TEM micrographs of LLDPE/nanocomposites with two particle size of nanosilica as a filler.

: 10 nm-SiO<sub>2</sub> (a) 0.1 g (b) 0.2 g (c) 0.3 g

: 15 nm-SiO<sub>2</sub> (d) 0.1 g (e) 0.2 g (f) 0.3 g

Figure 4.11a, 4.11b, and 4.11c represented LLDPE with 10 nm-SiO<sub>2</sub> at 0.1, 0.2, and 0.3 g of SiO<sub>2</sub>, respectively. Figure 4.11d, 4.11e and 4.11f showed LLDPE containing 15 nm-SiO<sub>2</sub> at 0.1 and 0.2 g of SiO<sub>2</sub>, respectively. The poor dispersion was probably due to interaction between particles leading to agglomeration. In addition, there was no pronouncedly different among each LLDPE/nano-SiO<sub>2</sub> sample. Thus, in order to obtain well dispersion, the modification of the nano-SiO<sub>2</sub> needs to be further investigated for future work.

#### 4.2.1.6 Characterization of LLDPE-nanocomposites with nuclear magnetic resonance (NMR)

Among a bunch of important aspects of making a polymer composite, one should mention how the filler affects the molecular structure of polymer produced. Then,  $^{13}\text{C}$  NMR is one of the most powerful techniques to identify the polymer microstructure, especially polyolefins. The resulted  $^{13}\text{C}$  NMR spectra (not shown) for all samples were assigned typically to the LLDPE obtained from copolymerization of ethylene/1-hexene. The triad distribution was identified based on the method described by Randall[73]. It can be observed that the LLDPE consisting of 10 and 15 nm- $\text{SiO}_2$  exhibited similar  $^{13}\text{C}$  NMR patterns indicating similar molecular structure of polymer. Based on calculations described by Galland et al.[74], the triad distribution of monomer is listed in Table 4.3. It indicated that all LLDPE samples were random copolymer with the difference in 1-hexene insertion.

**Table 4. 3** Triad distribution<sup>a</sup> obtained from  $^{13}\text{C}$  NMR of LLDPE- $\text{SiO}_2$  nanocomposites

Filler	Weight (g)	EEE	EEH	HEH	EHE	EHH	HHH
			+			+	
			HEE			HHE	
Nano- $\text{SiO}_2$ (10 nm)	0.1	0.66	0.09	0	0.04	0.21	0
	0.2	0.39	0.12	0.02	0.06	0.41	0
	0.3	0.47	0.13	0.02	0.07	0.31	0
Nano- $\text{SiO}_2$ (15 nm)	0.1	0.61	0.09	0	0.05	0.25	0
	0.2	0.31	0.12	0.03	0.07	0.47	0
	0.3	0.19	0.12	0.04	0.08	0.57	0

<sup>a</sup> E refers to ethylene and H refers to 1-hexene

This result was also similar with what we found in our previous works without the addition of nano-SiO<sub>2</sub>[75-78]. According to the triad distribution shown in Table 4.3, the 1-hexene insertion can be calculated based on ref. 74. The 1-hexene insertion in LLDPE/nano-SiO<sub>2</sub> is shown in Table 4.2. It can be observed that larger particle resulted in increased 1-hexene insertion due to less steric hindrance as also described by Scheme 4.1. Hence, the large molecule of 1-hexene can insert more. The melting temperature ( $T_m$ ) as also shown in Table 4.2 trended to decrease with more insertion of 1-hexene due to decreased crystallinity.

#### **4.2.2 Effect of the amount of nano-SiO<sub>2</sub>.**

In the first part, the ratios of  $[Al]_{MAO}/[Zr]$  were varied with the amounts of nano-SiO<sub>2</sub> used. This was because the amounts of MAO being present in 1 g of nano-SiO<sub>2</sub> were the same during MAO impregnation. Hence, larger amounts of nano-SiO<sub>2</sub> meant higher ratios of  $[Al]_{MAO}/[Zr]$ . In this part, the ratio of  $[Al]_{MAO}/[Zr]$  was kept constant at 2270 by changing the catalyst concentrations,  $[Zr]$ . Thus, the amounts of nano-SiO<sub>2</sub> can be varied without changing the  $[Al]_{MAO}/[Zr]$  ratio. In fact, only 15 nm-SiO<sub>2</sub> was chosen for study the effect of amounts of nano-SiO<sub>2</sub>.

##### **4.2.2.1 Effect of the amount of nano-SiO<sub>2</sub> on activity and characteristics of LLDPE-SiO<sub>2</sub> nanocomposites.**

Using the similar ways as mentioned in 3.1, activities and characteristics of LLDPE/15 nm-SiO<sub>2</sub> composite were obtained as shown in Table 4.4.

**Table 4.4** Activity and characteristics of LLDPE-SiO<sub>2</sub> nanocomposites at [Al]<sub>MAO</sub>/[Zr] = 2270

Filler	Weight (g)	Polym. yield (g)	Time (s)	Activity <sup>a</sup>	%SiO <sub>2</sub> <sup>b</sup>	T <sub>m</sub> <sup>c</sup> (°C)	1-Hexene insertion <sup>d</sup> (%)
Nano-SiO <sub>2</sub> (15 nm)	0.1	0.1000	717	386	50	107.6	19.86
	0.2	0.9555	149	17758	20.9	89.7	54.5
	0.3	0.7545	248	8425	39.8	101.2	67.5

<sup>a</sup> Activities (kg of polym/mol of Zr.h) were measured at polymerization temperature of 70°C, [ethylene] = 0.018 mole, [1-hexene] = 0.018 mole, [Al]<sub>MAO</sub>/[Zr] = 2270, [Al]<sub>TMA</sub>/[Zr] = 2500, in toluene with total volume = 30 ml and [Zr] = 5 to 15, x 10<sup>-5</sup> M

<sup>b</sup> The amount of SiO<sub>2</sub> present in the LLDPE composites based on yield

<sup>c</sup> Melting temperature (T<sub>m</sub>) was obtained from the DSC measurement

<sup>d</sup> 1-hexene insertion or incorporation was calculated based on <sup>13</sup>C NMR

It was found that at the specified condition the activity went to a maximum with the certain amount of nano-SiO<sub>2</sub> (0.2 g), then went down with increased amount of nano-SiO<sub>2</sub> (0.3 g). Increased activity with increasing the amount of nano-SiO<sub>2</sub> at the beginning can be attributed to increased distribution of MAO. Consequently, this also resulted in increased 1-hexene insertion as also shown in Table 4.5. However, increased amounts of nano-SiO<sub>2</sub> more resulted in decreased activity. This was probably due to stronger interaction between particles.

#### 4.2.2.2 The effect of the amount of nanopowder-silica on the morphologies of LLDPE-nanocomposites.

Morphologies of LLDPE/nano-SiO<sub>2</sub> composites are shown in Figure 4.12.

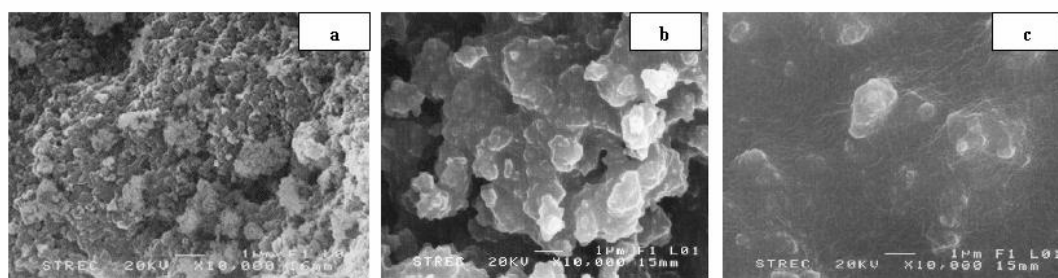
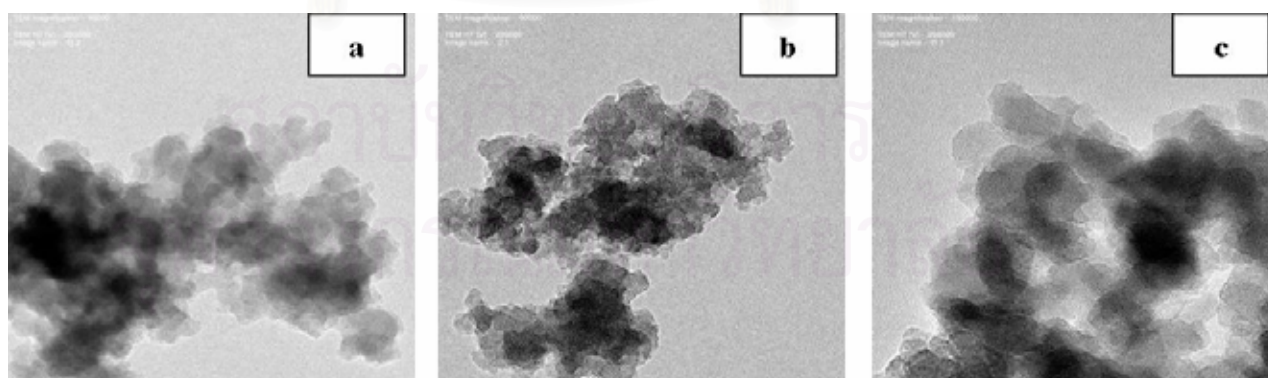


**Figure 4.12** Morphologies of LLDPE/nano composites with 15nm silica as a filler. (a) 0.1 g (b) 0.2 g (c) 0.3 g

Figure 4.12a, 4.12b, and 4.12c represented LLDPE with 15 nm-SiO<sub>2</sub> at 0.1, 0.2, and 0.3 g of SiO<sub>2</sub>, respectively. Significant differences can be observed with changing amounts of nano-SiO<sub>2</sub> in the LLDPE composites. This result was similar to that of the previous part (4.2.1.4). So, we can confirm that the amount of nano-silica affects the morphology of LLDPE-nanocomposite even the ratio of [Al]<sub>MAO</sub>/[Zr] was kept constant.

#### 4.2.2.3 Characterization of LLDPE-nanocomposites ( fixed ratio of [Al]<sub>MAO</sub>/[Zr] ) with Transmission electron microscope (TEM).

The TEM micrographs of LLDPE/nano-SiO<sub>2</sub> are shown in Figure 4.13.



60 nm

**Figure 4.13** TEM micrographs of LLDPE/nano-SiO<sub>2</sub> with 15 nm silica as a filler.

(a) 0.1 g (b) 0.2 g (c) 0.3 g

Figure 4.13a, 4.13b, and 4.13c represented LLDPE with 15 nm-SiO<sub>2</sub> at 0.1, 0.2, and 0.3 g of SiO<sub>2</sub>, respectively. There was no pronouncedly different among each LLDPE/nano-SiO<sub>2</sub> sample similar to the previous part (4.2.1.5). So in the same way, the modification of the nano-SiO<sub>2</sub> needs to be further investigated for future work to obtain the good dispersion.

#### 4.2.2.4 Characterization of LLDPE-nanocomposites( fixed ratio of [Al]<sub>MAO</sub>/[Zr] ) with Nuclear Magnetic Resonance (NMR)

The triad distribution of monomer is listed in Table 4.5. It indicated that all LLDPE samples were random copolymer with the difference in 1-hexene insertion.

**Table 4.5** Triad distribution<sup>a</sup> obtained from <sup>13</sup>C NMR of LLDPE-SiO<sub>2</sub> nanocomposites

Filler	Weight (g)	EEE	EEH	HEH	EHE	EHH	HHH
			+ HEE			+ HHE	
Nano-SiO <sub>2</sub> (15 nm)	0.1	0.61	0.09	0	0.05	0.25	0
	0.2	0.31	0.12	0.03	0.07	0.47	0
	0.3	0.19	0.12	0.04	0.08	0.57	0

<sup>a</sup> E refers to ethylene and H refers to 1-hexene

## CHAPTER V

### CONCLUSIONS & RECOMMENDATIONS

#### 5.1 CONCLUSIONS

In the first part, the sol-gel silica was used as a filler for LLDPE-SiO<sub>2</sub> nanocomposite obtained via the *in situ* polymerization with MAO/metallocene catalyst. It was found that silica particles were well distribution in the polymer matrix at some certain amounts of them. However, activities and yields of polymerization were apparently low probably due to more steric hindrance arising from the nano-particles. Thus, polymerization conditions, catalysts used, and types of nano-particles need to be further investigated in order to increase productivity.

In the second part, it can be concluded that different particle size of the nano-SiO<sub>2</sub> had effect on catalytic properties for LLDPE/nano-SiO<sub>2</sub> composites. It was found that the larger particle (15 nm-SiO<sub>2</sub>) exhibited higher activity due to fewer interactions between SiO<sub>2</sub> and MAO. The larger particle also rendered higher insertion of 1-hexene. This was due to less steric hindrance arising from the larger particle. Apparently, higher 1-hexene insertion resulted in decreased melting temperature due to decreased crystallinity. No change in molecular structure of LLDPE was detected (only random copolymer was found). It should be noted that even with good distribution of the SiO<sub>2</sub>, the particle still exhibited poor dispersion inside the polymer matrix as seen by TEM due to agglomeration.

#### 5.2 RECOMMENDATIONS

In order to overcome the poor dispersion of particle, the SiO<sub>2</sub> needs to be modified prior to use. The modification of SiO<sub>2</sub> should be further investigated in the near future.

## REFERENCES

1. Clair, K. S. *Hydrocarbon Processing* (April 2004): 39-43.
2. Ajayan, P.M.; Schadler, L.S. and Braun, P.V. *Nanocomposite Science and Technology*, WILEY-VCH Verlag GmbH Co. KGaA, Weinheim: 2003.
3. Verbeek, C.J.R. *Mater. Lett.* 56 (2002): 226.
4. Nawang, R.; Danjaji, I.D.; Ishiaku, U.S.; Ismail, H. and Mohd Ishak, Z.A. *Polym. Testing* 20 (2001): 167.
5. Haung, Y.; Jiang, S.; Wu, L. and Hua, Y. *Polym. Testing* 23 (2004): 9.
6. Huang, Y.Q.; Zhang, Y.Q. and Hua, Y.Q. *J. Mater. Sci. Lett.* 22 (2003): 997.
7. Danjaji, I.D.; Nawang, R.; Ishiaku, U.S.; Ismail, H. and Mohd Ishak, Z.A. *Polym. Testing* 21 (2002): 75.
8. Verbeek, C.J.R. *Mater. Lett.* 52 (2002): 453.
9. Kashiwa, N. and Imuta, J. *Catalysis Surveys from Japan* 1 (1997): 125-142.
10. Sinclair, K. B. and Wilson, R. B. *Chemistry & Industry* 7 (1994): 857-862.
11. Gupta, V. K.; Satish, S. and Bhardwaj, I. S. *J. M. S.-Rev. Macromol. Chem. Phys.* C34(3) (1994): 439-514.
12. Naga, N. and Imanishi, Y. *Macromol. Chem. Phys.* 203 (2002): 159-165.
13. Lauher, J. W. and Hoffmann, R. J. *Am. Chem. Soc.* 98 (1976): 1729.
14. Castonguay, L. A. and Rappe, A. K. *J. Am. Chem. Soc.* 114 (1992): 5832-5842.
15. Kaminsky, W. and Laban, K. *Applied Catalysis A: General* 222 (2001): 47-61.
16. Yang, X.; Stern, C. L. and Marks, T. J. *J. Am. Chem. Soc.* 113 (1991): 3623-3625.
17. Chien, J. C. W. and Wang, B. P. *J. Polym. Sci.: Part A: Polym. Chem.* 26 (1988): 3089-3102.
18. Pedeutour, J. N.; Radhakrishnan, K.; Cramail, H. and Deffieux, A. *J. Mol. Cat. A: Chem.* 185 (2002): 119-125.
19. Pedeutour, J. N.; Cramail, H. and Deffieux, A. *J. Mol. Cat. A: Chem.* 176 (2001): 87-94.
20. Cam, D. and Giannini, U. *Makromol. Chem.* 193 (1992): 1049-1055.
21. Soga, K.; Kim, H. J. and Shiono, T. *Makromol. Chem., Rapid Commun.* 14 (1993): 765-770.



22. Katayama, H.; Shiraishi, H.; Hino, T.; Ogane, T. and Imai, A. *Macromol. Symp.* 97 (1995): 109-118.
23. Przybyla, C.; Tesche, B. and Fink, G. *Macromol. Rapid Commun.* 20 (1999): 328-332.
24. Harkki, O.; Lehmus, P.; Leino, R.; Luttikhedde, H. J. G.; Nasman, J. H. and Seppala, J. V. *Macromol. Chem. Phys.* 200 (1999): 1561-1565.
25. Cheruvu, S. US Pat 5608019 (1997).
26. Albano, C.; Sanchez, G. and Ismayel, A. *Polym. Bull.* 41 (1998): 91-98.
27. Shan, C. L. P.; Soares, J. B. P. and Penlidis, A. *J. Polym. Sci.: Part A: Polym Chem.* 40 (2002): 4426-4451.
28. Pietikainen, P. and Seppala, J.V. *Macromolecules* 27 (1994): 1325-1328.
29. Soga, K. and Kaminaka, M. *Makromol. Chem. Rapid Commun.* 13 (1992): 221-224.
30. Nowlin, T. E.; Kissin, Y. V. and Wagner, K. P. *J. Polym. Sci.: Part A: Polym. Chem.* 26 (1988): 755-764.
31. Chu, K. J.; Soares, J. B. P. and Penlidis, A. *Macromol. Chem. Phys.* 201 (2000): 340-348.
32. Soga, K.; Uozumi, T.; Arai, T. and Nakamura, S. *Macromol. Rapid Commun.* 16 (1995): 379-385.
33. de Fatima, V.; Marques, M.; Conte, A.; de Resende, F. C. and Chaves, E. G. J. *App. Polym. Sci.* 82 (2001): 724-730.
34. Kim, J. D. and Soares, J. B. P. *Macromol. Rapid Commun.* 20 (1999): 347-350.
35. Chu, K. J.; Soares, J. B. P. and Penlidis, A. *Journal of Polymer Science:Part A: Polymer Chemistry.* 38 (2000): 462-468.
36. Chu, K. J.; Shan, C. L. P.; Soares, J. B. P. and Penlidis, A. *Macromol. Chem. Phys.* 200 (1999): 2372-2376.
37. Shan, C. L. P.; Chu, K. J.; Soares, J. and Penlidis, A. *Macromol. Chem. Phys.* 201 (2000): 2195-2202.
38. Steinmetz, B.; Tesche, B.; Przybyla, C.; Zechlin, J. and Fink, G. *Acta Polymer* 48 (1997): 392-399.
39. Tait, P. J. T. and Monterio, M. G. K. Mecton'96, Houston, TX, USA June (1996).
40. Quijada, R.; Rojas, R.; Alzamora, L.; Retuert, J. and Rabagliati, F. M. *Catalysis letters* 46 (1997): 107-112.

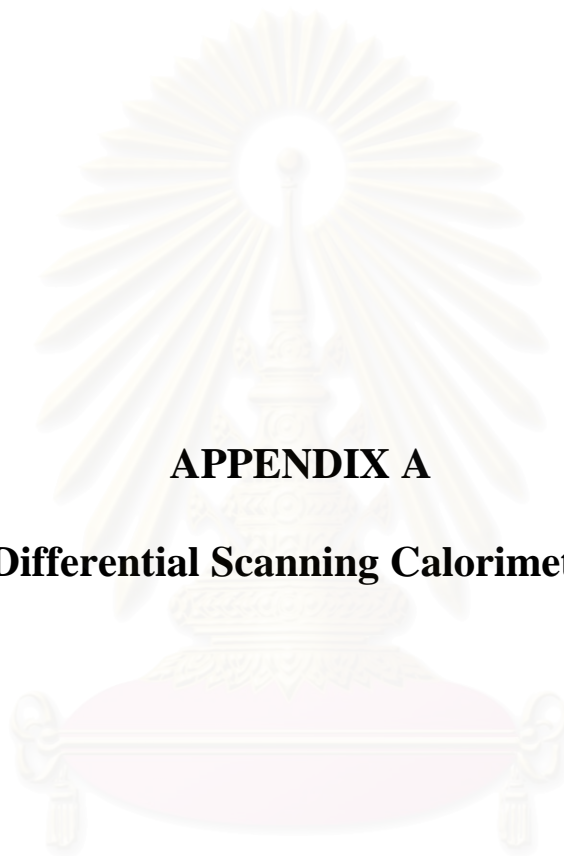
41. Chen, Y. X.; Rausch, M. D. and Chein, J. C. W. *J. Polym. Sci.: Part A: Polym. Chem.* 33 (1995): 2093-2108.
42. Ban, H.; Arai, T.; Ahn, C. H.; Uozumi, T. and Soga, T. *Recent Development in Heterogeneous Metallocene Catalyst.*
43. Ferreira, M. L.; Belelli, P. G.; Juan, A. and Damiani, D. E. *Macromol. Chem. Phys.* 201 (2000): 1334-1344.
44. Jordana, J.; Jacob, K.I.; Tannenbaum, R. Sharaf, M.A. and Jasiuk, I. *Materials Science and Engineering A* 393 (2005): 1-11.
45. Chan, C.M.; Wu, J.; Li, J.X. and Cheung, Y.K. *Polymer* 43 (2002): 2981-2992.
46. Vollenberg, P.H.T. and Heikens, D. *Polymer* 30 (1989): 1656-1662.
47. Petrovic, Z.S.; Javni, I. A.; Waddon, G. and Banhegyi, J. *Appl. Polym. Sci.* 76 (2000): 133-151.
48. Ash, B.J.; Stone, J.; Rogers, D.F.; Schadler, L.S.; Siegel, R.W.; Benicewicz, B.C. and Apple, T. *Mater. Res. Soc. Symp. Proc.* 661 (2000).
49. Ash, B.J.; Schadler, L.S. and Siegel, R.W. *Mater. Lett.* 55 (2002): 83-87.
50. Tadd, E.; Zeno, A.; Zubris, M.; Dan, N. and Tannenbaum, R. *Macromolecules.* 36 (2003): 6497-6502.
51. Wang, K.H.; Chung, I.J.; Jang, M.C.; Keum, J.K. and Song, H.H. *Macromolecules.* 35 (2002): 5529-5535.
52. Reynaud, E.; Jouen, T.; Gautheir, C. and Vigier, G. *Polymer* 42 (2001): 8759-8768.
53. Ranade, A., D'Souza, N.A. and Gnade, B. *Polymer* 43 (2002): 3759-3766.
54. Lopez, D.; Cendoya, I.; Torres, F.; Tejada, J. and Mijangos, C. *J. Appl. Polym. Sci.* 82 (2001): 3215-3222.
55. Masenelli-Varlot, K.; Reynaud, E.; Vigier, G. and Varlet, J. *J. Polym. Sci. B: Polym. Phys.* 40(2002): 272-283.
56. Zhang, Y.; Ge, S.; Tang, B.; Rafailovich, M.H.; Sokolov, J.C.; Peiffer, D.G.; Li, Z.; Dias, A.J.; McElrath, K.O.; Satija, S.K.; Lin, M.Y. and Nguyen, D. *Langmuir* 17 (2001): 4437-4442.
57. Friedlander, S.K.; Ogawa, K. and Ullmann, M. *J. Polym. Sci. B: Polym. Phys.* 38 (2000): 2658-2665.
58. Hotta, S. and Paul, D.R. *Polymer* 45 (2004): 7639-7654.
59. Wang, K. H.; Choi, M. H.; Koo, C. M.; Choi, Y. S. and Chung, I. J. *Polymer*, 42 (2001): 9819-9826 .

60. Lew, C. Y.; Murphy, W. R. and McNally, G. M. *Polym. Eng. Sci.* 44 (2004): 1027-1035.
61. Chuang, T. H.; Guo, W.; Cheng, K. C.; Chen, S.W.; Wang, H.T. and Yen, Y. Y. *Journal of Polymer Research* 11(2004): 169 – 174.
62. Mameri, F.; Bourhis, E. L.; Rozes L. and Sanchez C. *Journal of the European*, Available online 21 January 2005,
63. Liu, Y.; Lee J. Y. and Hong, L. *Journal of Power Sources* 129 (2004): 303-311.
64. Qiu, F. X.; Zhou, Y. M. and Liu, J. Z. *European Polymer Journal* 40 (2004): 713-720.
65. Papageorgiou, G. Z.; Achilias, D. S.; Bikiaris, D. N. and Karayannidis, G. P. *Thermochimica Acta* 427 (2005): 117-128.
66. Buckley, M. and Greenblatt, M. *J.Chem. Edu.* 71 (1994): 599.
67. Jongsomjit, B.; Praserttham, P. and Kaewkrajang, P. *Mater. Chem. Phys.* 86 (2004): 243.
68. Jongsomjit, B.; Chaichana, E. and Praserttham, P. *Sci.* 40 (2005): 2043-2045.
69. Jongsomjit, B.; Kaewkrajang, P.; Shiono, T. and Praserttham, P. *Ind. Eng. Chem. Res.* 43 (2004): 7959.
70. Chao, C.; Praserttham, P.; Khorbunsongserm, S. and Rempel, G.L. *J.Macromol. Sci., Part A: Pure Appl. Chem.* 40 (2003): 181.
71. Kogelbauer, A.; Weber, J. C. and Goodwin, Jr., J. G. *Catal. Lett.* 34 (1995): 259.
72. Jongsomjit, B.; Panpranot, J.; Goodwin, Jr., J. G. *J. Catal.* 204 (2001): 98.
73. Randall, J. C. *J. Macromol. Sci., Rev. Macromol. Chem. Phys.* C29 (1989): 201.
74. Galland, G. B.; Quijada, P.; Mauler, R. S. and de Menezes, S. C. *Macromol. Rapid Commun.* 17 (1996): 607.
75. Jongsomjit, B.; Kaewkrajang, P.; Wanke, S. E. and Praserttham, P. *Catal. Lett.* 94 (2004): 205.
76. Jongsomjit, B.; Ngamposri, S. and Praserttham, P. *Catal. Lett.* 100 (2005): 139.
77. Jongsomjit, B.; Ngamposri, S. and Praserttham, P. *Molecules.* 10 (2005): 672.
78. Jongsomjit, B.; Ngamposri, S. and Praserttham, P. *Ind. Eng. Chem. Res.* 44 (2005): 9059.



**APPENDICES**

สถาบันวิทยบริการ  
จุฬาลงกรณ์มหาวิทยาลัย



**APPENDIX A**

**Differential Scanning Calorimeter**

สถาบันวิทยบริการ  
จุฬาลงกรณ์มหาวิทยาลัย

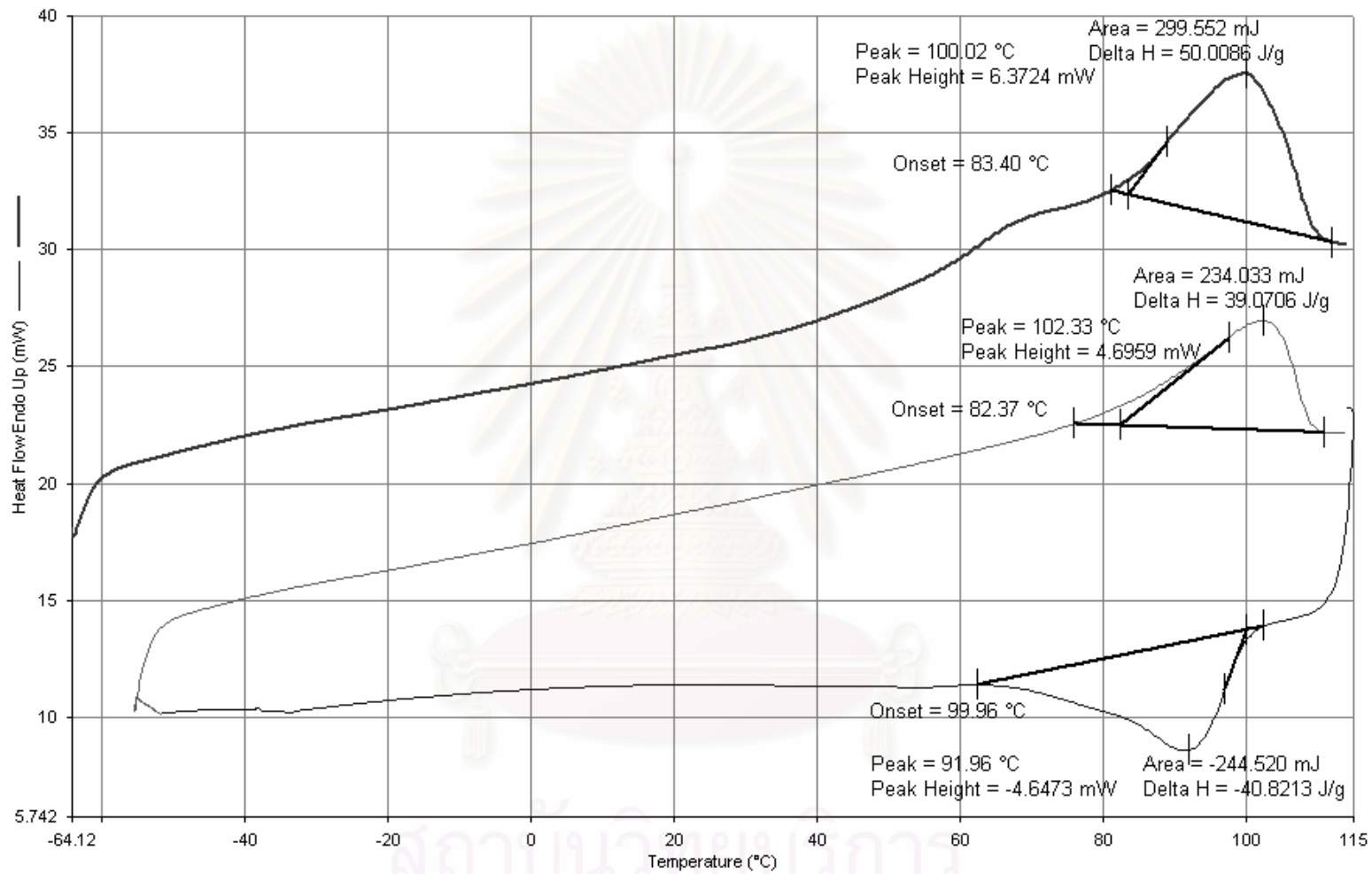


**Figure A-1.** DSC curve of LLDPE-nanocomposites with 0.1 g of 10 nm-silica

จุฬาลงกรณ์มหาวิทยาลัย

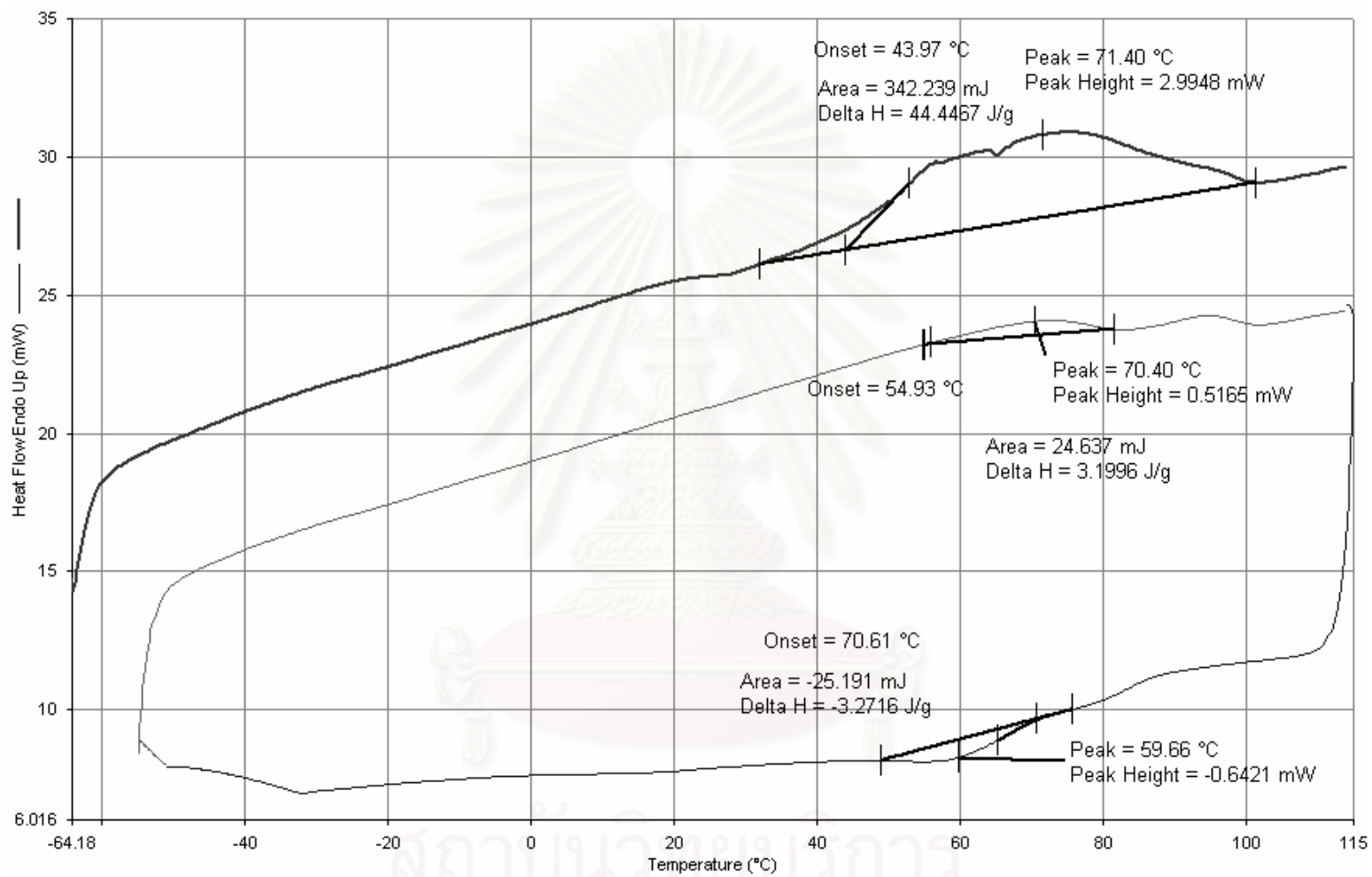


**Figure A-2.** DSC curve of LLDPE-nanocomposites with 0.2 g of 10 nm-silica

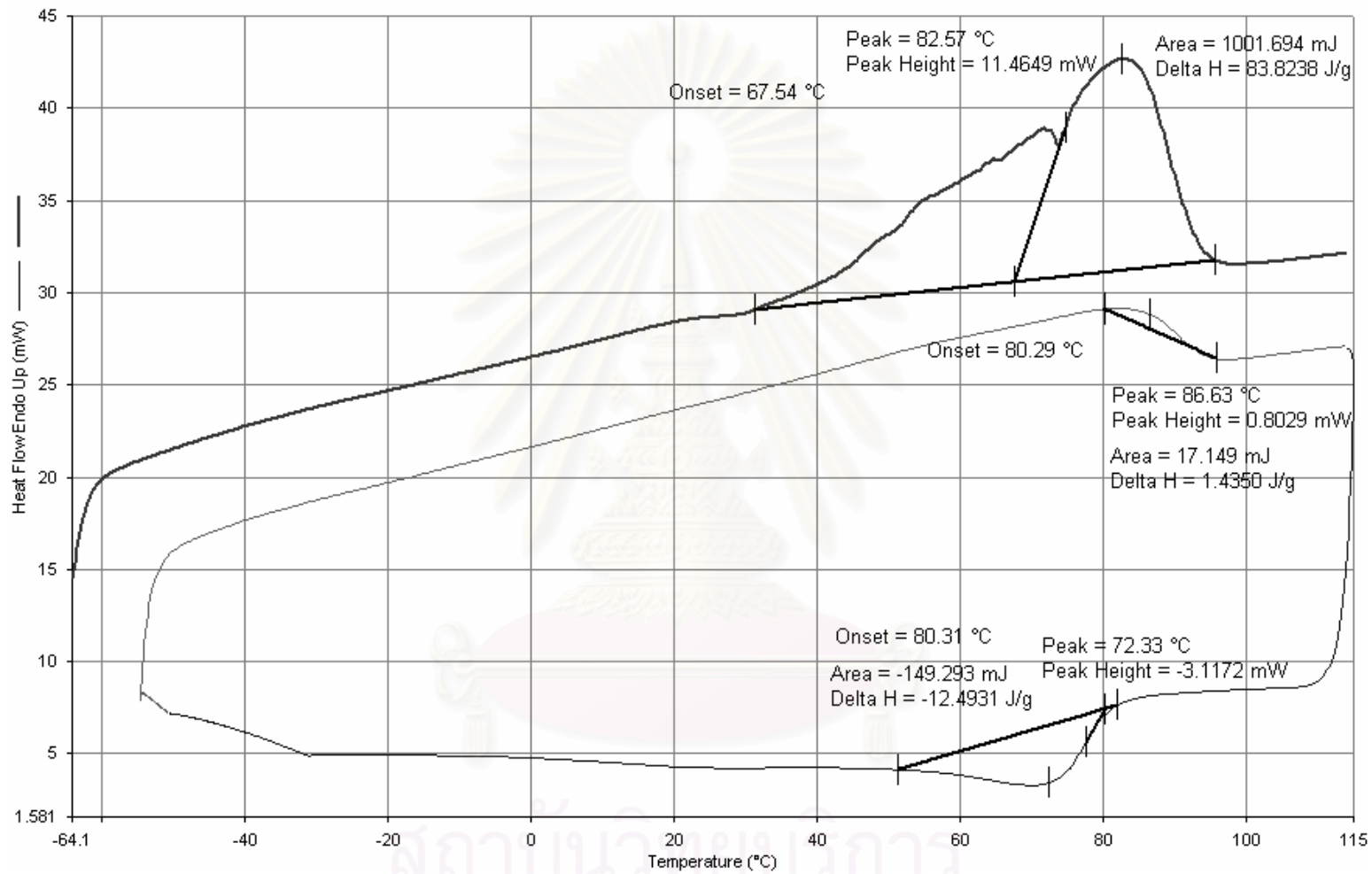


**Figure A-3.** DSC curve of LLDPE-nanocomposites with 0.3 g of 10 nm-silica



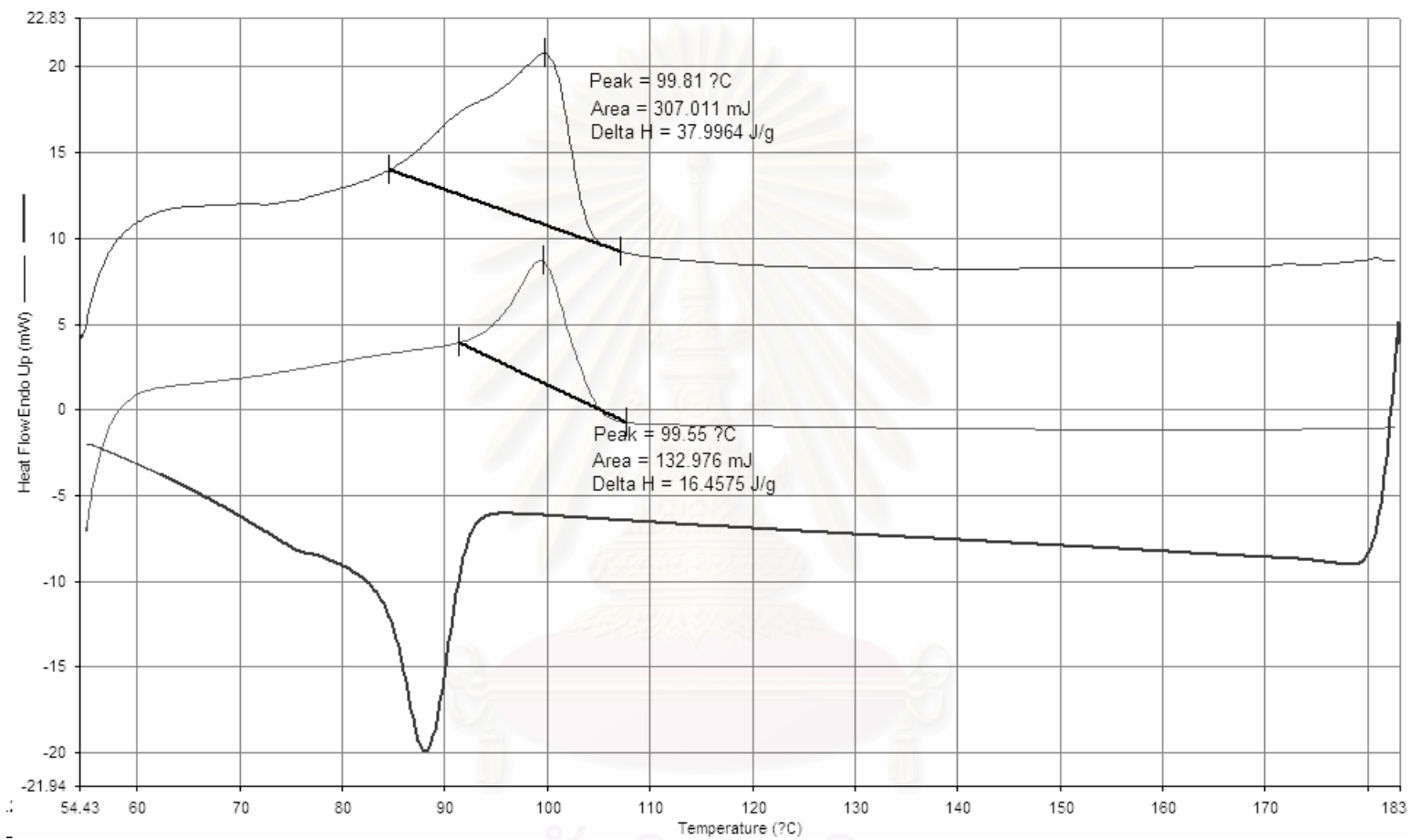


**Figure A-4.** DSC curve of LLDPE-nanocomposites with 0.1 g of 15 nm-silica

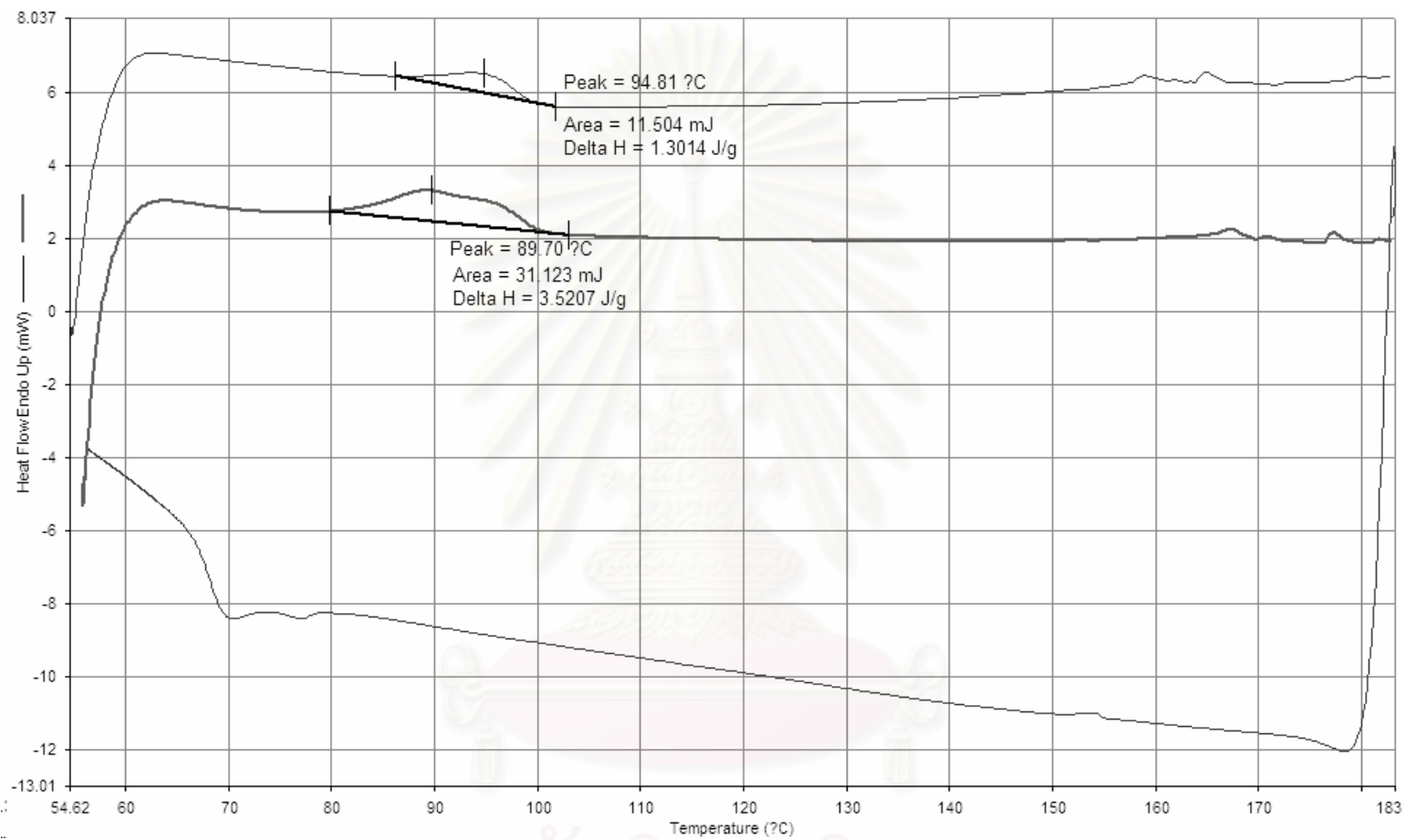


**Figure A-5.** DSC curve of LLDPE-nanocomposites with 0.2 g of 15 nm-silica

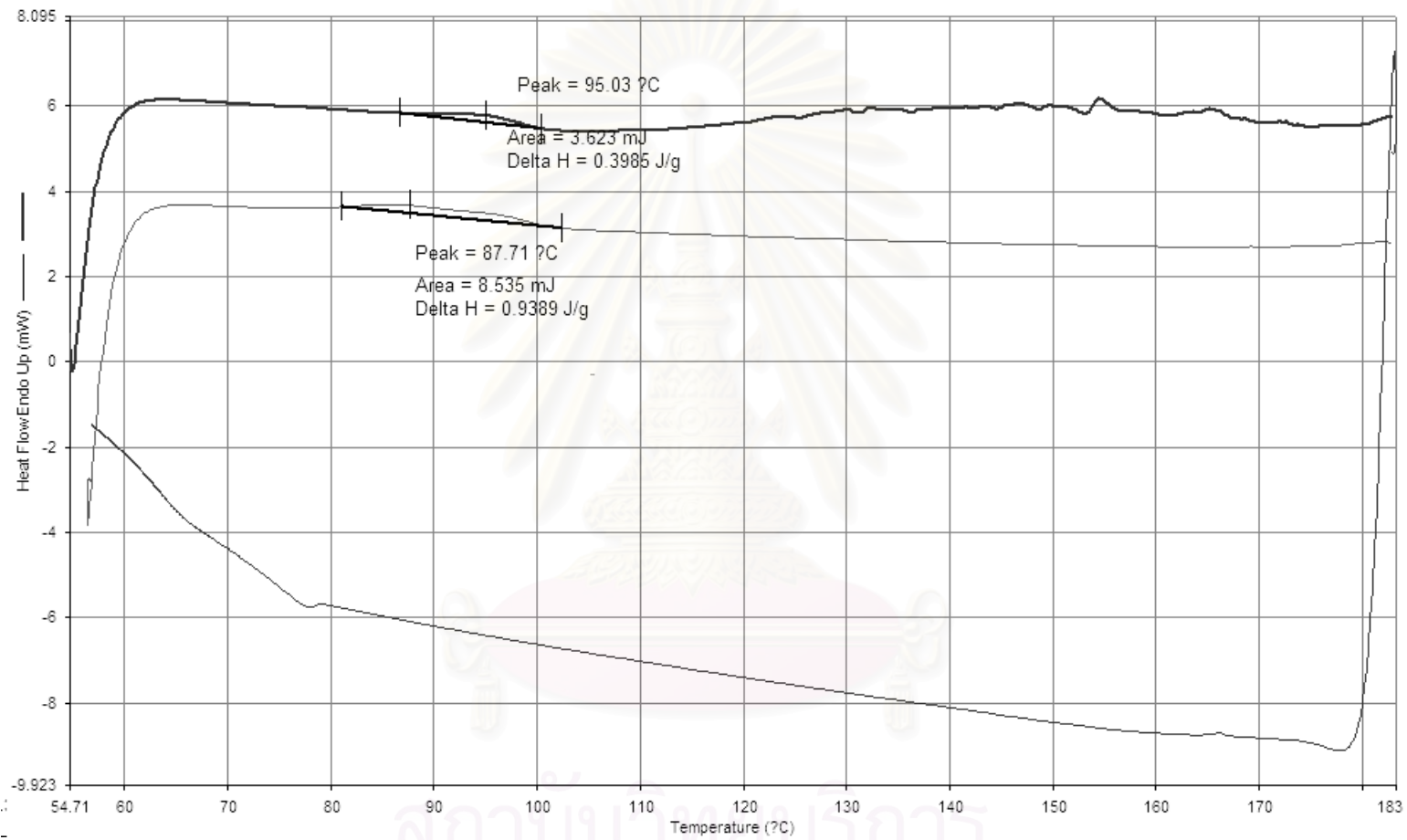


**Figure A-6.** DSC curve of LLDPE-nanocomposites with 0.3 g of 15 nm-silica

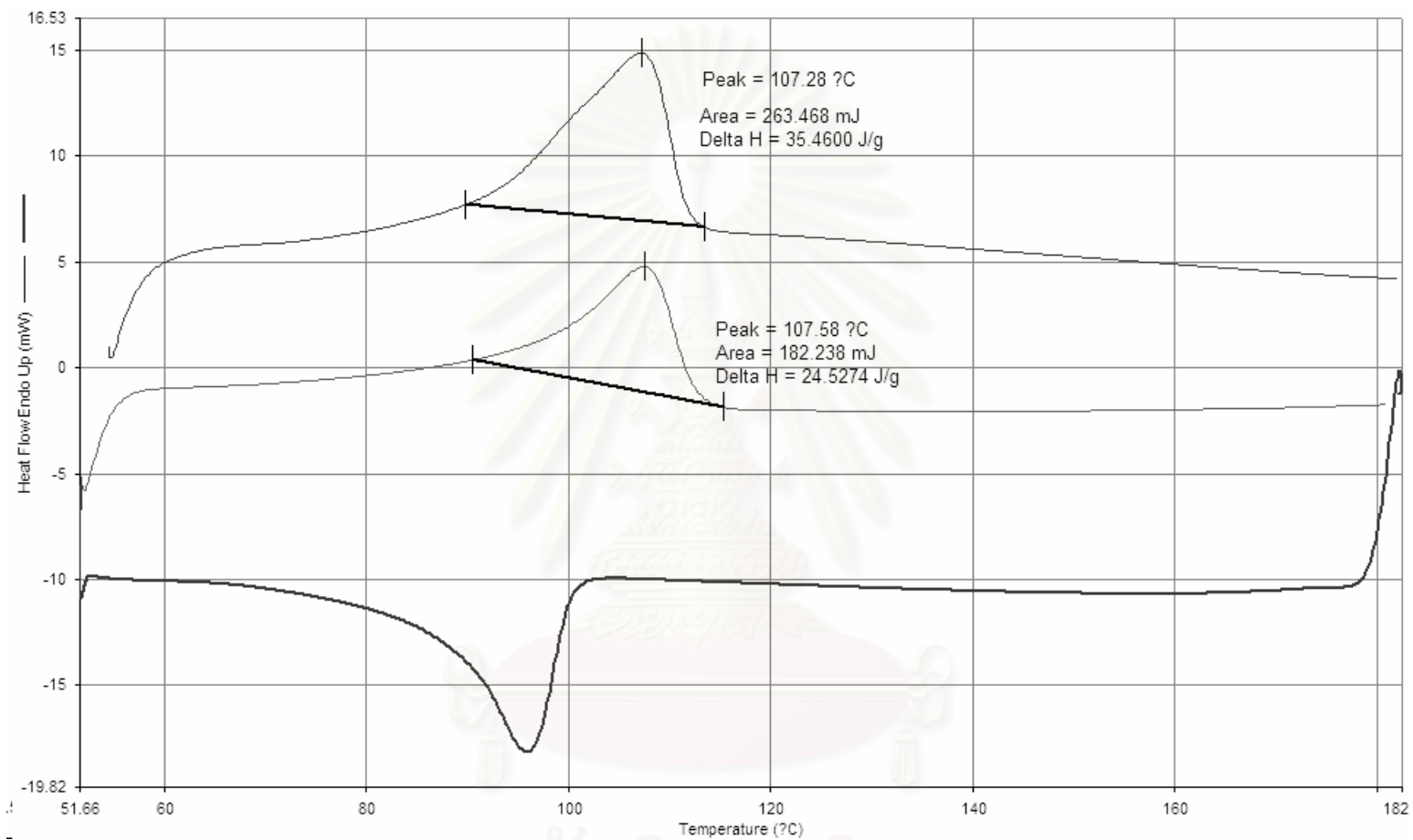


**Figure A-7.** DSC curve of LLDPE-nanocomposites with 0.1 g of 15 nm-silica ( fixed ratio of Al/Zr)

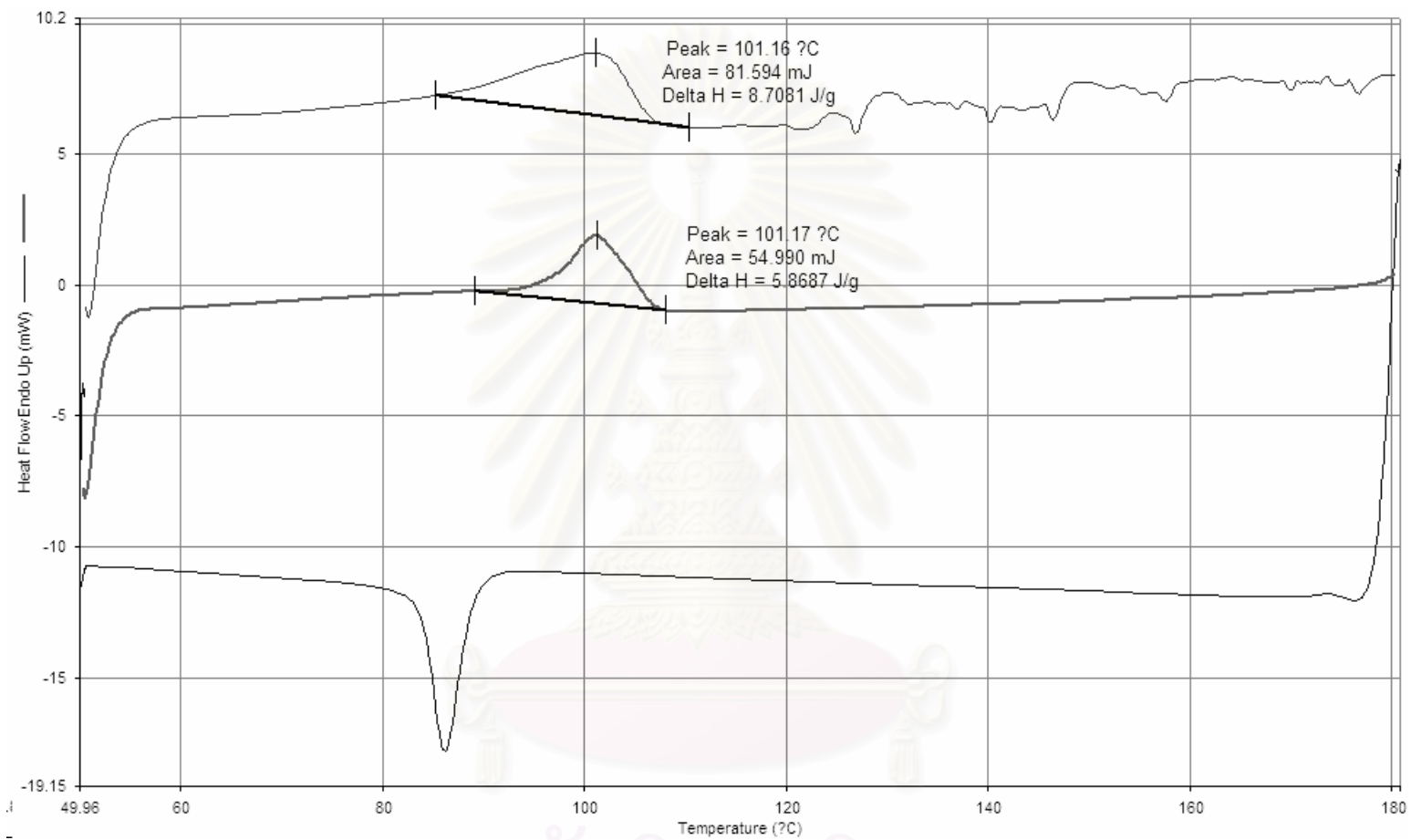
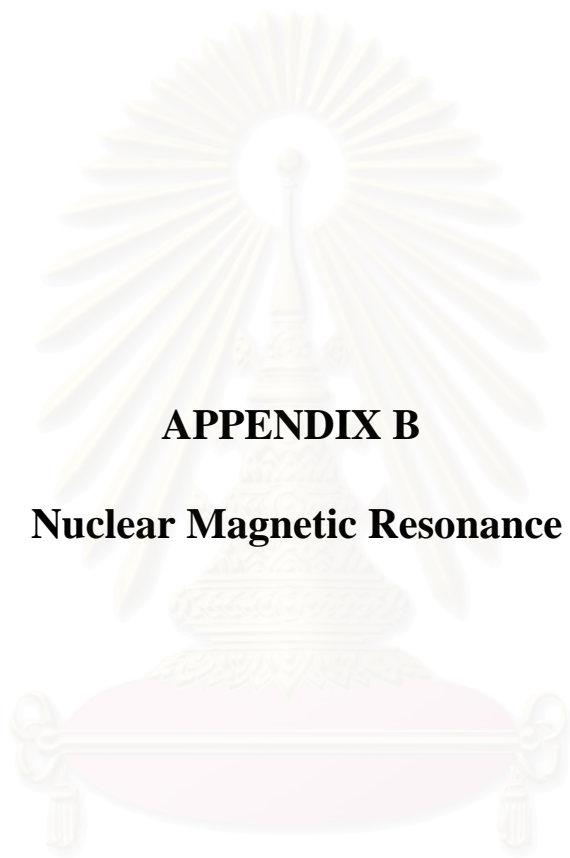


**Figure A-8.** DSC curve of LLDPE-nanocomposites with 0.3 g of 15 nm-silica ( fixed ratio of Al/Zr)

สถาบันวิทยบริการ  
จุฬาลงกรณ์มหาวิทยาลัย



**APPENDIX B**

**Nuclear Magnetic Resonance**

สถาบันวิทยบริการ  
จุฬาลงกรณ์มหาวิทยาลัย

Department of Science Service  
 Chemistry Division  
 Lab. no. - VC 419  
 Name of sample: LLDPE 1  
 Instrument : Avance JEK-400  
 Solvent : o-dichlorobenzene/CDCl<sub>3</sub>  
 (at 120°C)  
 Operator : Nongnuch D.  
 Date : 20-10-2005

page 2/7

Current Data Parameters  
 NAME polter  
 EXPRNO 7  
 PROCNO 1

F2 - Acquisition Parameters  
 Date\_ 000000  
 Time 15.16  
 INSTRUM cpw100  
 PROBR0 5 mm QNP 1H  
 PRFRAG rgdc  
 TD 151072  
 SOLVENT CDCl<sub>3</sub>  
 NS 4.59  
 ts 0  
 SNU 25125.628 Hz  
 FIDRES 0.191493 Hz  
 AQ 2.6003027 sec  
 RG 4096  
 DN 15.900 usec  
 DE 7.14 usec  
 TE 300.2 K  
 dA1 0.0300000 sec  
 dL12 19.08 usec  
 QDPR2 Waltz16  
 PCPD2 136.00 usec  
 GC2 400.1317160 MHz  
 NE2 15  
 PL1 150.00 dB  
 SE 3.0600500 sec  
 FI 6.80 usec  
 FE 7.14 usec  
 SFO1 100.6262885 MHz  
 NU01 70  
 PL -6.00 dB

F1 - Processing parameters  
 SI 65536  
 SF 100.6127004 MHz  
 MDW 60  
 SSI 0  
 LB 3.00 Hz  
 GB 0  
 PC 1.00

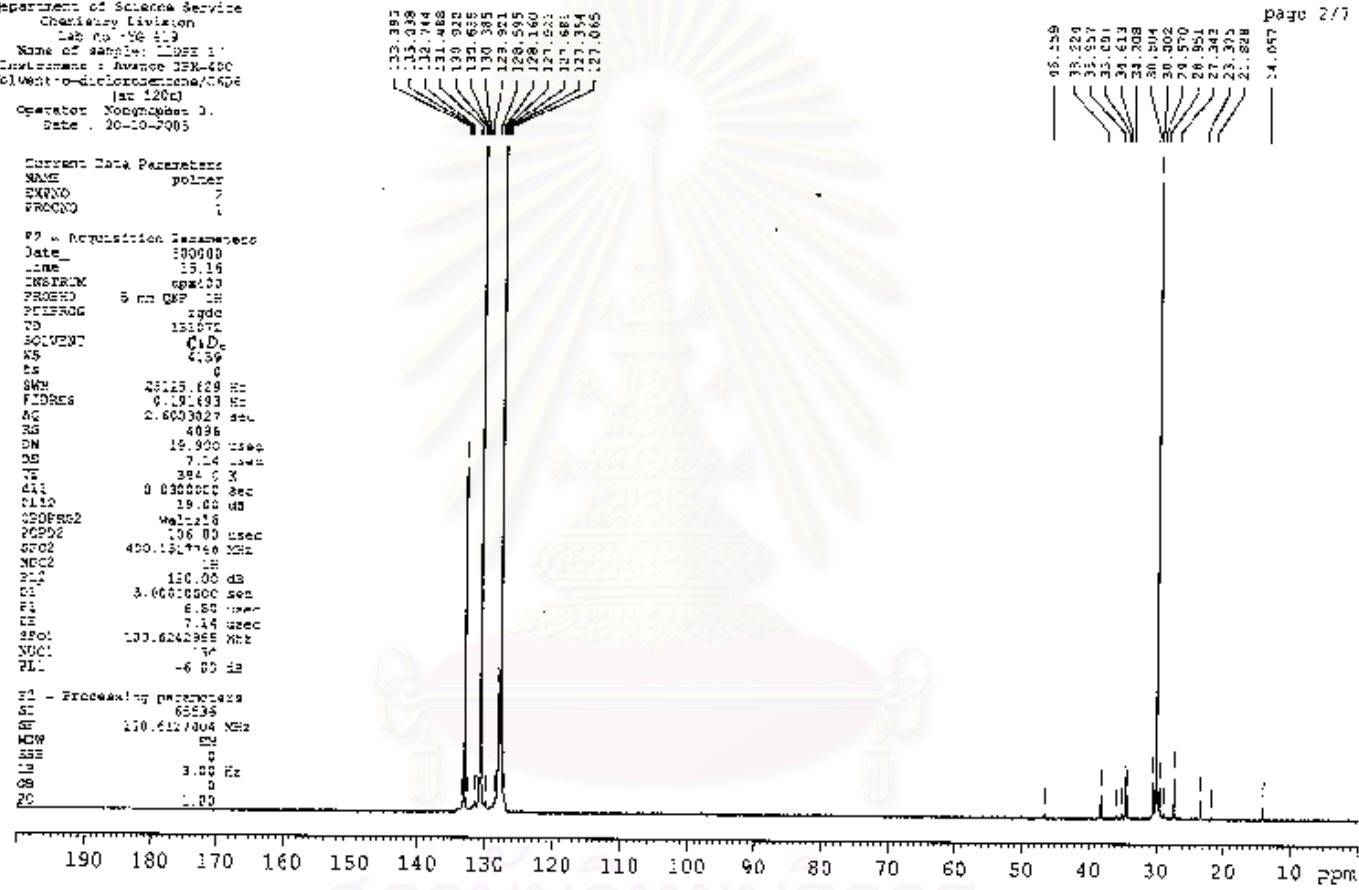


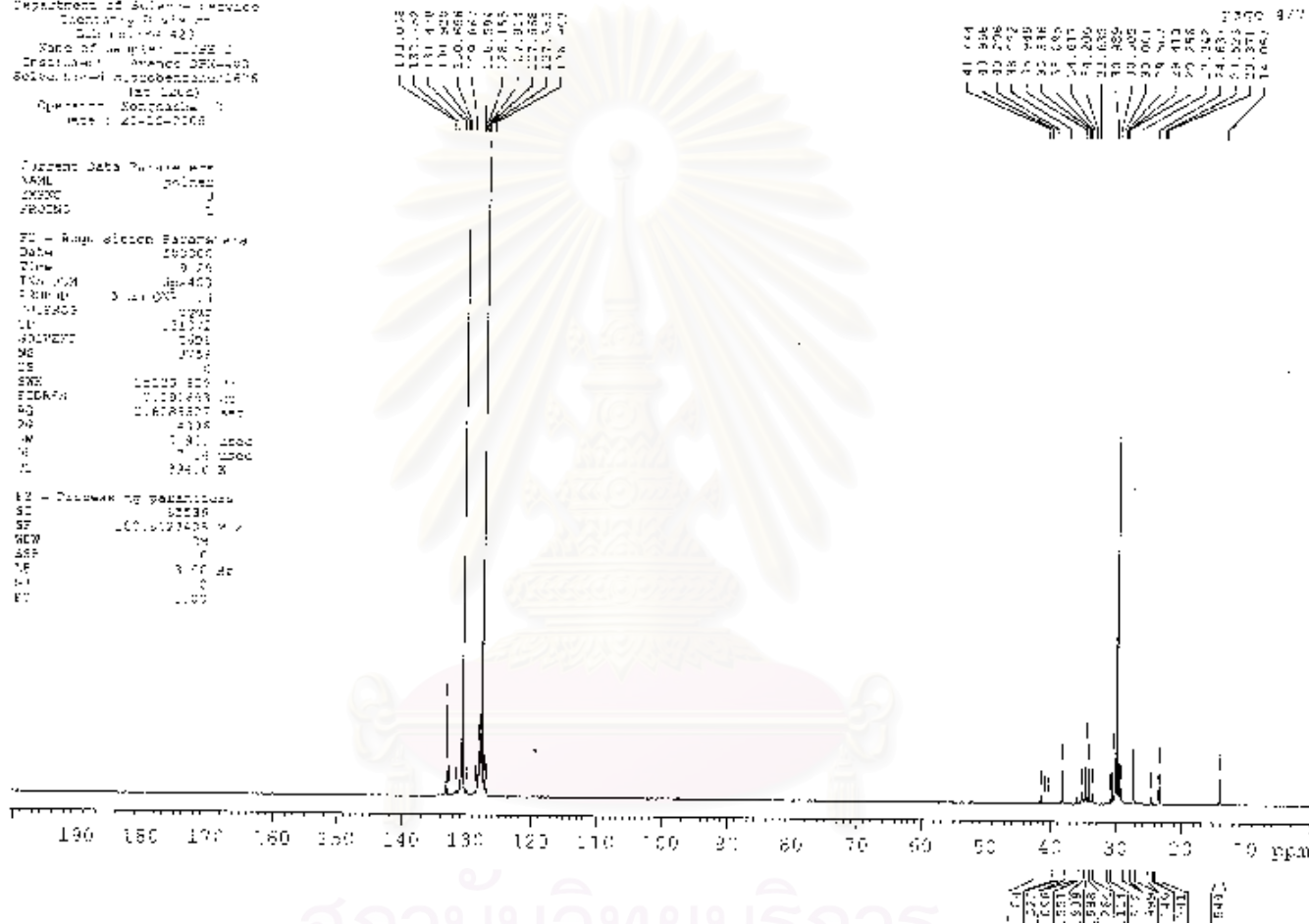
Figure B-1. <sup>13</sup>C-NMR spectrum of LLDPE-nanocomposites with 0.1g of 10 nm-silica

Department of Science - Physics  
 Chemistry (9th Flr.)  
 Faculty of Science - Chiang Mai  
 Institute of Advanced Study (IAS)  
 800.101-14, Phrao, Chiang Mai 50200  
 Thailand  
 Project: Nanocomposites  
 Date: 20-10-2008

Current Data Parameters  
 NAME: Untitled  
 USER: J  
 PRGNO: 1

PE - Acquisition Parameters  
 Date\_: 20080907  
 Time: 9:26  
 T2\*: 0.443  
 F2: 125.760  
 A: 1  
 INSTRUM: spect  
 NU: 65536  
 SFO: 125.760  
 ACQUIS: 0001  
 ME: JMS  
 DS: 0  
 SWH: 16000.000  
 FIDRES: 0.000493  
 AQ: 0.6678500  
 RG: 320  
 HW: 1.300  
 VS: 1.98  
 CS: 0.00000

PE - Processing parameters  
 SI: 32768  
 SF: 125.760000  
 SEW: 32  
 SGP: 0  
 TE: 300.2  
 SI: 0  
 FT: 1.00





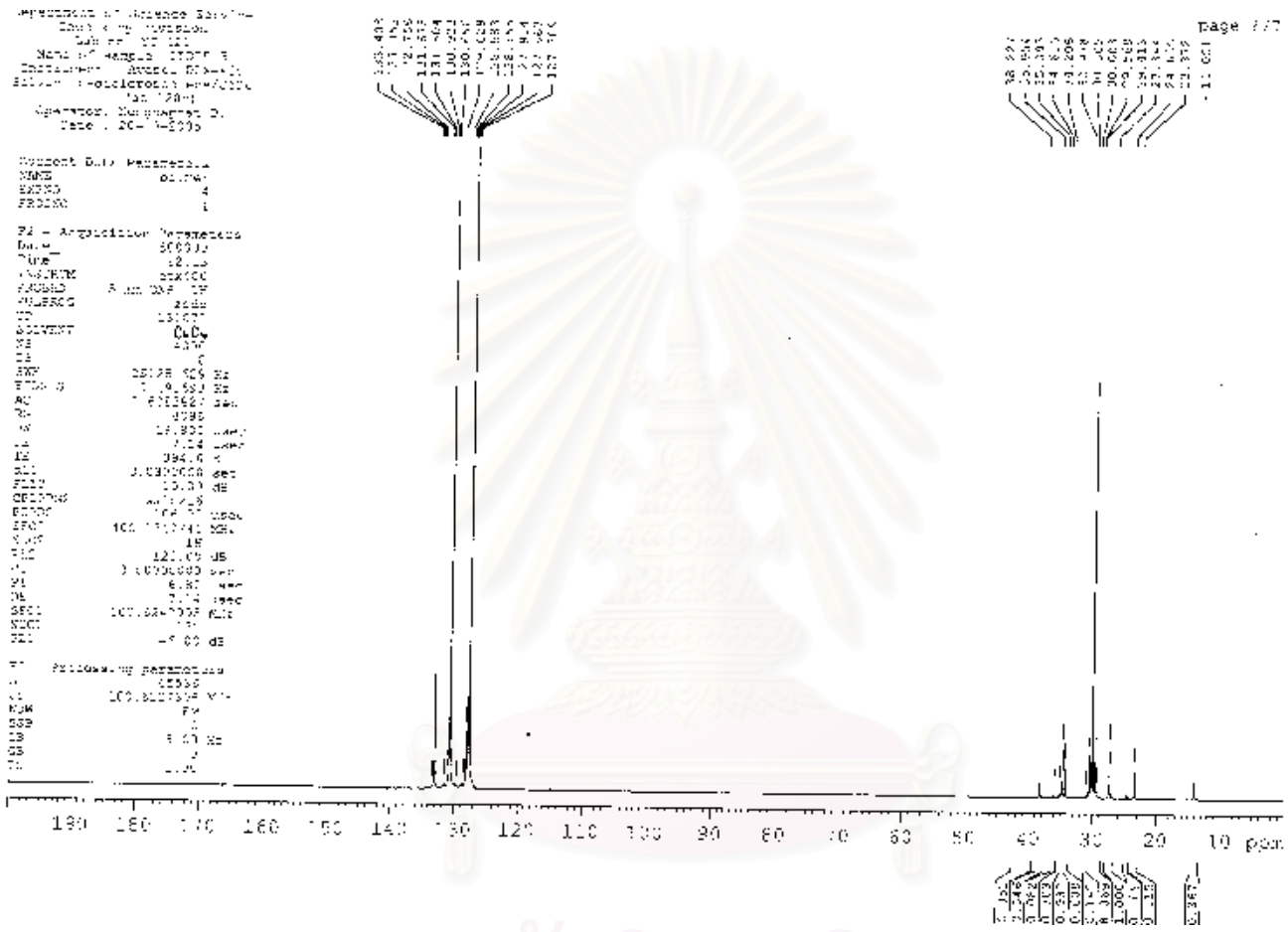


Figure B-3. <sup>13</sup>C-NMR spectrum of LLDPE-nanocomposites with 0.3 g of 10 nm-silica

สภากงวิทยงรกร  
 จุฬาลงกรณมหาวิทยาลัย

Instrument: Avance 400  
 Solvent: CDCl<sub>3</sub>  
 Date: 12-22-2005

Current Data Parameters  
 NAME: LLDPE  
 PROC: 2  
 ACQNO: 1

F1 - 13C NMR  
 Date\_: 05/05/06  
 Time: 10:01  
 INSTRUM: spect-400  
 PRGNAME: 13c-400  
 B1PRG: zgpg30  
 B1PROG: zgpg30  
 F1: 125.761  
 SCANS: 64  
 DS: 4  
 DB: 0  
 SFO: 125.76117  
 P1: 0.15000000  
 AC: 0.00000000  
 DE: 0.00200000  
 DW: 19.00000000  
 EQ: 0.15000000  
 EI: 0.00000000  
 FID: 125.76117  
 GPCPRG: zgpg30  
 GPCPR2: zgpg30  
 GPCPR3: zgpg30  
 GPCPR4: zgpg30  
 GPCPR5: zgpg30  
 GPCPR6: zgpg30  
 GPCPR7: zgpg30  
 GPCPR8: zgpg30  
 GPCPR9: zgpg30  
 GPCPR10: zgpg30  
 GPCPR11: zgpg30  
 GPCPR12: zgpg30  
 GPCPR13: zgpg30  
 GPCPR14: zgpg30  
 GPCPR15: zgpg30  
 GPCPR16: zgpg30  
 GPCPR17: zgpg30  
 GPCPR18: zgpg30  
 GPCPR19: zgpg30  
 GPCPR20: zgpg30  
 GPCPR21: zgpg30  
 GPCPR22: zgpg30  
 GPCPR23: zgpg30  
 GPCPR24: zgpg30  
 GPCPR25: zgpg30  
 GPCPR26: zgpg30  
 GPCPR27: zgpg30  
 GPCPR28: zgpg30  
 GPCPR29: zgpg30  
 GPCPR30: zgpg30  
 GPCPR31: zgpg30  
 GPCPR32: zgpg30  
 GPCPR33: zgpg30  
 GPCPR34: zgpg30  
 GPCPR35: zgpg30  
 GPCPR36: zgpg30  
 GPCPR37: zgpg30  
 GPCPR38: zgpg30  
 GPCPR39: zgpg30  
 GPCPR40: zgpg30  
 GPCPR41: zgpg30  
 GPCPR42: zgpg30  
 GPCPR43: zgpg30  
 GPCPR44: zgpg30  
 GPCPR45: zgpg30  
 GPCPR46: zgpg30  
 GPCPR47: zgpg30  
 GPCPR48: zgpg30  
 GPCPR49: zgpg30  
 GPCPR50: zgpg30  
 GPCPR51: zgpg30  
 GPCPR52: zgpg30  
 GPCPR53: zgpg30  
 GPCPR54: zgpg30  
 GPCPR55: zgpg30  
 GPCPR56: zgpg30  
 GPCPR57: zgpg30  
 GPCPR58: zgpg30  
 GPCPR59: zgpg30  
 GPCPR60: zgpg30  
 GPCPR61: zgpg30  
 GPCPR62: zgpg30  
 GPCPR63: zgpg30  
 GPCPR64: zgpg30  
 GPCPR65: zgpg30  
 GPCPR66: zgpg30  
 GPCPR67: zgpg30  
 GPCPR68: zgpg30  
 GPCPR69: zgpg30  
 GPCPR70: zgpg30  
 GPCPR71: zgpg30  
 GPCPR72: zgpg30  
 GPCPR73: zgpg30  
 GPCPR74: zgpg30  
 GPCPR75: zgpg30  
 GPCPR76: zgpg30  
 GPCPR77: zgpg30  
 GPCPR78: zgpg30  
 GPCPR79: zgpg30  
 GPCPR80: zgpg30  
 GPCPR81: zgpg30  
 GPCPR82: zgpg30  
 GPCPR83: zgpg30  
 GPCPR84: zgpg30  
 GPCPR85: zgpg30  
 GPCPR86: zgpg30  
 GPCPR87: zgpg30  
 GPCPR88: zgpg30  
 GPCPR89: zgpg30  
 GPCPR90: zgpg30  
 GPCPR91: zgpg30  
 GPCPR92: zgpg30  
 GPCPR93: zgpg30  
 GPCPR94: zgpg30  
 GPCPR95: zgpg30  
 GPCPR96: zgpg30  
 GPCPR97: zgpg30  
 GPCPR98: zgpg30  
 GPCPR99: zgpg30  
 GPCPR100: zgpg30

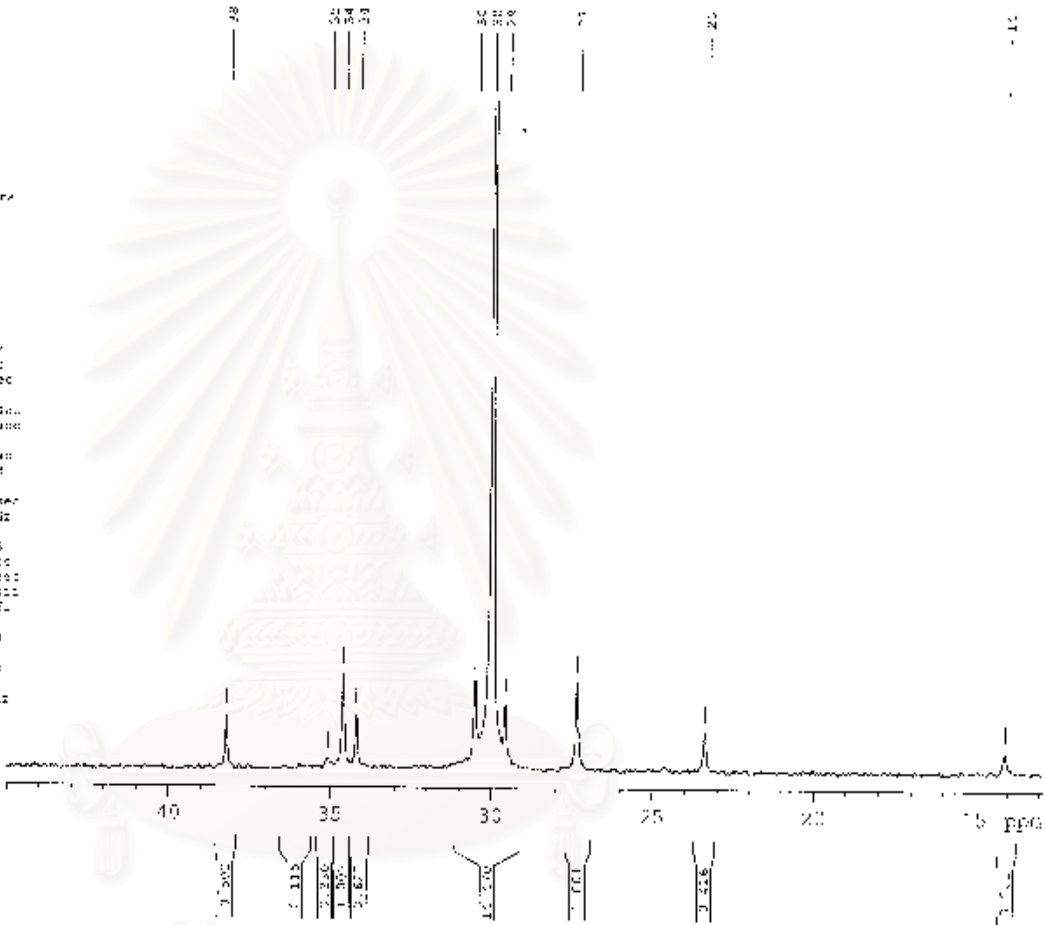


Figure B-4. <sup>13</sup>C-NMR spectrum of LLDPE-nanocomposites with 0.1 g of 15 nm-silica

สถาบันวิทยบริการ  
 จุฬาลงกรณ์มหาวิทยาลัย

Department of Polymer Science  
 Chemistry Division  
 Institute of Chemistry  
 Kasornburi Road, Bangkok 10132  
 Thailand  
 Date: 22/11/2005

Customer: Poly. Experiment  
 Name: 130-1  
 EMail: 2  
 Phone: 1

DE Acq. P1. Log Parameters  
 Date: 200511  
 Time: 13:55  
 File Name: 130-100  
 Processor: 5 - 1 - 0000 DE  
 Processor: 0000  
 P1: 130-100  
 Software: v3.0  
 AS: 000  
 P1: 0  
 QM1: 11100.000 Hz  
 P1: 0.111693 Hz  
 AQ: 1.0000000 sec  
 RC: 0.00  
 DR: 10.000 sec  
 DF: 7.14 sec  
 CF: 100.0 Hz  
 S.F.: 0.000000 sec  
 S.F.: 0.00 DE  
 P1: 00000  
 P1: 10.00 sec  
 S.F.: 40.00000 Hz  
 NDC: 10  
 S.F.: 100.00 Hz  
 P1: 10.00 sec  
 S.F.: 7.14 sec  
 S.F.: 100.00000 Hz  
 P1: 10.00 sec  
 P1: 10.00 sec

P1 - Processing: 000000  
 S.F.: 60.00  
 SF: 100.00000 Hz  
 P1: 10.00  
 S.F.: 10.00  
 P1: 10.00  
 S.F.: 10.00

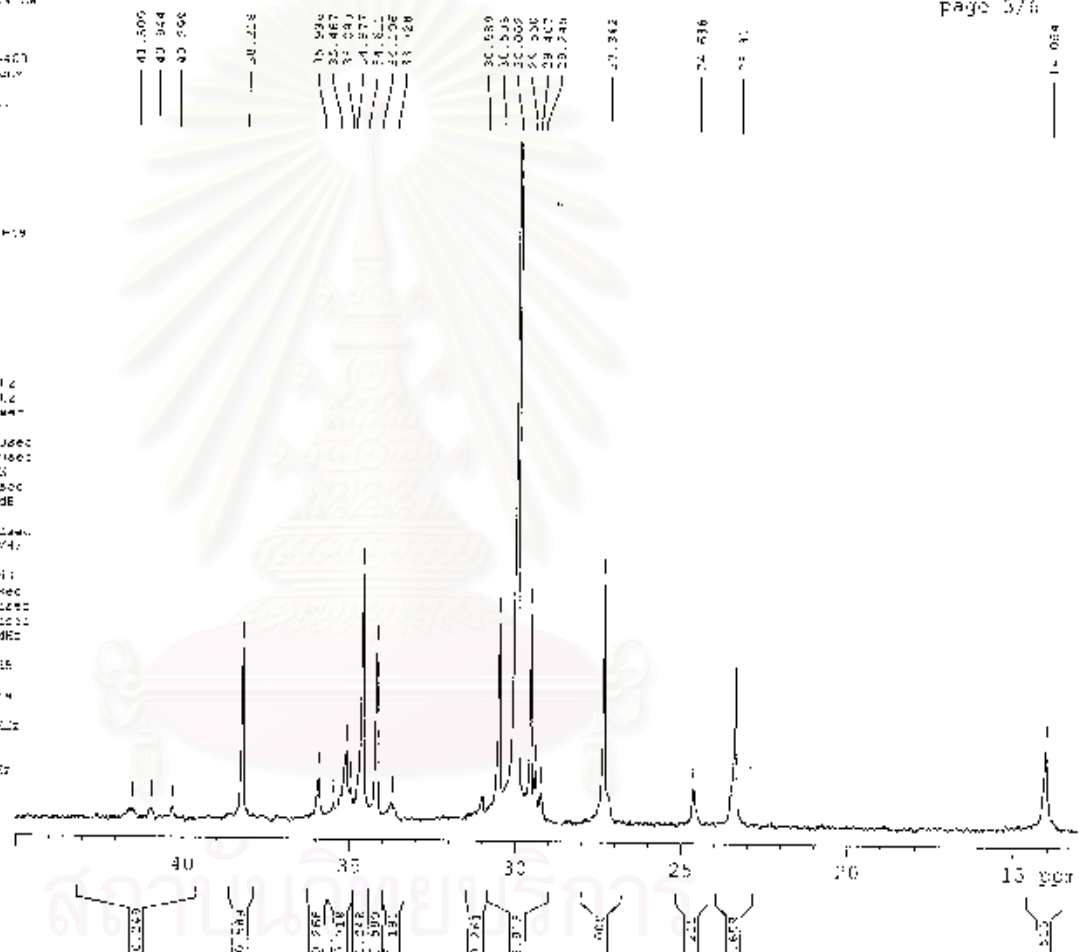


Figure B-5. <sup>13</sup>C-NMR spectrum of LLDPE-nanocomposites with 0.2 g of 15 nm-silica

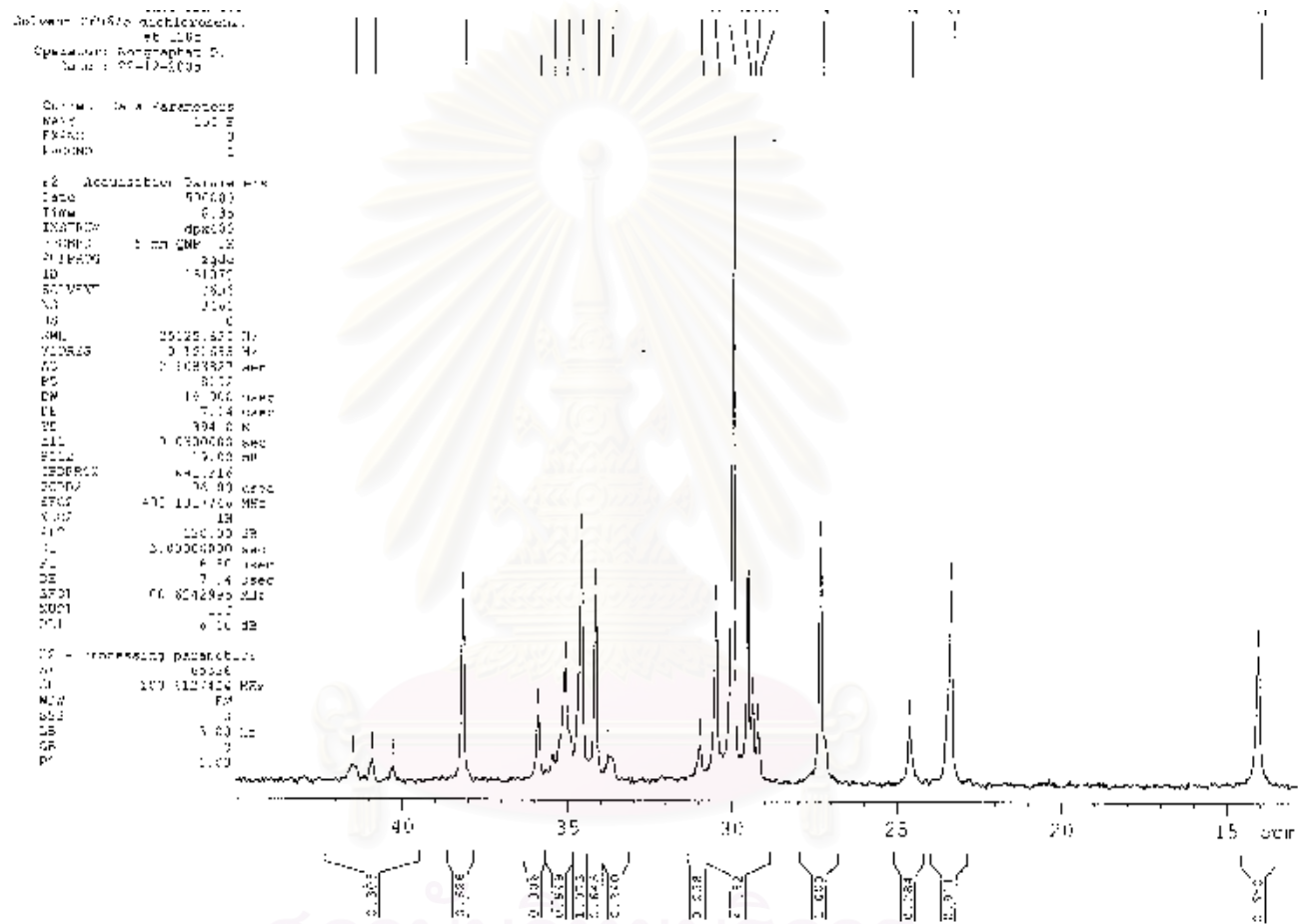


Figure B-6. <sup>13</sup>C-NMR spectrum of LLDPE-nanocomposites with 0.3g of 15 nm-silica

Sample name: F-11  
 Instrument: Avance DEB-400  
 File name: 03067-0-1101020001  
 at 1200  
 Operator: Rajakumar P.  
 Date: 02-11-2022

Experiment Parameters  
 Name: F-11  
 LIXNO: -  
 PROCNO: -

F2 - Acquisition Parameters  
 Date\_UTC: 202209  
 Time: 12:58  
 INSTRUM: spect  
 PROCNO: 11  
 F2: 125.762  
 SOLVENT: CDCl3  
 NS: 640  
 DS: 4  
 SWH: 15000.000 Hz  
 L1: 125.762 MHz  
 A2: 2.0000000 sec  
 PC: 0.152  
 DP: 4096.000000  
 DE: 19.140000  
 FE: 0.000000  
 ST1: 7.000000 sec  
 FID1: 1.000000  
 SFO1: 125.762 MHz  
 EQ1: 10.000000 sec  
 SF02: 400.1463636 MHz  
 WID2: 14  
 FID2: 1.000000  
 SFO2: 313.7453333 MHz  
 E1: 5.000000 sec  
 DE: 19.140000  
 SF03: 100.6261667 MHz  
 NUC1: 13C  
 P1: 12.000000 sec

F2 - Processing parameters  
 SI: 32768  
 SF: 125.7621474 MHz  
 NU1: 13C  
 SFO1: 125.762 MHz  
 FID1: 1.000000  
 SFO2: 400.1463636 MHz  
 WID2: 14  
 FID2: 1.000000

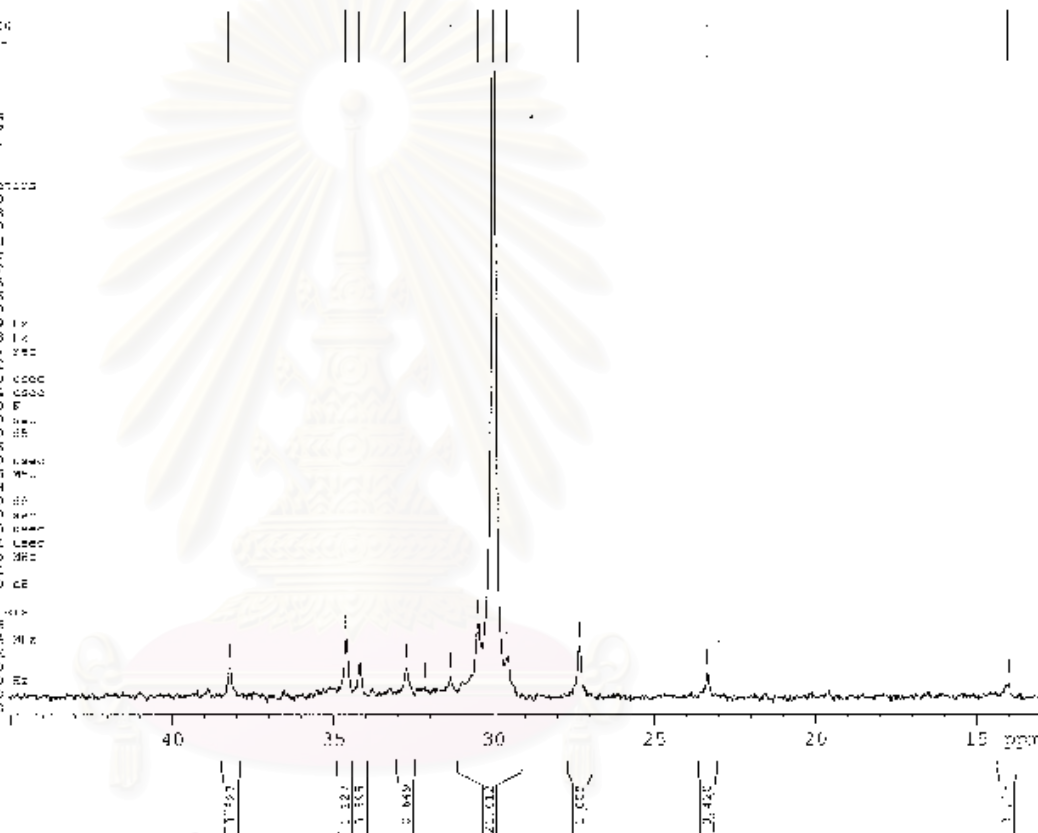
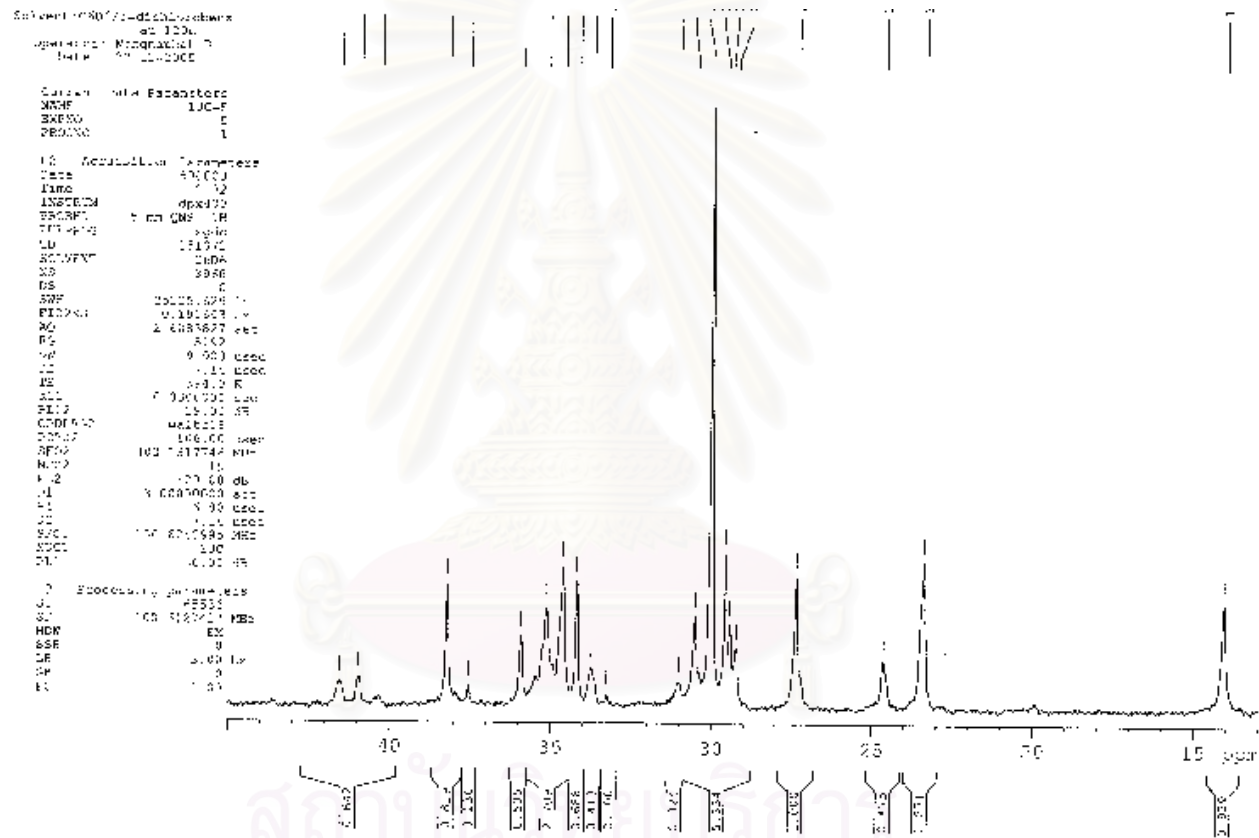


Figure B-7  $^{13}\text{C}$ -NMR spectrum of LLDPE-nanocomposites with 0.1g of 15 nm-silica (fixed ratio of Al/Zr)



**Figure B-8**  $^{13}\text{C}$ -NMR spectrum of LLDPE-nanocomposites with 0.3g of 15 nm-silica (fixed ratio of Al/Zr)



**APPENDIX C**

**The specification of commercial nano-SiO<sub>2</sub>**

สถาบันวิทยบริการ  
จุฬาลงกรณ์มหาวิทยาลัย

**Nano-SiO<sub>2</sub> 10 nm, 99.5%**

Aldrich Silica

Molecular Formula SiO<sub>2</sub>

Molecular Weight 60.08

CAS Number 7631-86-9

MDL number MFCD00011232

Properties

form spherical (porous)

surface area BET surf. area 590-690 m<sup>2</sup>/g

bp &gt;100 °C(lit.)

2230 °C(lit.)

mp &gt;1600 °C(lit.)

density 2.2-2.6 g/mL at 25 °C

bulk density 0.068 g/mL

References

Merck Merck 13,8567

Reference Corp MSDS 1 (2), 3090:A / RegBook 1 (3), 3535:B / Sax 6, 2395

Safety

Safety Statements 22-24/25

WGK Germany 2

RTECS VV7310000

สถาบันวิทยบริการ  
จุฬาลงกรณ์มหาวิทยาลัย



**Nano-SiO<sub>2</sub> 15 nm, 99.5%**

Aldrich Silica

Molecular Formula SiO<sub>2</sub>

Molecular Weight 60.08

Propertiessurface area BET surf. area 140-180 m<sup>2</sup>/g

bp &gt;100 °C(lit.)

2230 °C(lit.)

mp &gt;1600 °C(lit.)

density 2.2-2.6 g/mL at 25 °C

bulk density .011 g/mL

References

Merck Merck 13,8567

Reference Corp MSDS 1 (2), 3090:A / RegBook 1 (3), 3535:B / Sax 6, 2395

Safety

Safety Statements 22-24/25

WGK Germany 2

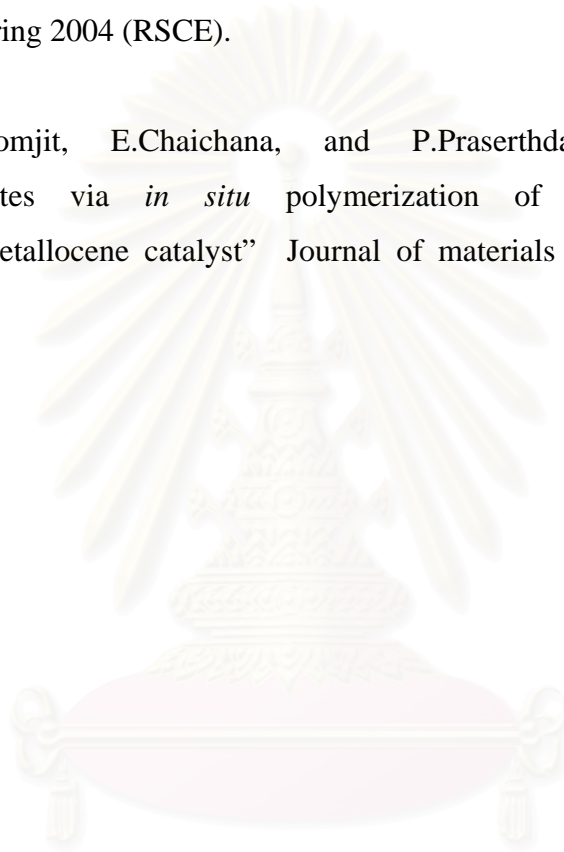
RTECS VV7310000

สถาบันวิทยบริการ  
จุฬาลงกรณ์มหาวิทยาลัย

## APPENDIX D

### LIST OF PUBLICATION

1. E.Chaichana, B.Jongsomjit, and P.Praserthdam “LLDPE/silica doped alumina-nanocomposites synthesized via *in situ* polymerization of ethylene/1-hexene with MAO/zirconocene catalyst” The regional symposium on chemical engineering 2004 (RSCE).
2. B.Jongsomjit, E.Chaichana, and P.Praserthdam “LLDPE/nano-silica composites via *in situ* polymerization of ethylene/1-hexene with MAO/metallocene catalyst” Journal of materials science 40(2005) 2043-2045.



สถาบันวิทยบริการ  
จุฬาลงกรณ์มหาวิทยาลัย

## VITAE

Mr. Ekrachan Chaichana was born in March 5<sup>th</sup>, 1980 in Samutsakorn, Thailand. He finished high school from Samutsakorn Vitthayalai School, Samutsakorn and received bachelor's degree in Science from the department of Chemistry, Faculty of Science, Silpakorn University, Bangkok, Thailand in 2000.



สถาบันวิทยบริการ  
จุฬาลงกรณ์มหาวิทยาลัย

## LLDPE/nano-silica composites synthesized via *in situ* polymerization of ethylene/1-hexene with MAO/metallocene catalyst

BUNJERD JONGSOMJIT\*, EKKRACHAN CHAICHANA, PIYASAN PRASERTHDAM  
Center of Excellence on Catalysis and Catalytic Reaction Engineering, Department of Chemical Engineering,  
Faculty of Engineering, Chulalongkorn University, Bangkok 10330, Thailand  
E-mail: bunjerd.j@chula.ac.th

It is known that the copolymerization of ethylene with higher 1-olefins is a commercial importance for productions of elastomer and linear low-density polyethylene (LLDPE). LLDPE (density 0.920 to 0.940) is one of the most widely used polyolefins in many applications, especially, for plastic films. However, in some cases, the use of polyolefins or LLDPE is limited by their drawbacks such as low mechanical strength, low thermal resistance, poor optical properties and so on. Thus, in order to improve the specific properties of these polymers, some additives need to be blended with them.

It has been reported that blending polymer with inorganic materials is considered as a powerful method to produce new materials called polymer composites or filled polymers. However, due to the significant development in nano-technologies in the recent years, nano-inorganic materials such as  $\text{SiO}_2$ ,  $\text{Al}_2\text{O}_3$  and  $\text{TiO}_2$  have brought much attention to this research field. Therefore, the polymer composites filled with nano-inorganic materials are well recognized as polymer nano-composites. Essentially, addition of the nano-materials into polymers may lead to overcome the drawbacks and produce new materials, which are considered to be robust. Basically, there are three methods used to produce the filled polymer; (i) melt mixing, (ii) solution blending, and (iii) *in situ* polymerization. Due to the direct synthesis via polymerization along with the presence of nano-materials, the *in situ* polymerization is perhaps considered to be the most powerful techniques to produce polymer nano-composites with good dispersion of the nano-particles into polymer matrix. Although, many authors [1–6] have studied LLDPE composites only synthesized via melt mixing and solution blending, no further reports have been done on synthesizing polymer nano-composites via the *in situ* polymerization with metallocene catalysts.

In the present study, LLDPE/nano- $\text{SiO}_2$  composites synthesized via the *in situ* polymerization with MAO/metallocene catalyst was investigated for the first time. The nano- $\text{SiO}_2$  and nano- $\text{SiO}_2$  doped  $\text{Al}_2\text{O}_3$  filled materials were synthesized using sol-gel method [7] to obtain the nano- $\text{SiO}_2$  with particle size of ca. 50 nm. The amounts of nano-materials filled were also varied. Yields, activities, and polymer morphologies were discussed.

The preparation of LLDPE/nano-composites via *in situ* polymerization was performed as follows; all chemicals [nano- $\text{SiO}_2$ , nano- $\text{SiO}_2$  doped  $\text{Al}_2\text{O}_3$ , toluene, rac-ethylenebis (indenyl) zirconium dichloride  $[\text{Et}(\text{Ind})_2\text{ZrCl}_2]$ , methylaluminoxane (MAO), trimethylaluminum (TMA) and 1-hexene] were manipulated under an inert atmosphere using a vacuum glove box and/or Schlenk techniques. The nano-materials were heated under vacuum at  $400^\circ\text{C}$  for 6 hr prior to impregnation with MAO. In order to impregnate MAO onto the nano-materials, the method was described as follows. One gram of the nano-materials was reacted with the desired amount of MAO at room temperature and stirred for 30 min. The solvent was then removed from the mixture. About 20 ml of toluene was added into the obtained precipitate, the mixture was stirred for 5 min, and then the solvent was removed. This procedure was done for five times to ensure the removal of impurities. Then, the solid part was dried under vacuum at room temperature to obtain white powder of nano-materials/MAO.

Polymerization was conducted upon the methods as follows. The ethylene/1-hexene copolymerization reaction was carried out in a 100-ml semi-batch stainless steel autoclave reactor equipped with a magnetic stirrer. At first, 0.1, 0.2, and 0.3 g of the nano-materials/MAO ( $[\text{Al}]_{\text{MAO}}/[\text{Zr}] = 1135, 2270, \text{ and } 3405$ ) and 0.018 mole of 1-hexene along with toluene (to make the total

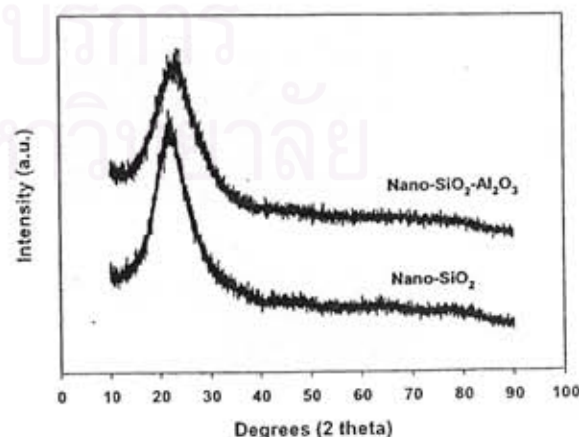


Figure 1 XRD patterns of nano- $\text{SiO}_2$  and nano- $\text{SiO}_2\text{-Al}_2\text{O}_3$ .

\*Author to whom all correspondence should be addressed.

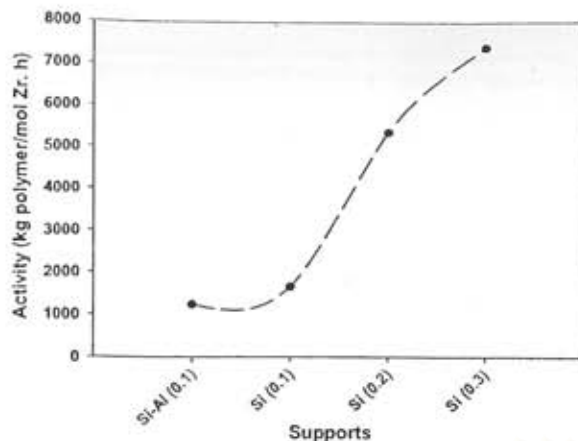


Figure 2 Activity profile with various amounts of support used.

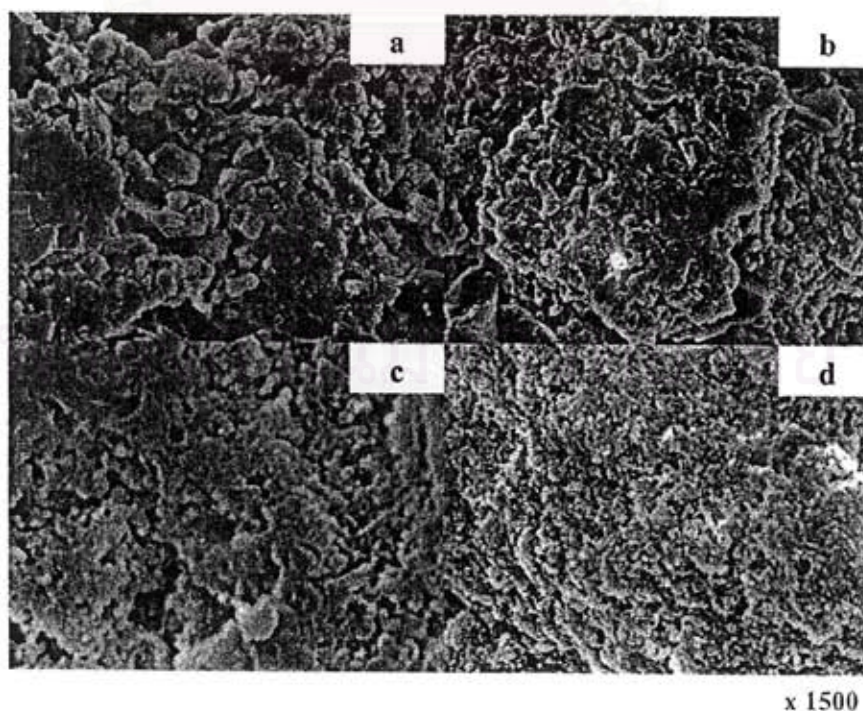
volume of 30 ml) were put into the reactor. The desired amount of  $\text{Et}(\text{Ind})_2\text{ZrCl}_2$  ( $5 \times 10^{-5}$  M) and TMA ( $[\text{Al}]_{\text{TMA}}/[\text{Zr}] = 2500$ ) was mixed and stirred for 5-min aging at room temperature, separately, and then was injected into the reactor. The reactor was frozen in liquid nitrogen to stop reaction for 15 min and then the reactor was evacuated to remove argon. The reactor was heated up to polymerization temperature ( $70^\circ\text{C}$ ). To start reaction, 0.018 mole of ethylene was fed into the reactor containing the comonomer and catalyst mixtures. After all ethylene was consumed, the reaction was terminated by addition of acidic methanol (0.1% HCl in methanol) and stirred for 30 min. After filtration, the obtained copolymer (white powder) was washed with methanol and dried at room temperature. The LLDPE/nano- $\text{SiO}_2$  composites obtained were characterized using scanning electron microscopy (SEM) and energy dispersive X-ray spectroscopy (EDX)

TABLE I Activity and yield of LLDPE/nano-composites via *in situ* polymerization with metallocene catalyst

Nano-filled	Amounts/Run (g)	Yield (g)	Time (s)	Activity ( $\text{kg pol./mol. Zr.h}$ )
$\text{SiO}_2\text{-Al}_2\text{O}_3$	0.1	0.2006	450	1234
$\text{SiO}_2$	0.1	0.2147	360	1652
$\text{SiO}_2$	0.2	0.6070	318	5288
$\text{SiO}_2$	0.3	0.8382	315	7369

to study morphologies and elemental distribution, respectively.

XRD patterns of nano- $\text{SiO}_2$  and nano- $\text{SiO}_2\text{-Al}_2\text{O}_3$  are shown in Fig. 1. It was found that XRD patterns for both materials exhibited similar patterns assigning to amorphous silica. No XRD peaks of  $\text{Al}_2\text{O}_3$  were detected indicating highly dispersed forms of it. After impregnation of MAO onto the nano-particles, copolymerization of ethylene/1-hexene was performed with various conditions based on changing types and/or amounts of the nano-particles used. Activities and yields of LLDPE/nano-composites are shown in Table I. It was observed that activities and yields dramatically increased with increasing the amounts of  $\text{SiO}_2$  particles used due to increased MAO as a cocatalyst. However, at the same amount (0.1 g) of particles, the  $\text{SiO}_2\text{-Al}_2\text{O}_3$  exhibited the lowest yield and activity of any other samples. A comparison of activities is also shown in Fig. 2. It should be noted that activities of LLDPE/nano- $\text{SiO}_2$  composites obtained in this present study were much lower (about three times) compared to the LLDPE/micron- $\text{SiO}_2$  composite as reported by our group [8]. This was probably due to more steric hindrance arising from the nano-particles. Morphologies of LLDPE/nano composites are shown in Fig. 3.



x 1500

Figure 3 Morphologies of LLDPE/nano composites with: (a)  $\text{SiO}_2\text{-Al}_2\text{O}_3$  (0.1 g), (b)  $\text{SiO}_2$  (0.1 g), (c)  $\text{SiO}_2$  (0.2 g), and (d)  $\text{SiO}_2$  (0.3 g).

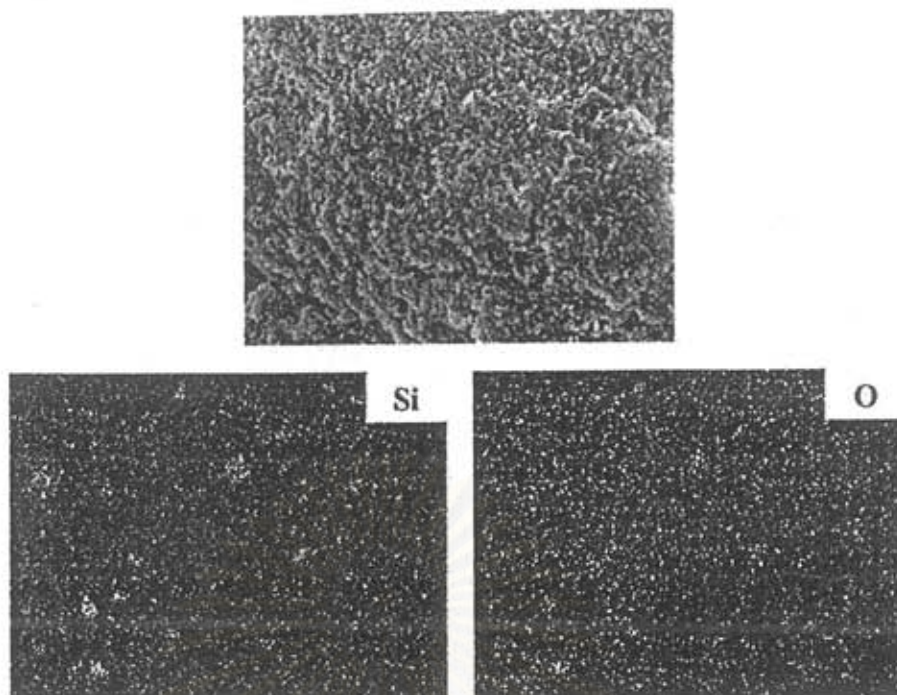


Figure 4 EDX mapping of LLDPE/nano-SiO<sub>2</sub> composite with SiO<sub>2</sub> (0.3 g) indicating distribution of Si and O.

It can be observed that with using SiO<sub>2</sub>-Al<sub>2</sub>O<sub>3</sub> (0.1 g), SiO<sub>2</sub> (0.1 g), and SiO<sub>2</sub> (0.2 g), morphologies [Fig. 3a-c] were found to be similar indicating only the polymer texture as seen in ref. [8]. However, with increasing the amount of nano-SiO<sub>2</sub> to 0.3 g, the morphology as shown in Fig. 3d was significantly changed indicating better combination between the silica and polymer textures. This was suggested that the LLDPE/nano-SiO<sub>2</sub> composite can be obtained at a certain amount of the nano-SiO<sub>2</sub> particles used. In order to identify the distribution of SiO<sub>2</sub> particles in the polymer matrix, EDX mapping was performed on the distribution of Si and O elements as shown in Fig. 4. It can be observed that Si and O elements exhibited good distribution all over the polymer matrix indicating good dispersion of nano-SiO<sub>2</sub> particles.

In summary, LLDPE/nano-SiO<sub>2</sub> composites can be obtained via the *in situ* polymerization with MAO/metallocene catalyst. It was found that silica particles were well dispersed in the polymer matrix at some certain amounts of them. However, activities and yields of polymerization were apparently low probably due to more steric hindrance arising from the nano-particles. Thus, polymerization conditions, catalysts used, and types of nano-particles need to be further investigated in order to increase productivity.

#### Acknowledgments

The authors would like to thank the Thailand Research Fund (TRF), National Research Council of Thailand (NRCT) and Thailand-Japan Transfer Technology Project (TJTTP-JBIC) for the financial support of this work. The authors would also like to thank Prof. Takeshi Shiono at Hiroshima University, Japan, for his kind advice throughout this project.

#### References

1. C. J. R. VERBEEK, *Mater. Lett.* **56** (2002) 226.
2. R. NAWANG, I. D. DANJAJI, U. S. ISHIKU, H. ISMAIL and Z. A. MOHD ISHAK, *Polym. Testing*, **20** (2001) 167.
3. Y. HAUNG, S. JIANG, L. WU and Y. HUA, *ibid.* **23** (2004) 9.
4. Y. Q. HUANG, Y. Q. ZHANG and Y. Q. HUA, *J. Mater. Sci. Lett.* **22** (2003) 997.
5. I. D. DANJAJI, R. NAWANG, U. S. ISHIKU, H. ISMAIL and Z. A. MOHD ISHAK, *Polym. Testing* **21** (2002) 75.
6. C. J. R. VERBEEK, *Mater. Lett.* **52** (2002) 453.
7. M. BUCKLEY and M. GREENBLATT, *J. Chem. Edu.* **71** (1994) 599.
8. B. JONGSOMJIT, P. PRASERTHDAM and P. KAEWKRAJANG, *Mater. Chem. Phys.* **86** (2004) 243.

Received 20 September  
and accepted 7 October 2004